NASA TECHNICAL NOTE

NASA TN D-3311


NASA TN D-3311



# FURTHER INVESTIGATION OF EFFECT OF AIR INJECTION THROUGH SLOTS AND POROUS SURFACES ON FLAT-PLATE TURBULENT SKIN FRICTION AT MACH 3

*by John B. Peterson, Jr., Donald I. McRee, Jerry B. Adcock, and Albert L. Braslow*

*Langley Research Center*
*Langley Station, Hampton, Va.*


NATIONAL AERONAUTICS AND SPACE ADMINISTRATION • WASHINGTON, D. C. • MARCH 1966

NASA TN D-3311

# FURTHER INVESTIGATION OF EFFECT OF AIR INJECTION THROUGH SLOTS AND POROUS SURFACES ON FLAT-PLATE TURBULENT SKIN FRICTION AT MACH 3

By John B. Peterson, Jr., Donald I. McRee, Jerry B. Adcock, and Albert L. Braslow

Langley Research Center
Langley Station, Hampton, Va.

NATIONAL AERONAUTICS AND SPACE ADMINISTRATION

For sale by the Clearinghouse for Federal Scientific and Technical Information
Springfield, Virginia 22151 – Price $0.95

# FURTHER INVESTIGATION OF EFFECT OF AIR INJECTION THROUGH SLOTS AND POROUS SURFACES ON FLAT-PLATE TURBULENT SKIN FRICTION AT MACH 3

By John B. Peterson, Jr., Donald I. McRee, Jerry B. Adcock, and Albert L. Braslow
Langley Research Center

## SUMMARY

An investigation was made at a Mach number of 3 and a Reynolds number per foot of $9.75 \times 10^6$ ($32 \times 10^6$ per meter) of the effectiveness of injection of air into the turbulent boundary layer through partial-chord porous surfaces, multiple-normal-flush slots, and rearward-inclined flush and step slots in reducing the level of supersonic skin friction. This investigation is an extension of a previous investigation reported in NASA TN D-2427 in which the results of injection through a full-chord-porous surface and through larger sizes of rearward-inclined-flush and step slots were presented.

The local and average skin friction near the end of the flat plate are presented for each configuration. In addition, boundary-layer velocity profiles and average skin-friction coefficients were measured at various positions behind the last point of injection to determine the development of the boundary layer after the injection.

The results of the partial-chord porous injection configurations and the three-normal-flush slot configuration show that they are about as effective as the full-chord porous configuration, which gave a 20-percent reduction in average skin friction. The 0.018-inch (0.046-cm) wide rearward-inclined-flush slot was more effective than any of the new slot configurations through the range of injection mass flows tested and provided a reduction in average skin friction of almost 15 percent. The velocity profiles measured behind the 0.018-inch (0.046-cm) wide rearward-inclined-flush slot indicated that most of the skin-friction reduction took place close behind the point of injection. The effectiveness of the various slot configurations appears to be largely dependent on the manner in which the injected air mixes with the original boundary layer. Although the distributed air injection resulted in a greater decrease in skin friction than the rearward-inclined-flush slots, other considerations such as recovery of the thrust available from the injection of air can make rearward-inclined slots more effective in reducing overall drag.

## INTRODUCTION

An investigation of the effect of air injection on average and local turbulent skin friction was conducted at a Mach number of 3 at the Langley Research Center. The use of air injection into the turbulent boundary layer offers a possibility of reducing the turbulent skin friction on supersonic cruise aircraft. Preliminary results of distributed injection through a porous surface, injection through rearward-inclined flush slots of various widths and injection through a rearward-inclined step slot are presented in reference 1. The present investigation was initiated to obtain more complete information on some of the slots tested in the preliminary investigation and to test several new injection configurations.

One of the new configurations tested consisted of partial-chord distributed injection through a porous surface. Since a full porous surface at this time is impractical from a structural standpoint, it was considered desirable to determine the drag-reducing effectiveness of smaller areas of distributed injection near the leading edge of the model. Multiple normal slots were also investigated to determine whether distributed injection could be simulated by a series of normal slots. Two slots previously tested - a rearward-inclined flush slot and a rearward-inclined step slot - were more thoroughly investigated in order to attempt to explain results obtained in the preliminary investigation. Since the smallest slot previously tested produced the best results, a smaller slot of each of the two rearward-inclined configurations was also tested.

The tests were made at a free-stream Reynolds number per foot of $9.75 \times 10^6$ ($32 \times 10^6$ per meter) through a range of air-injection rates. Average turbulent skin-friction coefficients were obtained along the plate surfaces at various locations. Local skin-friction coefficients were measured with a local skin-friction balance located 20 inches (51 cm) from the leading edge. Since the results of reference 1 indicate that effectiveness of the various configurations in reducing skin friction appeared to depend on the manner in which the injected air mixed with the boundary layer, boundary-layer profiles were measured in front of and behind the porous areas and slots to determine the effect of the injected air on the boundary layer.

## SYMBOLS

Measurements for this investigation were taken in the U.S. Customary System of Units. Equivalent values are indicated herein in the International System (SI) in the interest of promoting use of this system in future NASA reports. Details concerning the use of SI, together with physical constants and conversion factors, are given in reference 2.

$C_{D,meas}$ drag coefficient, $\frac{2\theta}{x_v}$

$C_{D,air}$ drag coefficient due to taking free-stream air on board and bringing it to rest, $\frac{\dot{m}U_\infty}{\frac{1}{2}\rho_\infty U_\infty^2 S}$, or $2F$

$C_{D,m}$ model drag coefficient, $C_{D,meas} - C_{D,air}$

$C_f$ local skin-friction coefficient

$C_F$ average skin-friction coefficient

$C_T$ thrust coefficient, $\frac{\text{Thrust}}{q_\infty S}$

$\frac{2F}{C_{F,o}}$ mass-flow parameter, $\frac{2\dot{m}}{\rho_\infty U_\infty S C_{F,o}}$

$l$ span of slot, 14 inches (35.56 cm)

$\dot{m}$ injection air mass-flow rate

$n$ power velocity profile index

$p$ static pressure

$p_t$ total pressure

$q$ dynamic pressure, $\frac{1}{2}\rho_\infty U_\infty^2$

$S$ reference area, $x_v l$

$u$ velocity

$U_\infty$ free-stream velocity

$w$ width of slot

$x$ distance measured from leading edge along axis of plate

$x_v$ distance measured from virtual origin of turbulence along axis of plate

$y$ perpendicular distance from plate

$\delta$ boundary-layer thickness

$\phi$ inclination of slot

$\theta$ momentum thickness of boundary layer

$\rho$ density

Subscripts:

$\infty$ free-stream conditions

o solid flat plate

## APPARATUS

### Wind Tunnel

The investigation was conducted in the 20-inch (51-cm) Langley variable supersonic tunnel which is an intermittent blowdown-type wind tunnel. Flexible nozzle walls, actuated by hydraulic motors, are used to vary the Mach number from 2.0 to 4.5. A schematic diagram of the tunnel is presented in reference 1.

### Models

The test model was a sharp-leading-edge (leading-edge radius less than 0.0008-inch) (0.0020-cm)) flat-plate configuration mounted vertically on a strut off the side wall of the tunnel at zero angle of attack. Photographs and sketches of the models are presented as figures 1 to 3. Three basic type configurations consisting of a solid surface, a porous surface, and a slotted surface were investigated. Three porous-surface configurations 14 inches (35.6 cm) wide, extended from 3 to 11 inches (7.6 to 28 cm or 15 to 57 percent chord), 3 to 8.33 inches (7.6 to 21 cm or 15 to 43 percent chord), and 3 to 7 inches (7.6 to 17.8 cm or 15 to 36 percent chord) from the leading edge. The porous surface was made of sintered bronze. These varying lengths of porous surface correspond to one-half, one-third, and one-fourth the length of the porous surface tested in reference 1. Two different multiple-normal-slot configurations, a series of 3 slots and a series of 6 slots, were investigated. Each of the slots on both multiple-slot configurations were flush with the surface, 0.045-inch (0.115-cm) wide and separated by 0.746 inch (1.895 cm). The six slots of the six-slot configuration were evenly spaced from 3.00 to 7.00 inches (7.61 to 17.8 cm), the same area as that covered by one of the porous-surface configurations. The three slots of the three-slot configuration were located at the same location as the first three slots of the six-slot configuration. Also investigated were two different single flush slots and two different single step slots all inclined 15° to the direction of flow and located approximately 3 inches (7.6 cm) from the leading edge. These slots included the most effective flush slot (the 0.018-inch (0.046-cm) slot) and the 0.065-inch (0.165-cm) step slot from the preliminary investigation (ref. 1) to investigate more thoroughly the boundary-layer mixing phenomena involved. In addition, a smaller flush slot (0.0085-inch (0.0216-cm) wide) and a 0.015-inch (0.038-cm) step slot were tested. All slots were 14 inches (35.6 cm) in span.

A boundary-layer trip consisting of distributed three-dimensional roughness (no. 60 carborundum) was placed 1 inch (2.54 cm) from the leading edge of all configurations to insure turbulent flow over the models. Reference 3 was used to calculate the height of roughness required to trip the boundary layer.

## Instrumentation

The surface static pressure was measured with static orifices in each model. The positions of the static orifices in each model are shown as circles in figure 2. The solid-surface configuration was equipped with static pressure orifices at 3, 4, 6, 8, 12, 16, 18, and 20 inches (7.6, 10.2, 15.2, 20.3, 30.5, 40.6, 45.7, and 51 cm) from the leading edge. All the slot-injection configurations had static orifices 0.1, 0.5, and 1.0 inch (0.25, 1.27, and 2.54 cm) behind the rearmost point of injection. Static orifices were also located at 12, 16, and 18 inches (30.5, 40.6, and 45.7 cm) from the plate leading edge for the multiple normal-slot and single-slot configurations. Static orifices were located at 20 inches (51 cm) from the plate leading edge for the porous configuration. Located in the plenum chamber of all configurations were a total-pressure tube to measure chamber total pressure and a thermocouple to measure chamber total temperature. A total-pressure boundary-layer survey apparatus was mounted opposite the model surface and is shown in figure 4. This apparatus allowed the movement of a total-pressure probe 10.5 inches (26.7 cm) in the streamwise direction and 1.0 inch (2.54 cm) normal to the model surface. The thickest boundary layer encountered was approximately 0.55 inch (1.40 cm). The height of the boundary-layer survey probe from the plate surface could be recorded to an accuracy of 0.0005 inch (0.00127 cm). Close-up photographs of the two probes used in the investigation are shown in figure 5. The extended probe was necessary in order to obtain boundary-layer surveys ahead of the 8-inch (20.3-cm) station.

The air for injection was taken from the supply tank of the variable supersonic tunnel and piped through a line containing pressure-reducer valves and a venturi to the plenum chamber. Measurements were made of venturi total pressure, venturi differential pressure, and venturi total temperature in order to calculate the mass flow passing into the model. A micromanometer was used to measure the venturi differential pressure.

A 1-inch (2.54-cm) diameter floating-disk local skin-friction balance, similar to those of reference 4, was mounted 20 inches (51 cm) from the leading edge of all configurations. The load range of the local skin-friction balance used was 0 to 0.029 pound (0 to 0.129 newton).

## PROCEDURE

All tests were conducted at a free-stream Mach number of 3 and a free-stream Reynolds number per foot of $9.75 \times 10^6$ ($31.95 \times 10^6$ per meter). The tunnel stagnation pressure was 65 pounds per square inch (44.8 newtons per square centimeter) absolute and the stagnation temperature was 110° F (43° C).

All tests were made with zero heat transfer to the plate surface. The total temperature of the injected air was 70° F (21° C) (that is, approximately equal to the flat-plate recovery temperature). The mass rate of flow of the injected air ranged from 0 to 0.075 pound per second (0 to 0.034 kilogram per second). The flow rate, in terms of the nondimensional mass-flow parameter $2F/C_{F,o}$ ranged from 0 to 0.85. The mass-flow rate was regulated by use of a valve located between the venturi and model.

The solid-surface model was first tested to determine the turbulent solid-plate local and average skin-friction coefficients. Boundary-layer pitot-pressure surveys were measured on the solid configuration at 3.0, 4.0, 6.0, 8.0, and 19.3 inches (7.6, 10.2, 15.2, 20.3, and 49.0 cm) from the leading edge.

Boundary-layer pitot-pressure surveys were made on all injection configurations at the 19.3-inch (49.0-cm) station for all injection rates. For the injection rate of 0.038 pound per second (0.017 kilogram per second), which corresponds to a $2F/C_{F,o}$ of 0.43 at the 19.3-inch (49-cm) station, surveys were also made at different stations along the model surface. For the porous configurations, these surveys were made at 11.2 and 14 inches (28.5 and 35.6 cm) from the plate leading edge. For the slot configurations, the locations varied somewhat, but, in general, surveys were made 0.1 inch (0.25 cm) ahead of the initial point of injection, at several stations within about 1 inch (2.54 cm) behind the final point of injection, and at 8 and 14 inches (28.5 and 35.6 cm) from the plate leading edge. A dimensional injection rate of 0.038 pound (0.017 kilogram) per second is used for identification for surveys other than at the 19.3-inch (49-cm) station inasmuch as the nondimensional parameter $2F/C_{F,o}$ is different at different stations for a constant injection mass flow due to the fact that $2F/C_{F,o}$ depends on the surface area ahead of the measuring station and the solid-plate average skin-friction coefficient at the measuring station.

The boundary-layer momentum thickness $\theta$ was calculated from the pitot pressure surveys by assuming that the static pressure and total temperature equal to the free-stream values were constant through the boundary layer. The assumption of a constant total temperature appears to be reasonable for the air-injection cases since only about 4 percent of the air in the boundary layer passing the survey probe is injected air for the highest mass-flow rate. In the cases of boundary-layer surveys taken close behind the slots with air injection, the $\theta$ value was calculated only where the static pressure measured on the surface was essentially equal to free stream so that the static pressure could be assumed to be constant through the boundary layer. In these cases, the Mach number measured by the pitot probe at the edge of the boundary layer was essentially equal to the free-stream Mach number.

All the local skin-friction data presented were obtained from the local skin-friction balance. The center of the skin-friction balance was located at the 20-inch (51-cm) station. The measurements of the skin-friction balance were taken after the boundary-layer surveys were completed and the probe moved downstream of the balance. The reference area used to reduce the force data of the balance to coefficient form was the area of the floating disk plus one-half

the area of the gap around the disk. This reference area was 0.7949 square inch (5.125 $cm^2$).

## RESULTS AND DISCUSSION

### Solid Plate

Boundary-layer measurements were made on a solid flat plate to provide a basis for comparison of the effectiveness in reducing skin friction of the various air-injection configurations. The static pressures measured along the solid plate were essentially constant as shown in figure 6. The boundary-layer velocity profiles measured at 3, 4, 6, 8, and 19.3 inches (7.6, 10.2, 15.2, 20.3, and 49.0 cm) from the leading edge of the solid-plate configuration are presented in figure 7. These profiles were found to correspond closely to a n power velocity profile of the form $\frac{u}{U_\infty} = \left(\frac{y}{\delta}\right)^{1/n}$ with $n$ equal to 6.8. With the use of the pitot-probe surveys and the assumption of a constant static pressure and total temperature through the boundary layer, the momentum thickness $\theta$ was calculated from the relation $\theta = \int_0^\delta \frac{\rho u}{\rho_\infty u_\infty}\left(1 - \frac{u}{U_\infty}\right)dy$. The integrand was plotted against the height above the surface $y$ and graphically integrated. The variation of $\theta$ with distance along the plate is shown in figure 8.

Since transition from laminar to turbulent flow was attained through the use of boundary-layer trips near the model leading edge, it was necessary to determine the virtual origin of the turbulent boundary layer. The momentum thicknesses presented in figure 8 were used with the method of reference 5 to determine the virtual origin, which was found to be located at the leading edge of the model. Therefore, the distance from the virtual origin and the distance from the leading edge of the model to the position of any measurement were equal. This distance was used as the reference length and, when multiplied by the span over which the air was injected (14 inches or 35.6 cm), gave the reference area for the air-injection cases.

The average skin-friction coefficient measured on the solid plate is shown in figure 9. The average skin-friction coefficients were determined from the relation $C_{F,o} = \frac{2\theta}{x_v}$ inasmuch as $\theta$ for the solid plate includes skin friction only and $x_v$ is the distance between the virtual origin and the measuring station. The average skin-friction coefficient $C_{F,o}$ at the 19.3-inch (49-cm) station is 0.00191. This value compares with the $C_{F,o}$ of 0.00174 measured in reference 1. The difference between the $C_{F,o}$ values found in the two tests is probably due to the somewhat greater leading-edge bluntness (0.0075-inch (0.0191-cm) radius compared with less than 0.0008 inch (0.0020 cm) in the present test) of the model in reference 1 which reduced the skin friction immediately behind the leading edge. This reduction in skin friction results from the

reduction in total pressure on the surface of a flat plate behind a blunt leading edge (ref. 6). Also, the bluntness of the model used in reference 1 caused the virtual origin to be ahead of the leading edge and thus the effective Reynolds number of the boundary layer is increased and a lower skin-friction coefficient results.

The local skin-friction coefficients presented in figure 9 were obtained from the variation of $\theta$ with $x$ (fig. 8) with the relation $C_{f,o} = 2\frac{d\theta}{dx}$. Also shown is the local skin-friction coefficient as obtained with the local skin-friction balance located at the 20-inch (51-cm) station. The value obtained with the skin-friction balance was $1.44 \times 10^{-3}$; this value compares very closely with $1.47 \times 10^{-3}$ found from the variation of $\theta$ with $x$ at the 19.3-inch (49-cm) station (the location of the boundary-layer survey). This value also can be compared with the local skin-friction coefficient of $1.39 \times 10^{-3}$ obtained with a skin-friction balance in reference 1. The small difference is again probably due to the greater bluntness of the leading edge on the model used in reference 1 causing an increase in the effective Reynolds number of the boundary layer which results in a lower skin-friction coefficient.

## Air Injection

The experimental data were reduced in such a manner as to permit the determination of the effect of air injection on local and average turbulent skin-friction coefficients. In order to obtain the average turbulent skin-friction coefficient, the experimentally measured momentum thickness must be separated into contributing components. Not only does the momentum thickness $\theta$ include momentum losses due to skin-friction drag, but also any other drag inputs which take place ahead of the survey station. The following sketch, which also appeared in reference 1, illustrates the components involved and the manner in which the desired average skin-friction coefficients were obtained from the measurements of $\theta$.

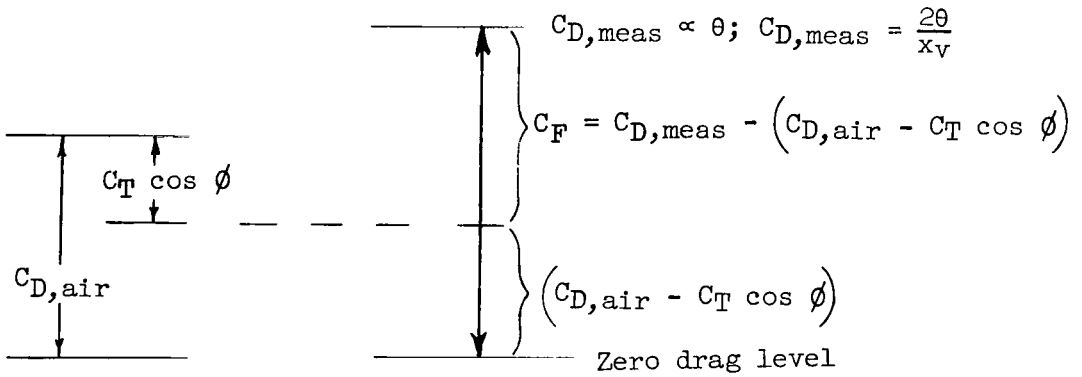


From the measured momentum thickness $\theta$, a drag coefficient $C_{D,meas}$ was obtained. For air injection normal to the plate surface, as in the case of the

distributed injection or multiple vertical slots, this drag coefficient includes not only the plate skin friction but also the complete momentum defect from free-stream conditions of the injected air, represented as $C_{D,air}$. For injection through rearward-inclined slots, some of the momentum loss is recovered and is defined in terms of a thrust coefficient $C_T$. This thrust coefficient, which includes both pressure and momentum components of thrust, was calculated by using the measured mass flow and chamber total pressure and temperature. From these measured values, the slot Mach number and slot pressure were obtained. By using these conditions, the thrust in the stream direction $C_T \cos \phi$ was calculated. For the slot tests, the momentum defect in the injected air is then $C_{D,air} - C_T \cos \phi$. This momentum defect will show up in the boundary layer at the survey station and therefore must be subtracted from $C_{D,meas}$ in order to obtain the average skin-friction coefficient, that is, $C_F = C_{D,meas} - \left(C_{D,air} - C_T \cos \phi\right)$.

Distributed injection.- Three different porous-surface configurations were investigated - 4, 5.33, and 8 inches (10.2, 13.5, and 20.3 cm) in streamwise extent. Results obtained from these configurations and from the configuration tested in the preliminary investigation (16 inches (40.6 cm) in streamwise extent) are shown in figures 10, 11, and 12. The ratios of the average and local skin-friction coefficient measured near the rear of the model with injection to the values measured on the solid plate without injection, $C_F/C_{F,o}$ and $C_f/C_{f,o}$, are plotted against the mass-flow parameter $2F/C_{F,o}$. With no injection the average skin-friction-coefficient ratios for the three smaller porous areas were 1.095. This value is believed to be due to a mismatch of the porous area with the solid surface of the model which caused small steps in the surface of the model. It was not due to the inherent distributed roughness of the porous surface because the piece of porous material used in this test was the same as that used in the previous investigation for which almost no increase was observed.

Some idea of the relative effectiveness of the various porous configurations can be obtained from the composite plot of all the configurations shown in figure 11. This figure shows that for the three partial-chord porous configurations, there is a rapid reduction of drag at first until a value of $2F/C_{F,o}$ of about 0.2 is reached and then the drag curve is parallel to the full-chord porous curve but slightly above it. It is believed that the first rapid reduction is primarily a reduction in the roughness drag of the partial-chord porous models as the low-energy injection air blankets and fills in the small steps or mismatches of the partial-chord porous model. The reduction that takes place at values of $2F/C_{F,o}$ greater than 0.2 would then be a reduction in skin friction due to the partial-chord porous injection. If this hypothesis is true, partial-chord porous injection appears to be about as effective as full-chord porous injection. Partial-chord porous injection may be preferred over full-chord porous injection because of the simplification that partial-chord porous injection offers in practical construction.

The average skin-friction-coefficient ratio at various stations behind the three porous configurations for a constant mass-flow rate of 0.038 pound (0.017 kilogram) per second (corresponding to a $2F/C_{F,o} = 0.43$ at the 19.3-inch (49-cm) station) are shown in figure 13 and the velocity profiles are shown in figures 14 and 15. As expected, all the porous configurations produced a greater reduction in skin friction at the 11.2-inch (28.4-cm) station than at stations farther downstream. The reason for this effect can be seen from the nondimensional velocity profiles shown in figure 15. The skin friction at the 11.2-inch (28.4-cm) station was reduced not only by thickening the boundary layer, but also by a favorable distortion of the boundary layer at points ahead of this station (both effects causing a lower velocity gradient at the surface). As the flow progresses downstream from the point of injection, the boundary layer tends toward the solid-plate profile where the reduction in skin friction that occurs is due only to the greater thickness of the injection boundary layer. Thus, there is a greater reduction in skin friction near the injection area and a lesser reduction downstream. It is of interest to note that at the 19.3-inch (49-cm) station, the velocities in the lower part of the nondimensional boundary-layer profile actually become higher than those in the solid-flat-plate nondimensional profile.

Multiple normal slots.- Since a large area of porous surface would be difficult to build and maintain on practical aircraft, alternate injection configurations using multiple normal slots to simulate distributed injection were also investigated. Both a three-slot configuration covering 1.63 inches (4.14 cm) and a six-slot configuration covering 4 inches or 10.2 centimeters (the same area as the smallest partial-chord porous configuration) were used. The static pressures measured along the surface of these configurations are presented in figure 16 for a mass-flow rate of 0.038 pound (0.017 kilogram) per second. Except in regions close behind the air injection slots, the static pressure is essentially constant and equal to the solid-flat-plate values shown in figure 6.

It was hoped that the six-slot configuration would be directly comparable to the 4-inch (10.2-cm) porous configuration. However, as shown in figure 17, there was a large increase in drag at zero-injection mass flow. This increase is probably due to the warping of the six-slot configuration which caused discontinuities or steps in the surface at the slot locations. There is some question as to whether the initial skin-friction reductions obtained with air injection are reductions in skin friction or reductions in the drag of the surface discontinuities caused by the warped model. In any case, it is evident that the six-normal-slot configuration did not reduce the skin friction as much as the porous configurations since the $C_F/C_{F,o}$ value decreased only from 1.1 to 1.0 and actually seems to be increasing at the higher mass flows. Paradoxically, however, the three-slot configuration, in which the three slots are concentrated in a smaller area nearer the leading edge of the model than either the six-slot configuration or any of the distributed injection configurations (ideally comparable to many slots), gave as much reduction in average skin friction as was obtained from the 16-inch (41-cm) porous surface configuration (15 percent at a $2F/C_{F,o}$ of 0.7). The local skin-friction reduction as measured by the skin-friction balance at the 20.0-inch (51-cm) station was approximately the same for the two multiple-slot configurations

(fig. 18). Evidently, the high average skin friction which occurred on the six-slot configuration was caused by a region of high local skin friction somewhere ahead of the skin-friction balance. This condition is also shown in figure 19 where the average skin friction at various distances along the plate is given at an injection mass flow of 0.038 pound (0.017 kilogram) per second. The fact that the skin friction on the six-slot configuration increases rapidly between 8 and 14 inches (20.3 and 35.6 cm) indicates that the local skin friction is high. Behind the 14-inch (20.3-cm) station, the average skin friction remains approximately constant and somewhat below the flat-plate values and indicates that the local skin friction is slightly lower than that on the solid plate. This result agrees with the indications of the skin-friction balance at the 20.0-inch (51-cm) station shown in figure 18(b).

The velocity ratio $u/U_\infty$ through the boundary layer at various stations behind the multiple normal-slot configurations at an injection mass flow of approximately 0.038 pound (0.017 kilogram) per second (corresponding to a $2F/C_{F,o}$ of 0.43 at the 19.3-inch (49-cm) station) are plotted against the dimensional height $y$ in figure 20 and against the nondimensional height $y/\delta$ in figure 21. The velocity ratio $u/U_\infty$ does not reach 1.0 at a $y/\delta$ of 1.0 in figure 21 for the stations close behind the injection slots because there was a shock wave from the injection air which created an entropy layer for a short distance above the plate. This entropy layer was absorbed into the boundary layer at distances further downstream from the last slot where the boundary-layer thickness $\delta$ was greater. A comparison between the nondimensional velocity profiles behind the six-slot and three-slot configurations in figures 21(a) and 21(b) shows the reason that the three-slot configuration was so effective. It is seen that there was a greater favorable distortion of the profile behind the three-slot configuration. This greater distortion was undoubtedly due to the greater velocity at which the air is injected through the three-slot configuration for the same mass flow. It is to be noted that the profiles for both multiple-slot configurations distort beyond the flat-plate profile at the 19.3-inch (49-cm) station in a manner similar to the profiles for the partial-chord porous injection.

It appears, then, that the same skin-friction reduction can be obtained from the three-normal-slot configuration as was obtained from the full-chord (16-inch or 40.6-cm) porous-injection configuration. However, both the normal-slot and porous configurations are wasteful of the thrust that might be obtained from the injection air and, therefore, these configurations should only be considered for use with very low-energy air. Also, the results obtained from the multiple normal-slot configurations in this investigation indicate that great care must be taken in the construction of the slots to prevent warping which can increase the drag at zero-injection mass flow.

Rearward-inclined flush slots.- An investigation of the effectiveness of rearward-inclined slots was made in order to see whether some of the thrust available in the injection air could be recovered. In the previous investigation (ref. 1), the narrowest flush slot tested (0.018-inch (0.046-cm) wide) proved to be the most effective slot in reducing drag. Therefore, a still narrower flush slot (0.0085-inch (0.0216-cm) wide) and the original 0.018-inch (0.046-cm) flush slot were tested in the present investigation.

The static-pressure distributions along the surface of these configurations are shown in figure 22 for the 0.038 pound (0.017 kilogram) per second mass-flow rate. As in the case of the multiple normal-slot configuration, the static pressures are essentially equal to the solid-flat-plate values shown in figure 6 except in the region close behind the slot.

The variation of average and local skin-friction coefficient ratios with mass-injection rate are shown in figures 23 and 24 for the two slots. The 0.018-inch (0.046-cm) flush slot from reference 1 was the more effective slot and produced a decrease in average skin friction of almost 15 percent as opposed to a decrease of approximately 10 percent for the 0.0085-inch (0.0216-cm) flush slot. Furthermore, this skin-friction reduction occurred at a lower flow rate with the 0.018-inch (0.046-cm) slot than the flow rate necessary to give the approximately 10-percent reduction with the 0.0085-inch (0.0216-cm) slot. However, if the downward trend of the 0.0085-inch (0.016-cm) slot would continue to higher mass-flow rates, a greater decrease in skin friction might be obtained at very high flow rates. The local skin-friction coefficients presented in figure 24 were measured by the local balance and show that the 0.0085-inch (0.016-cm) flush slot produces a greater skin-friction reduction at the 20.0-inch (51-cm) station for the higher mass flow rates. These trends indicate that the skin-friction reduction takes place near the 0.018-inch (0.046-cm) slot and further downstream of the 0.0085-inch (0.0216-cm) slot.

This is shown in figure 25 where the average skin-friction coefficients along the surface of the flush-slot configurations are shown for a mass-flow rate of 0.038 pound (0.017 kilogram) per second. It is seen that the skin friction slowly decreases with distance from the leading edge for the 0.0085-inch (0.0216-cm) slot, whereas for the 0.018-inch (0.046-cm) slot, average skin friction increases with distance from the leading edge. Thus, it is obvious that most of the skin-friction reduction occurs near the point of injection for the 0.018-inch (0.046-cm) slot whereas the skin-friction reduction is largest at the back of the plate for the 0.0085-inch (0.0216-cm) slot. When the velocity profiles of the two configurations (figs. 26 and 27) are compared, it can be seen that the velocities near the surface are lower for the 0.018-inch (0.046-cm) slot from just behind the slot to the 8-inch (20.3-cm) station. These lower velocities indicate a lower skin friction as was obtained for the 0.018-inch (0.046-cm) slot to the 8-inch (20.3-cm) station. The velocity profiles from the 8-inch (20.3-cm) station to the 19.3-inch (49-cm) station show that the velocities near the surface (primarily from the velocities indicated by the pitot tube on the surface) for the 0.018-inch (0.046-cm) slot are greater. The reduction in skin friction closer to the point of injection for the 0.018-inch (0.046-cm) slot, however, is large enough to produce a lower average skin friction at the 19.3-inch (49-cm) station (fig. 25).

The nondimensional profiles in figure 28 show that there is a more favorable distortion just behind the 0.018-inch (0.046-cm) slot than there is behind the 0.0085-inch (0.0216-cm) slot; this condition also indicates the reason that the 0.018-inch (0.046-cm) slot is more effective. (For clarity, only those profiles sufficient to show the trend are presented.) Again, it is to be noted that the nondimensional profiles are distorted beyond the flat-plate profile at

the 19.3-inch (49-cm) station, in a manner similar to the profiles for both the multiple-normal-slot and the partial-chord porous injection.

These results suggest that greater skin-friction reduction might be attained by using several rearward-facing flush slots at various chordwise positions. If they were used, the large skin-friction reduction immediately downstream of each slot should combine to give a large overall reduction in skin friction. For example, if an additional 0.018-inch (0.046-cm) rearward-facing flush slot were located midway between the original slot position at 3 inches (7.62 cm) from the leading edge and the downstream measuring station at 19.3 inches (49 cm) from the leading edge (at the 11.2-inch (28.4-cm) station) and 0.038 pound (0.017 kilogram) per second of air were injected through each of them, the skin-friction reduction which might be expected could be calculated from the results presented in figure 25. It can be calculated from this figure and the $C_{F,o}$ presented in figure 9 that the actual skin-friction drag to the 11.2-inch (28.4-cm) station would be 0.535 of the total solid-plate skin-friction drag back to the 19.3-inch (49-cm) station. In order to estimate the skin-friction drag behind the second slot, a reasonable, although unverified, assumption was made that the skin-friction drag over the surface behind this slot is reduced by the same percentage as it was reduced over the surface behind the slot at 3 inches (7.62 cm). With this assumption, then, the skin-friction drag from the 11.2-inch (28.4-cm) station to the 19.3-inch (49-cm) station would be 0.272 of the total solid-plate skin-friction drag. If these values of skin-friction ratio are combined, a two-slot configuration would give a skin-friction ratio of 0.807 at $2F/C_{F,o}$ of 0.86, a value comparable to that obtained with full-chord porous injection shown in figure 10. Such a configuration would have the additional advantages over full-chord porous injection of providing a thrust recovery from the injection air and having simpler construction and maintenance. Further wind-tunnel tests, however, would be necessary to verify these calculated skin-friction reductions for multiple rearward-inclined flush slots inasmuch as the skin-friction reductions are greatly dependent on the exact mixing process between the injection air and the boundary-layer air.

Rearward-inclined step slots.- The static pressure distribution for the rearward-inclined step slot configuration at an injection mass-flow rate of 0.038 pound (0.017 kilogram) per second is plotted in figure 29. Once again, the static pressure is essentially equal to the solid-flat-plate values, except in regions close behind the slot.

The average skin-friction coefficients at the 19.3-inch (49-cm) station for the two step-slot configurations, as a fraction of the solid-plate coefficients, are presented in figure 30. With no air injection through the slots, the average skin-friction coefficients were approximately 95 percent and 85 percent of that on the solid plate for the 0.015-inch (0.0381-cm) and 0.068-inch (0.173-cm) step slots, respectively. This skin-friction reduction was probably due to the separation of the flow over some length downstream of the rearward-facing step. However, this skin-friction reduction does not mean that the overall drag of the model was reduced by this amount, since there was an additional base-pressure drag on the back of the step slots. This base-pressure drag can be determined from the measurement of the model plenum chamber pressure

with no-injection mass flow. For the 0.065-inch (0.165-cm) step, the base-pressure drag was 0.21 of the flat-plate drag and, therefore, the total drag of this configuration was 1.06 of the flat-plate drag.

Injecting air through the 0.015-inch (0.0381-cm) slot increased the skin friction at first until the ratio $C_F/C_{F,o}$ reached approximately 0.98 at a value of $2F/C_{F,o}$ of 0.42. Further increases in mass flow reduced the skin friction until $C_F/C_{F,o}$ was only about 0.9 at the highest mass flow tested. The skin friction behind the larger 0.068-inch (0.173-cm) slot, however, increased over the entire range of mass flow tested, until at the highest mass flow there was almost no reduction in average skin friction. It seems reasonable to expect that even higher mass flows might result in skin-friction reductions if the same phenomenon observed with the 0.015-inch (0.0381-cm) slot occurred on the 0.068-inch (0.173-cm) slot configuration. Further tests would be required, however, to determine whether any similarity exists between the two configurations.

The local skin-friction coefficients for the step-slot configurations measured at the 20-inch (51-cm) station are presented in figure 31. This figure shows that the local skin friction was reduced by injection of air through the 0.015-inch (0.0381-cm) step slot, but that the local skin friction was increased by air injection through the 0.068-inch (0.173-cm) step slot for all values of the mass-flow parameter $2F/C_{F,o}$ used in this investigation.

The velocity profiles at various stations behind the two step-slot configurations at a mass-flow rate of 0.038 pound (0.017 kilogram) per second (corresponding to a $2F/C_{F,o}$ of 0.43 at the 19.3-inch (49-cm) station) are presented as dimensional profiles in figure 32 and as nondimensional profiles in figure 33. (Again for the sake of clarity, only those nondimensional profiles sufficient to show the trend are presented.) The velocity profiles close behind the step slots have a favorable distortion and a low velocity gradient at the surface which give low local skin frictions especially for the 0.068-inch (0.173-cm) slot. At the 19.3-inch (49-cm) station, however, it is seen that the 0.015-inch (0.0381-cm) slot profile has returned to the solid flat-plate profile, whereas the 0.068-inch (0.173-cm) slot profile is adversely distorted at the 19.3-inch (49-cm) station. Evidently, the mixing process caused the velocity profile behind the 0.068-inch (0.173-cm) step slot to change from a favorable distortion just behind the injection point to an unfavorable distortion at the 19.3-inch (49-cm) station, as it did for the multiple-normal-slot and rearward-inclined-flush-slot configurations. (See figs. 21 and 28.) This adverse distortion evidently caused the high local skin friction shown in figure 31 for the 0.068-inch (0.173-cm) step slot. It is apparent that the local skin friction at any given station along the model surface depends not only on the thickening of the boundary layer by the injection air but also on the amount of distortion of the boundary-layer profile.

The average skin friction at various stations behind the two step slots at a mass flow rate of 0.038 pound (0.017 kilogram) per second is shown in figure 34. The skin friction behind the 0.068-inch (0.173-cm) slot was lower than that for the 0.015-inch (0.0381-cm) slot at all stations for this mass flow.

Also, the skin friction was lower for both slots at the forward stations near the injection point. This low skin friction is due to the low velocity gradients at the surface in the separated regions behind the step slots.

Other considerations.- Although distributed injection produced the greatest decrease in skin friction, this fact does not necessarily mean that distributed injection has the greatest overall effectiveness. When distributed injection is used, the momentum or thrust of the air used for injection is lost. When the air is injected through rearward-inclined slots, however, most of the momentum of the air is recovered and a greater overall effectiveness might be obtained. An example of such a situation is shown in figure 35. The model drag coefficient $C_{D,m}$ is plotted against the mass-flow parameter $2F/C_{F,o}$. The lower curve presents the variation of $C_{D,m}$ with rate of air injection through the 0.018-inch (0.046-cm) rearward-facing inclined flush slot. This drag coefficient includes the reduction in skin friction as well as the momentum recovered from the injected air. The curve labeled $C_{F,o} - C_T$ indicates the reduction in $C_{D,m}$ that could be obtained if all the energy of the injection air used in the 0.018-inch (0.046-cm) rearward-facing slot were recovered as thrust in a sonic nozzle. It must be realized, however, that for the normal method used on aircraft, only about 70 percent of the thrust available from auxiliary air is recovered because of interaction of the air exhausting through the sonic nozzle with the passing free-stream air. (See ref. 7.) Therefore, the curve shown for the sonic nozzle is an idealistic one and would not be attained in practice.

The difference between the sonic nozzle curve and the lower curve indicates that a reduction in skin friction took place in the case of slot injection. The upper curve shows that distributed injection gives the least reduction in drag coefficient. This reduction is only a reduction in skin friction since there is no recovery of momentum from the injected air. As can be seen, the greatest overall effectiveness was obtained with the inclined flush slot. Also, since the reductions in drag coefficient shown by the sonic-nozzle curve probably would not be obtained in practice, the reductions obtainable from slot injection may be even more significant. These curves clearly indicate that only if very low energy air were available for injection would distributed injection be considered for reducing turbulent skin-friction drag. In this case, of course, the porous surface must be able to pass the required injection mass flow with a very low pressure drop.

Another advantage of using air injection into the boundary layer is a possible reduction of the drag of granular- and step-type surface roughness. Goddard (ref. 8) showed that drag due to the granular type of roughness is proportional to the dynamic pressure at the top of the roughness. Since air injection reduces skin friction by reducing the velocity gradient at the wall (through boundary-layer thickening, distortion, or both), it would also reduce the velocity at the top of surface roughness. Also, the results obtained in this test with the partial-chord porous-surface configurations suggest that the injection air reduced the drag due to the step-type surface roughness resulting from the mismatch of the porous surface and the solid plate. Drag due to waviness of the surface, however, probably could not be greatly reduced by air

injection, as indicated by the results of reference 8 which showed that most of the drag due to waviness is pressure or wave drag that occurs outside the boundary layer. Reference 9 indicated that a thick boundary layer did not insulate the outside flow from variations in surface shape due to waviness as much as might be expected. Therefore, an increase of the boundary-layer thickness by injection could not be expected to reduce appreciably the drag of wavy-type surfaces.

Application of the slot air-injection results obtained in the wind tunnel to flight conditions requires some explanation. From similarity considerations, it is apparent that the ratio of the slot width to the boundary-layer height $w/\delta$ is the important parameter that should be duplicated in flight. When $w/\delta$ is the same, it can be shown that the other parameters that are important to the interaction between the injection air and the boundary-layer air, such as the pressure and velocity ratios between the injection and the external airstreams, are duplicated when the mass-flow parameter $2F/C_{F,o}$ is duplicated. Under these conditions, then, it is reasonable to expect that the same skin-friction reductions can be obtained in flight as were obtained in the wind tunnel.

For example, the value of $w/\delta$ for the 0.018-inch (0.046-cm) rearward-facing inclined flush slot was 0.18 $\left(\frac{w}{\delta} = \frac{0.018 \text{ inch}}{0.10 \text{ inch}} \text{ or } \frac{0.046 \text{ cm}}{0.254 \text{ cm}}\right)$. If it were desired to duplicate air injection through a slot located the same relative distance from the leading edge of an aircraft flying at $M = 3$ and at a Reynolds number per foot of $0.975 \times 10^6$ or $3.20 \times 10^6$ per meter (one-tenth of the value of the wind-tunnel tests), the slot should be ten times as wide (0.18 inch (0.46 cm) wide), because the boundary-layer thickness would be ten times as thick at the injection position. With such a slot, the skin-friction reduction should be the same as that obtained on the wind-tunnel model back to the plate-length Reynolds number of the wind-tunnel test $\left(R_x = 15.7 \times 10^6\right)$. Thus, a 193-inch (490-cm) length on the airplane would correspond to the 19.3-inch (49-cm) length on the wind-tunnel model. At Reynolds numbers on the airplane greater than $15.7 \times 10^6$, the effect of the air injection on the skin friction is not quantitatively known. The thicker boundary layer resulting from the air injection, however, should reduce the values of local skin friction at all Reynolds numbers larger than $15.7 \times 10^6$. This reduction should occur because the adverse distortion that was noted at the 19.3-inch (49-cm) station on the model with the 0.018-inch (0.046-cm) wide slot was not severe enough to overcome the favorable effect of the boundary-layer thickening (evidenced by the always lower local skin friction due to injection at the 20-inch (51-cm) station).

## SUMMARY OF RESULTS

An investigation of the effect of air injection on local and average flat-plate turbulent skin friction has been conducted at a Mach number of 3 and at a

Reynolds number per foot of $9.75 \times 10^6$ ($32 \times 10^6$ per meter). The following results were obtained:

1. Partial-chord porous injection appeared to be about as effective as the full-chord porous injection in decreasing average skin friction. The decrease obtainable with full-chord porous injection was approximately 20 percent at a mass-flow parameter $\left(2F/C_{F,o}\right)$ of 0.8.

2. The reduction in average skin friction produced by the three-normal-slot configuration was almost equal to that produced by the 16-inch (41-cm) porous surface (full-chord porous) and indicated that distributed injection can be simulated by using vertical slots.

3. The 0.018-inch (0.046-cm) rearward-inclined flush slot was the most effective rearward-inclined slot investigated; it produced an almost 15-percent decrease in average skin friction at a mass-flow parameter of 0.5.

4. The 0.015-inch (0.038-cm) rearward-inclined step slot was the most effective step slot tested but it was not as effective as the flush slots in reducing average skin friction. The maximum reduction in average skin friction for the 0.015-inch (0.038-cm) rearward-inclined step slot was 10 percent at a mass-flow parameter of 0.85.

5. The effectiveness of all the slot configurations depended greatly on the distortion of the velocity profile behind the injection slot and upon the mixing of the injected stream with the boundary layer. Injection of air through all the configurations caused an increase in the boundary-layer thickness which tended to reduce the skin friction, but in many cases an adverse distortion of the boundary layer lessened the favorable effect of a thick boundary layer and tended to cause an increase in skin friction.

6. Possible recovery of part of the momentum of the injected air must be considered in evaluation of overall effectiveness of air injection in reducing drag. Although distributed injection proved to be more effective than the rearward-inclined flush slots in reducing average skin friction, recovery of most of the thrust available from the injection air by using rearward-inclined slots can make such slots more effective in overall drag reduction.

7. The boundary-layer velocity profiles at various stations behind the injection position (for an injection mass flow of 0.038 pound (0.017 kilogram) per second) showed that the greatest average skin-friction reductions occurred close behind the injection point, except in one case (the 0.0085-inch (0.0216-cm) rearward-inclined flush slot). These results indicate that the use of more than one slot spaced along the surface may offer the possibility of greater skin-friction reductions than injection in the forward region only. Further experimentation is required to validate this hypothesis, however, because the skin-friction reduction is greatly dependent on the exact mixing process of the injection air with the boundary-layer air.

Langley Research Center,
National Aeronautics and Space Administration,
Langley Station, Hampton, Va., November 3, 1965.

## REFERENCES


1. McRee, Donald I.; Peterson, John B., Jr.; and Braslow, Albert L.: Effect of Air Injection Through a Porous Surface and Through Slots on Turbulent Skin Friction at Mach 3. NASA TN D-2427, 1964.

2. Mechtly, E. A.: The International System of Units - Physical Constants and Conversion Factors. NASA SP-7012, 1964.

3. Braslow, Albert L.; and Knox, Eugene C.: Simplified Method for Determination of Critical Height of Distributed Roughness Particles for Boundary-Layer Transition at Mach Numbers From 0 to 5. NACA TN 4363, 1958.

4. Shutts, W. H.; Hartwig, W. H.; and Weiler, J. E.: Final Report on Turbulent Boundary-Layer and Skin-Friction Measurements on a Smooth, Thermally Insulated Flat Plate at Supersonic Speeds. DRL-364, CM-823 (Contract NOrd-9195), Univ. of Texas, Jan. 5, 1955.

5. Rubesin, Morris W.; Maydew, Randall C.; and Varga, Steven A.: An Analytical and Experimental Investigation of the Skin Friction of the Turbulent Boundary Layer on a Flat Plate at Supersonic Speeds. NACA TN 2305, 1951.

6. Bertram, Mitchel H.: Calculations of Compressible Average Turbulent Skin Friction. NASA TR R-123, 1962.

7. Vick, Allen R.: An Investigation To Determine the Discharge and Thrust Characteristics of Auxiliary-Air Outlets for a Stream Mach Number of 3.25. NASA TN D-1478, 1962.

8. Goddard, Frank E., Jr.: Effect of Uniformly Distributed Roughness on Turbulent Skin-Friction Drag at Supersonic Speeds. Rep. No. 20-113 (Contract No. DA-04-495-Ord 18), Jet Propulsion Lab., C.I.T., Sept. 3, 1957.

9. Czarnecki, K. R.; and Monta, William J.: Pressure Distributions and Wave Drag Due to Two-Dimensional Fabrication-Type Surface Roughness on an Ogive Cylinder at Mach Numbers of 1.61 and 2.01. NASA TN D-835, 1961.

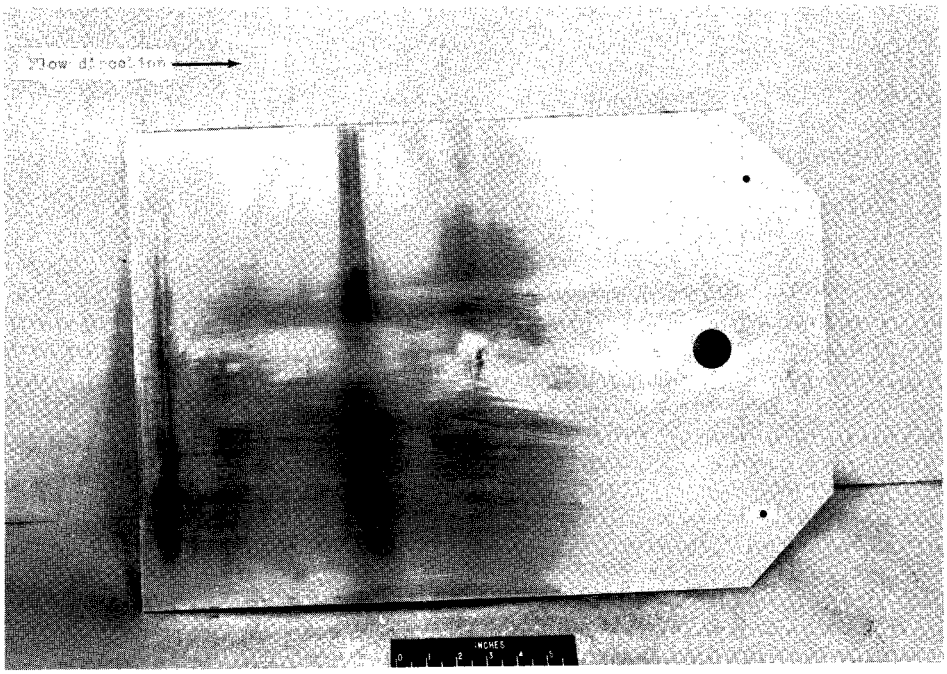


(a) Solid-plate configuration.

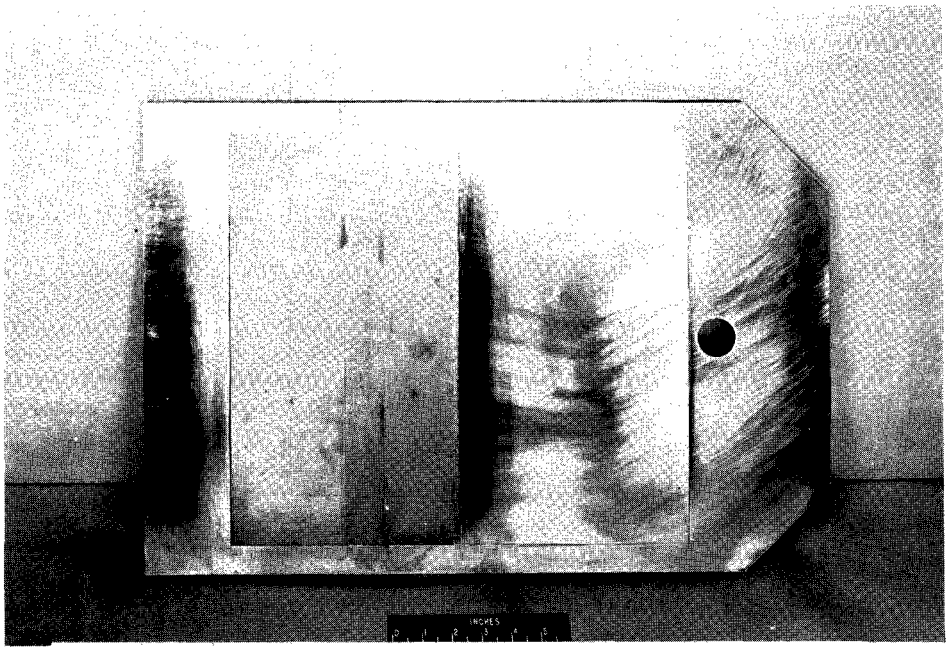


(b) Partial-chord porous-surface configuration.

Figure 1.- Photographs of configurations tested. L-65-9006

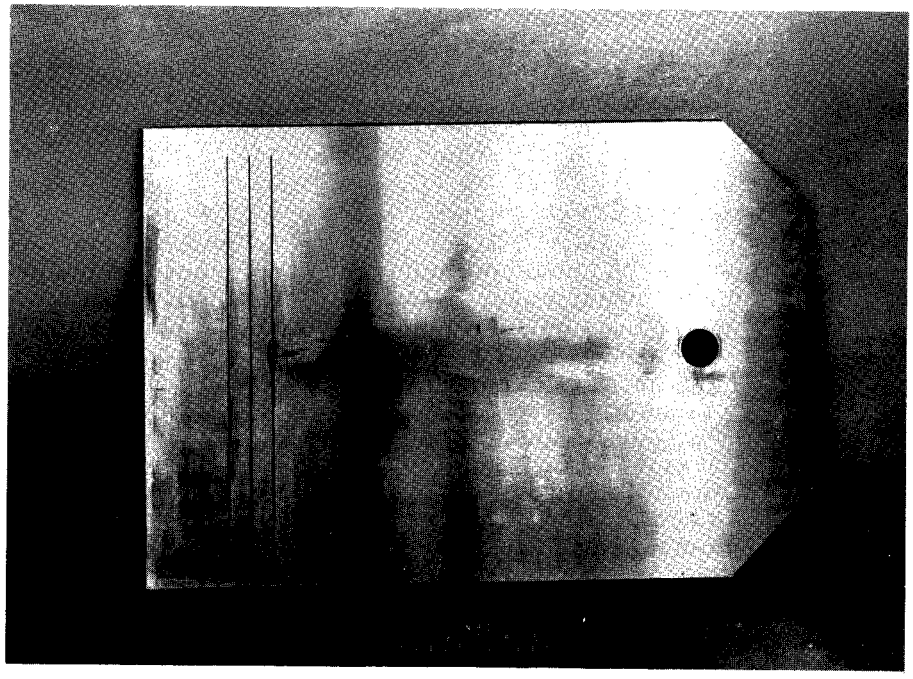

(c) Three-normal-slot configuration.

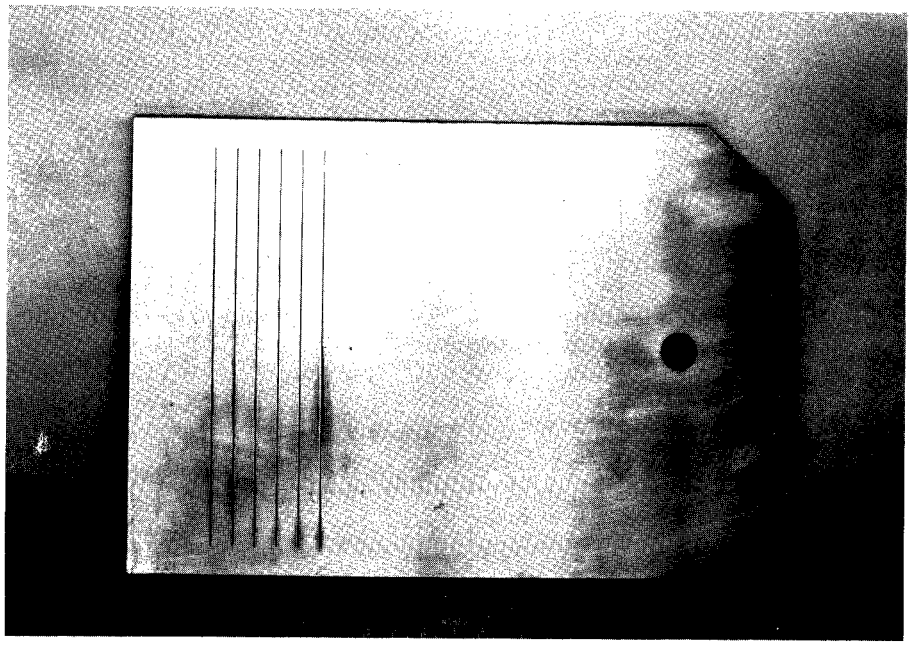

(d) Six-normal-slot configuration.

Figure 1.- Continued. L-65-9007

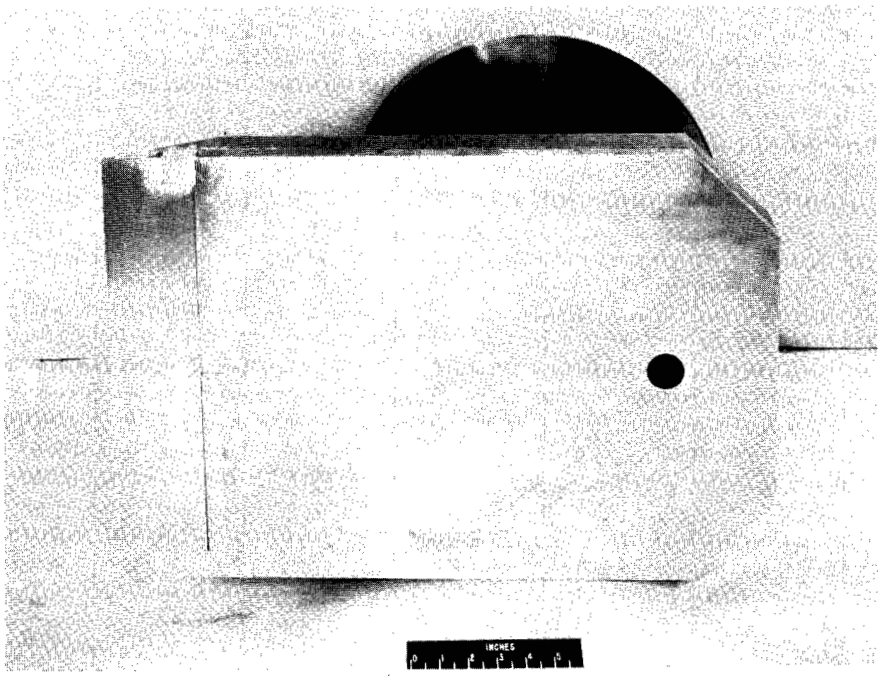


(e) Single rearward-inclined flush-slot configuration.

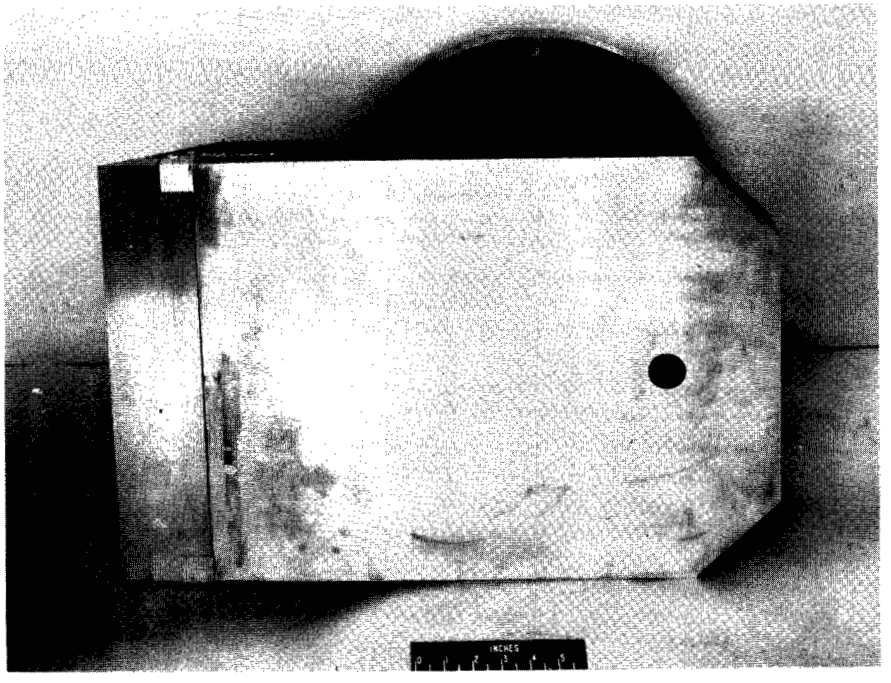


(f) Single rearward-inclined step-slot configuration.

Figure 1.- Concluded. L-65-9008

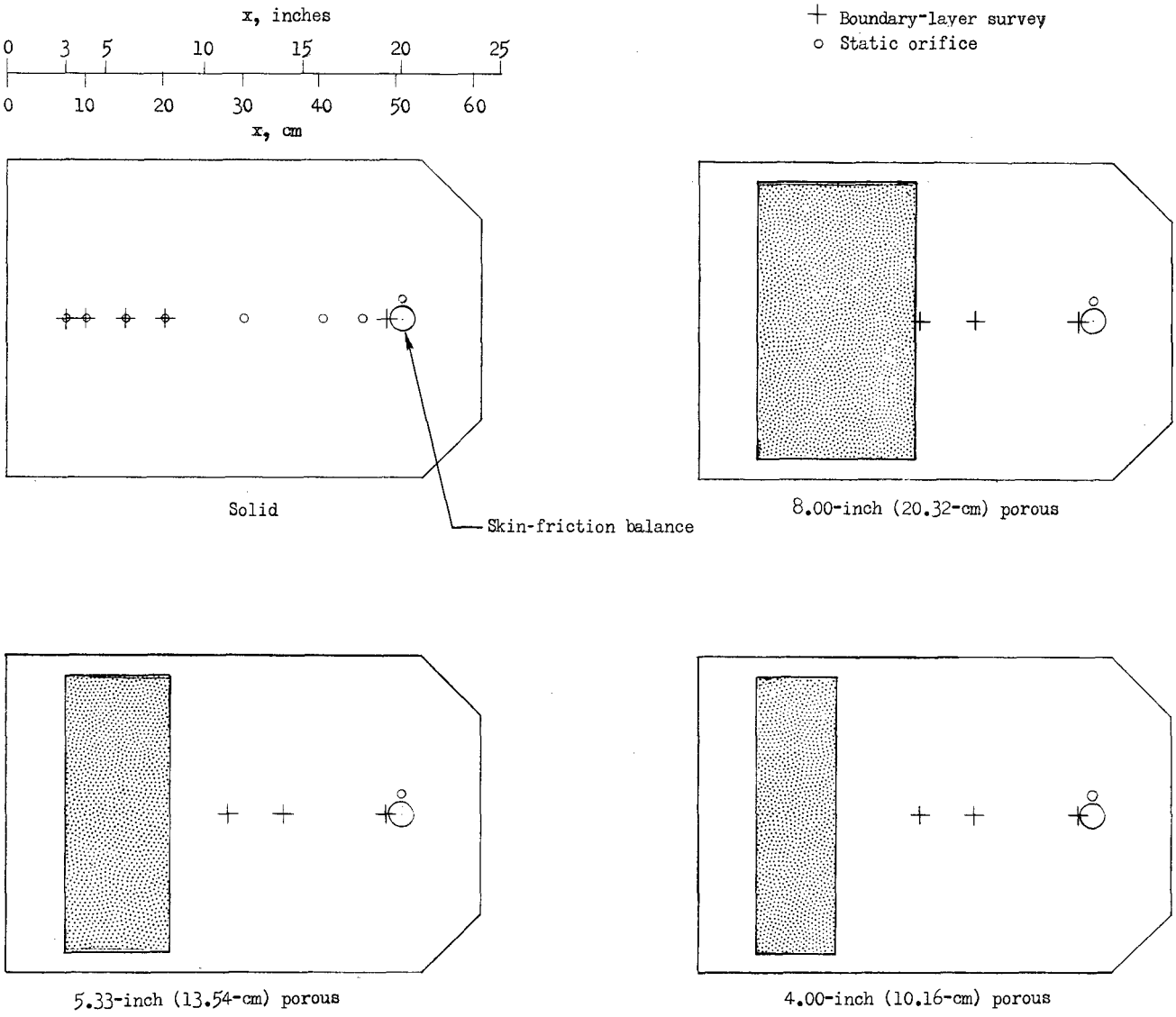


(a) Solid- and porous-surface configurations.

Figure 2.- Sketch of configurations showing location of boundary-layer surveys and static orifices.

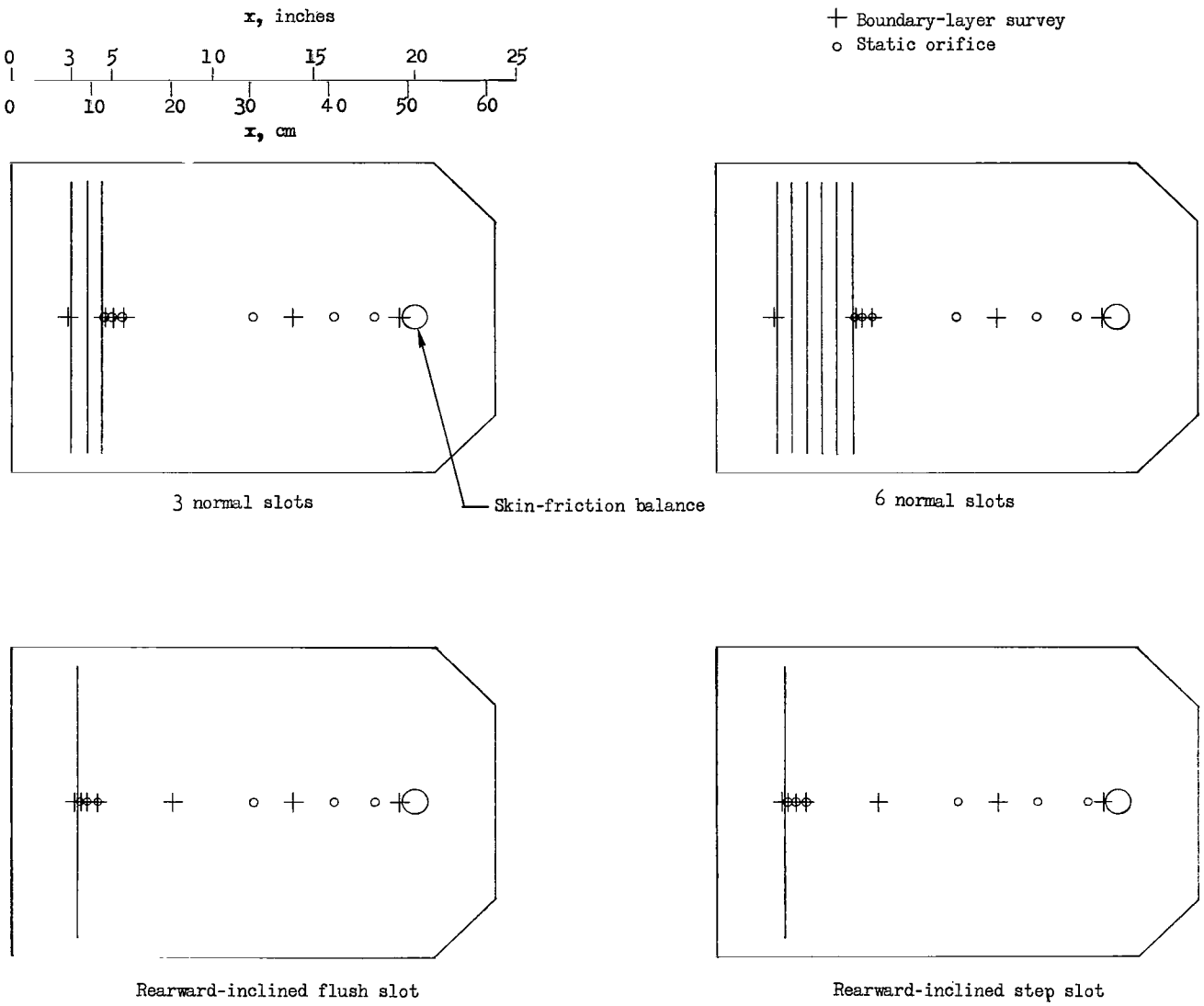


(b) Slotted-surface configurations.

Figure 2.- Concluded.

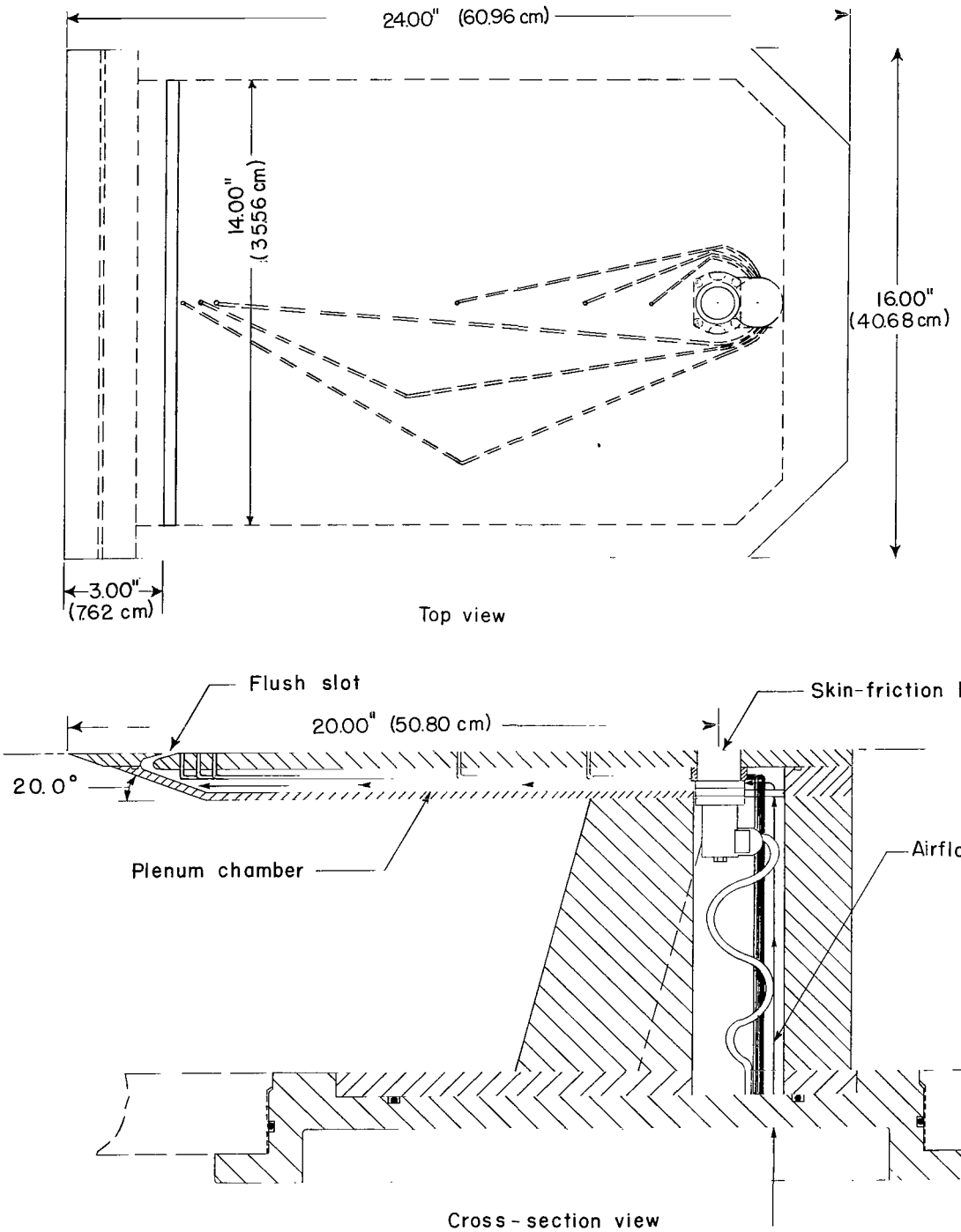


Figure 3.- Sketch of flush-slot air-injection model.

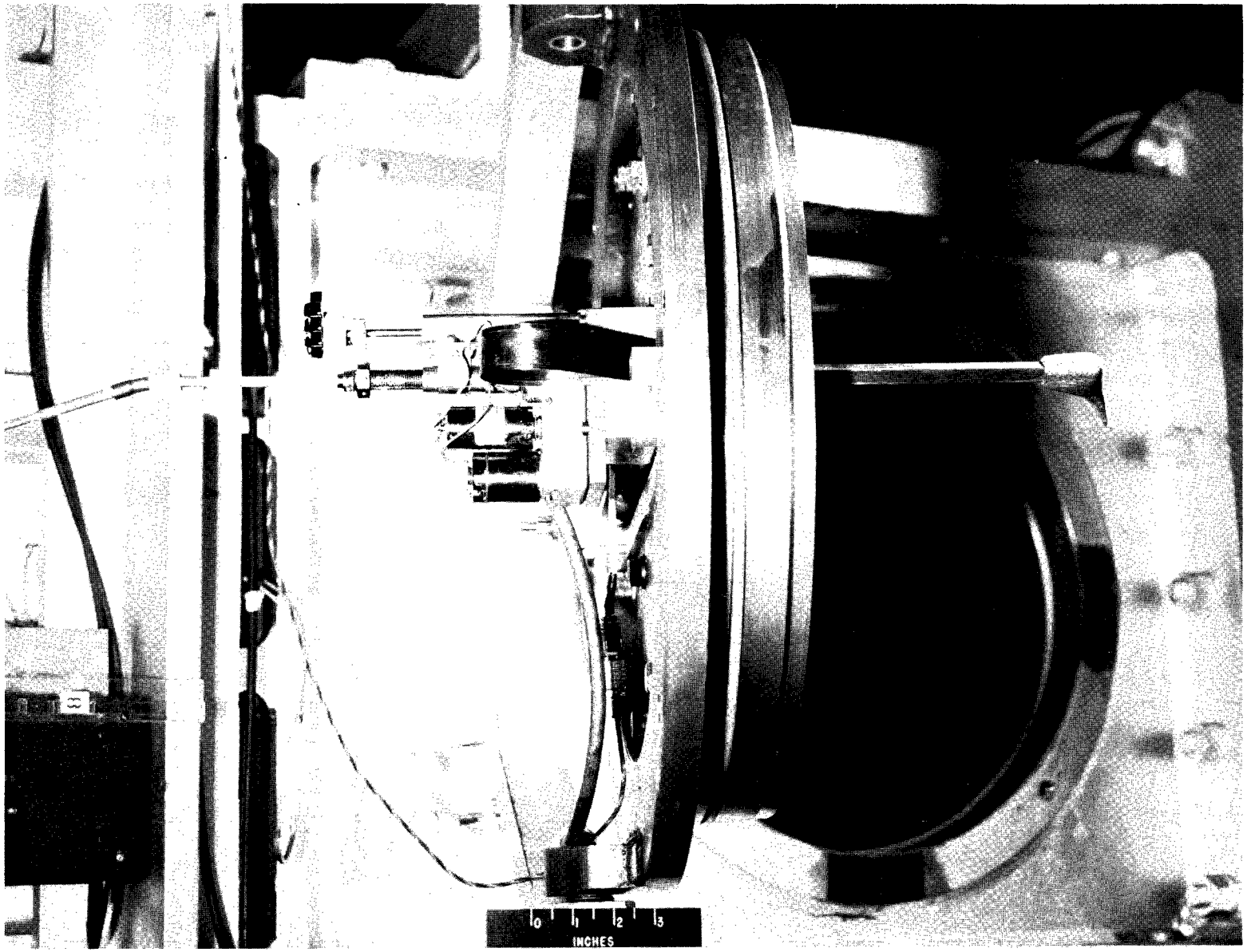


Figure 4.- Photograph of boundary-layer survey apparatus. L-63-802

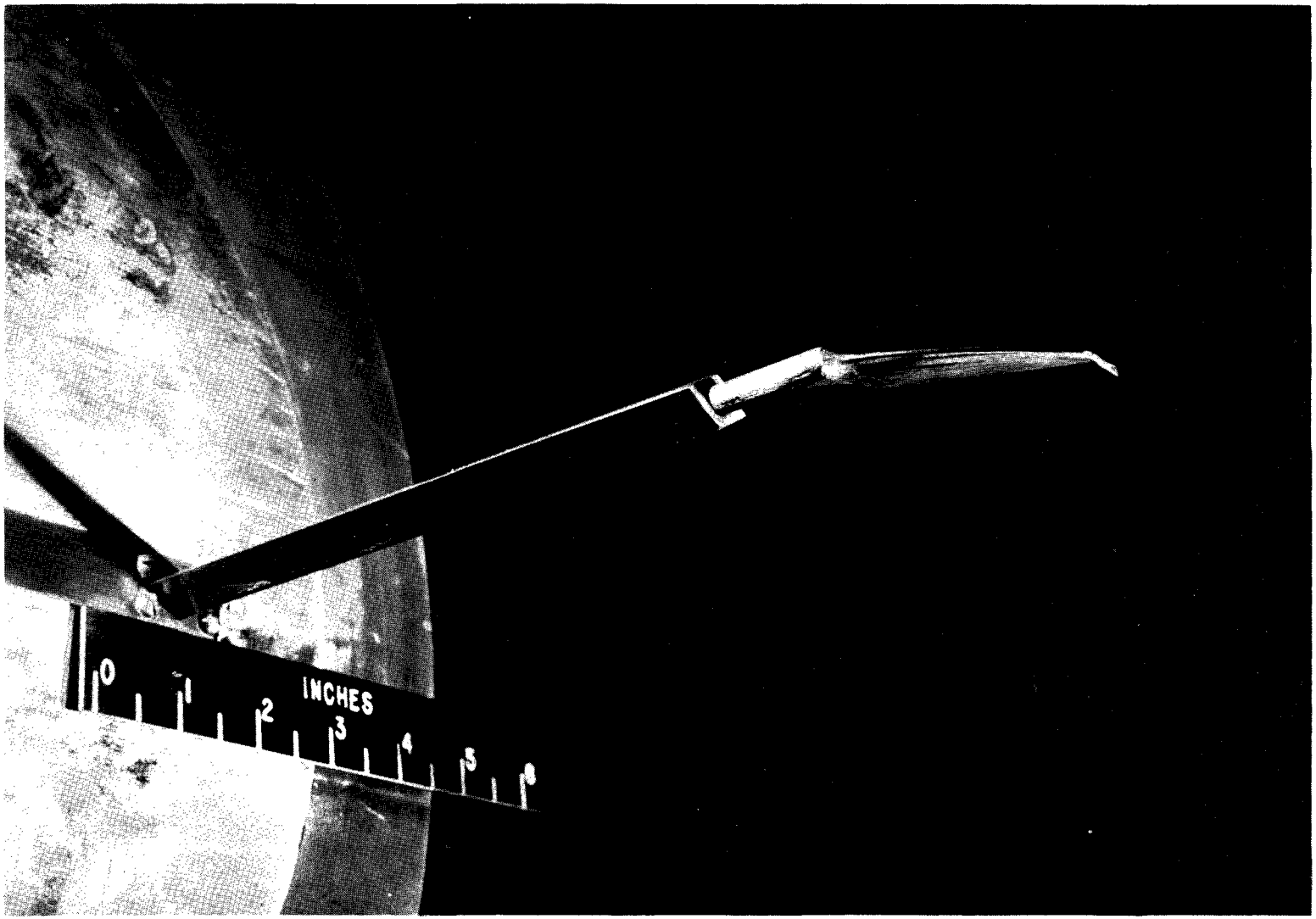


(a) Normal probe.

L-63-6005

Figure 5.- Photographs of the two probes used in this investigation.

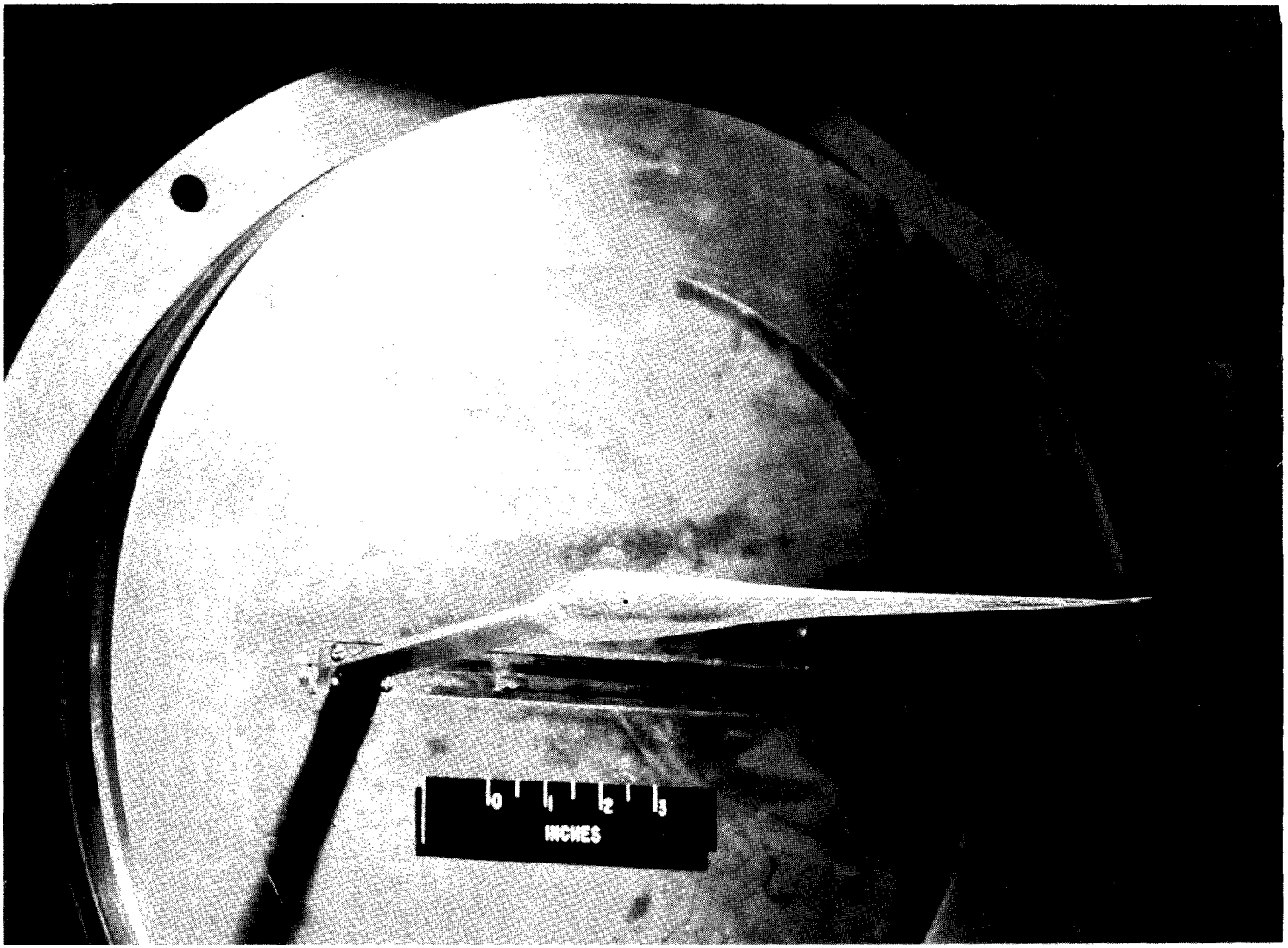


(b) Extended probe.

L-63-798

Figure 5.- Concluded.

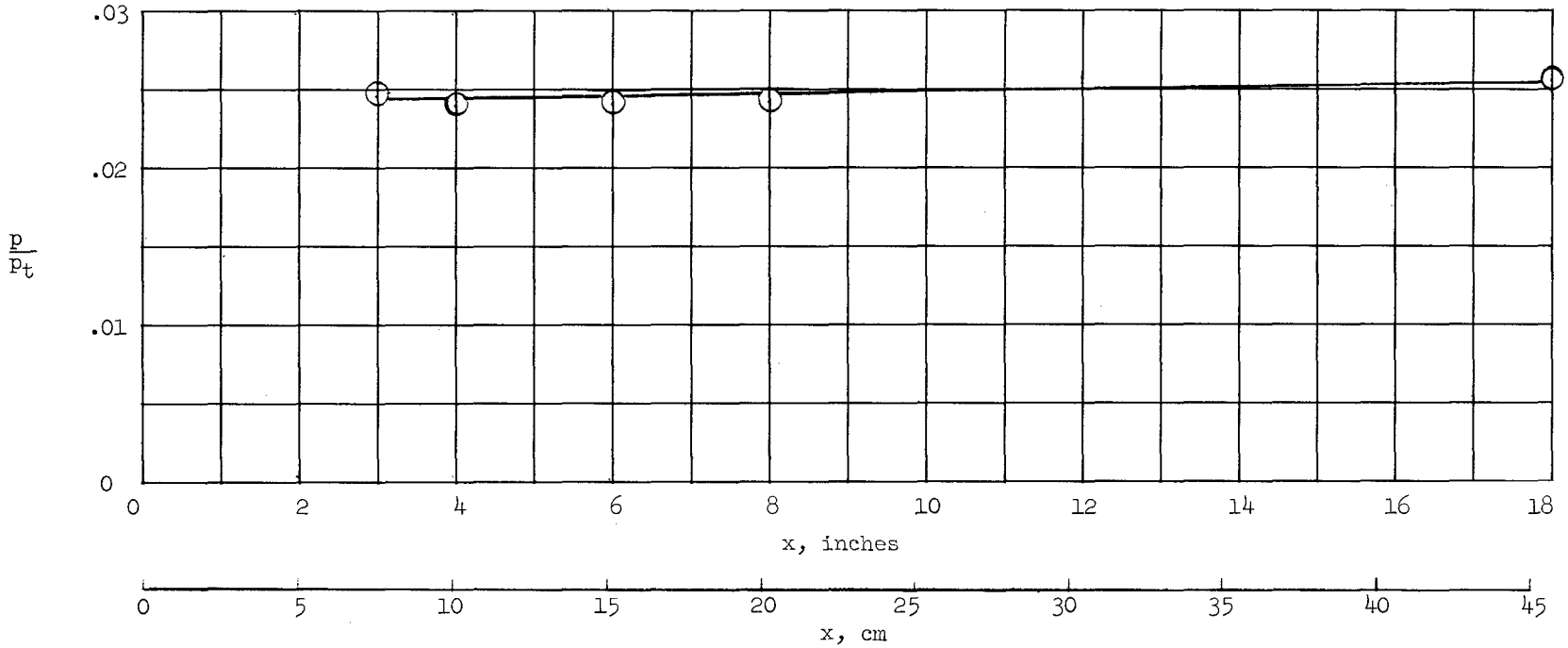


Figure 6.- Static-pressure distribution along surface of solid-plate configuration.

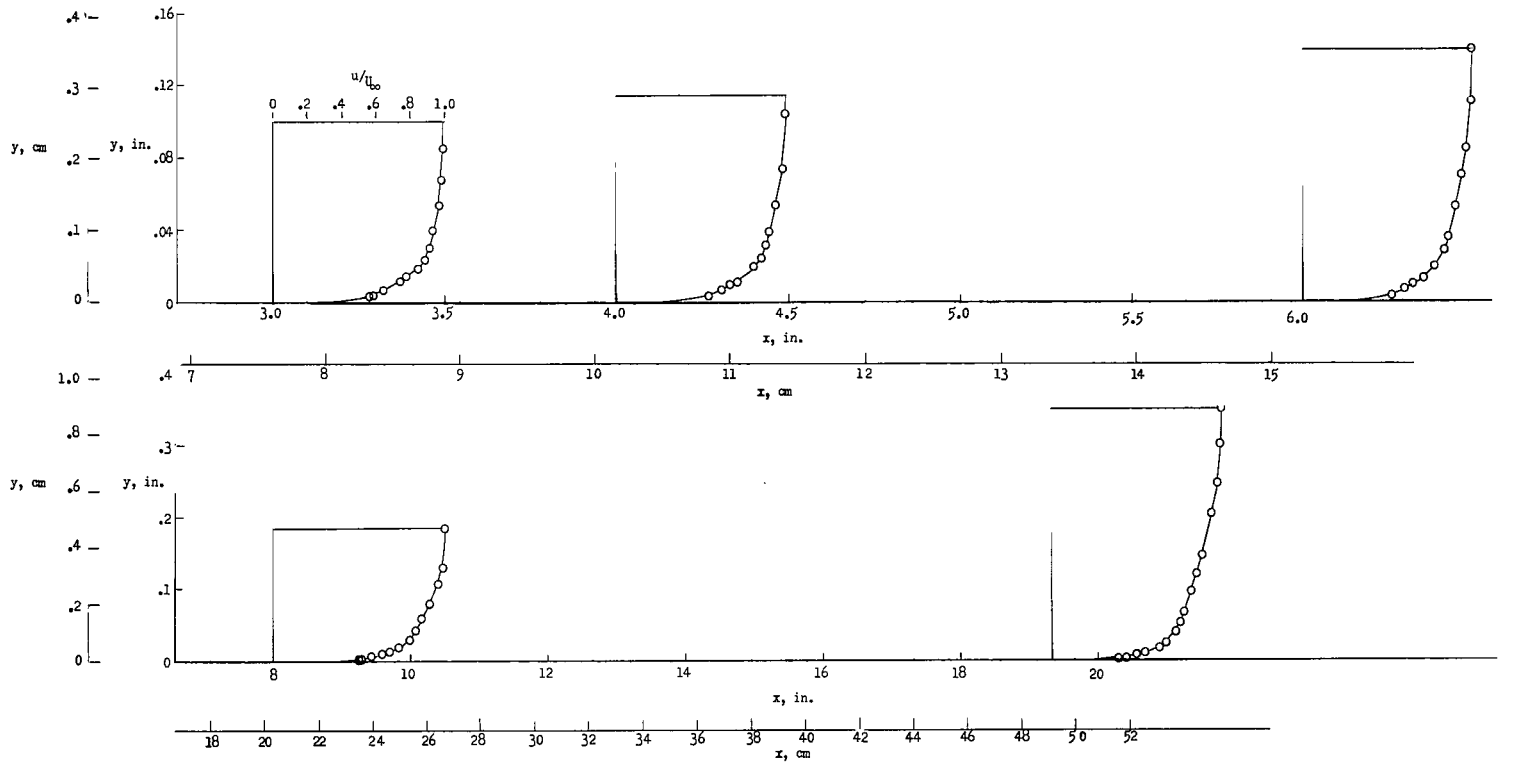


Figure 7.- Velocity profiles along surface of solid-plate configuration.

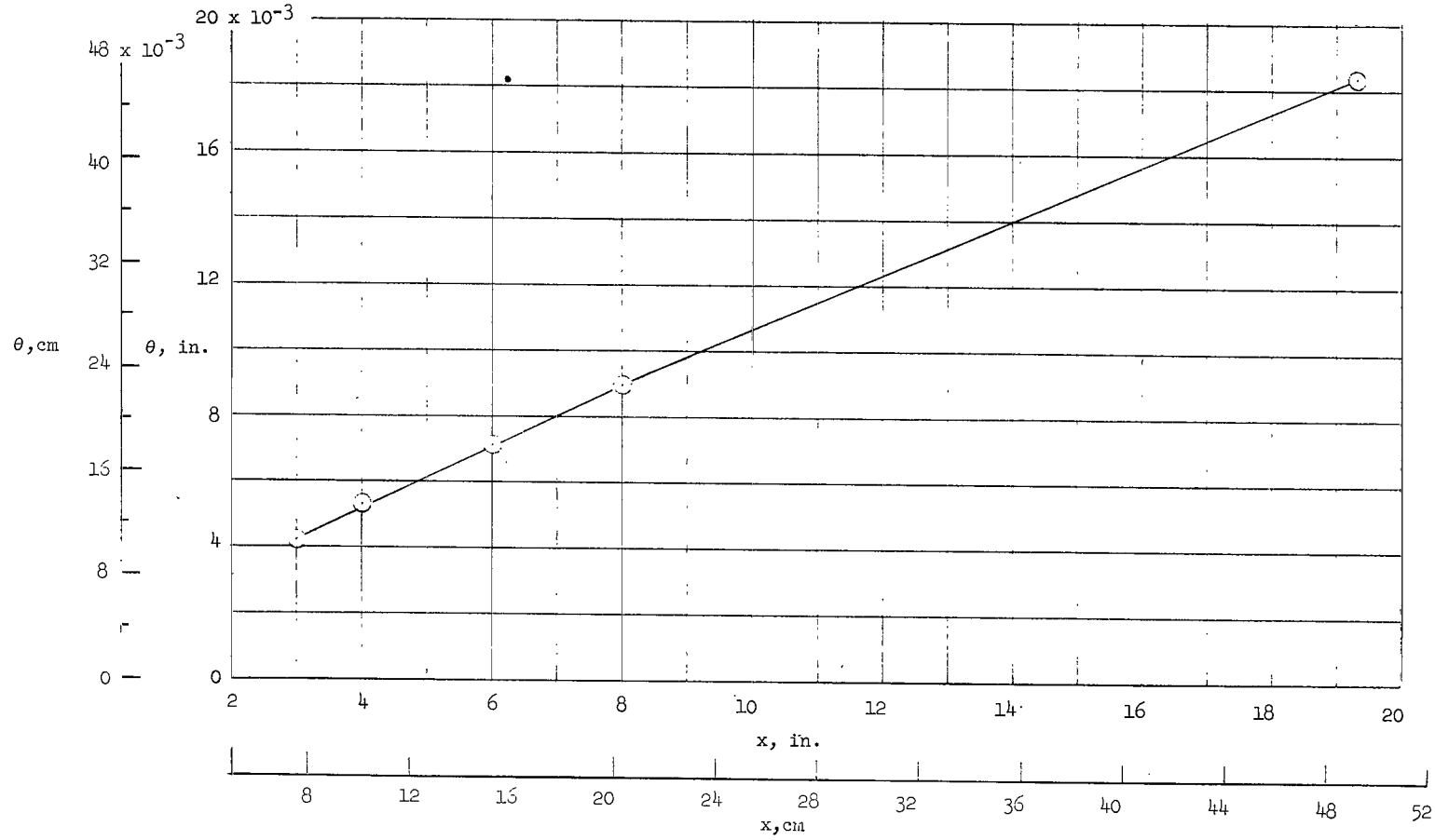


Figure 8.- Momentum thickness along surface of solid-plate configuration.

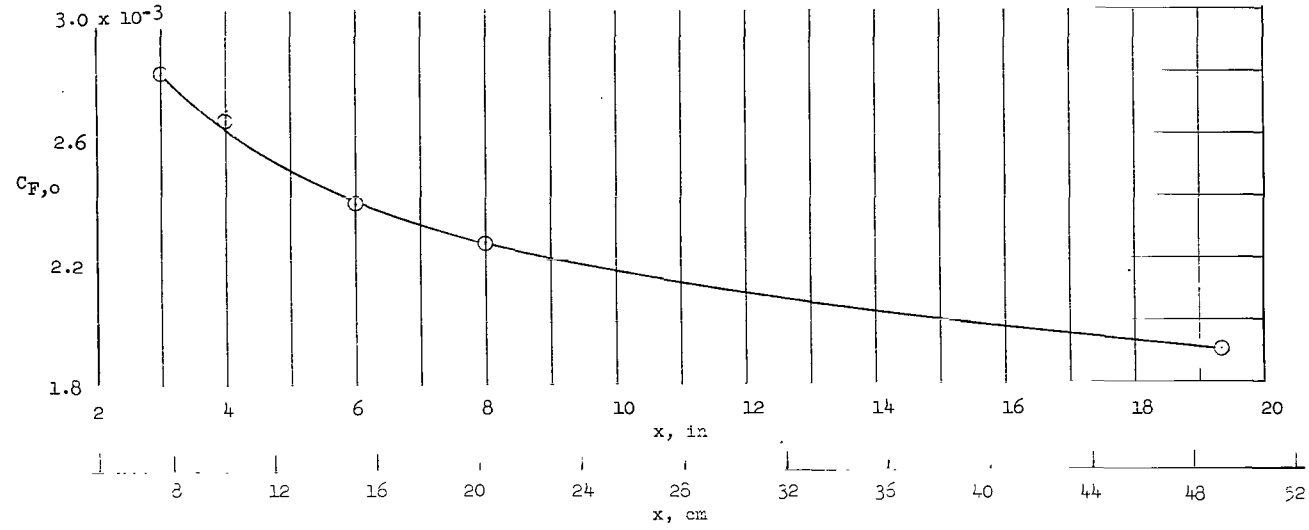


(a) Average skin-friction coefficient.

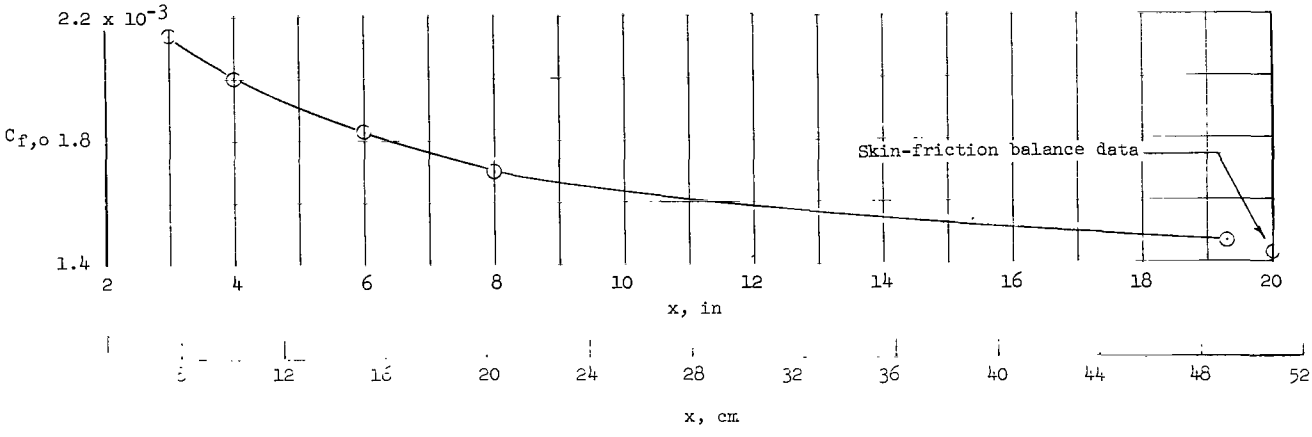


(b) Local skin-friction coefficient.

Figure 9.- Average and local turbulent skin-friction coefficient along solid-plate surface.

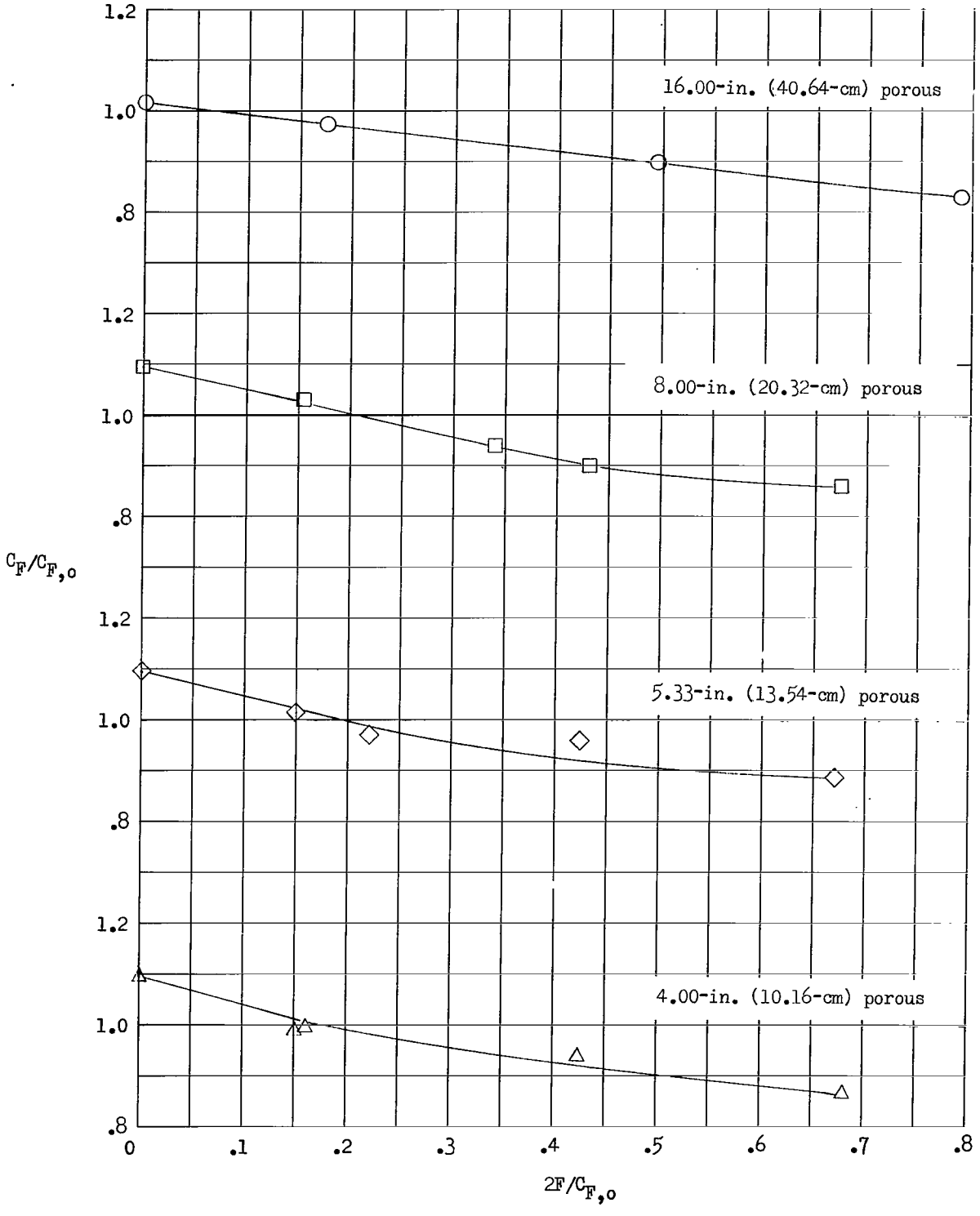


Figure 10.- Average skin-friction-coefficient ratios for porous configurations. x = 19.3 in. (49.02 cm).

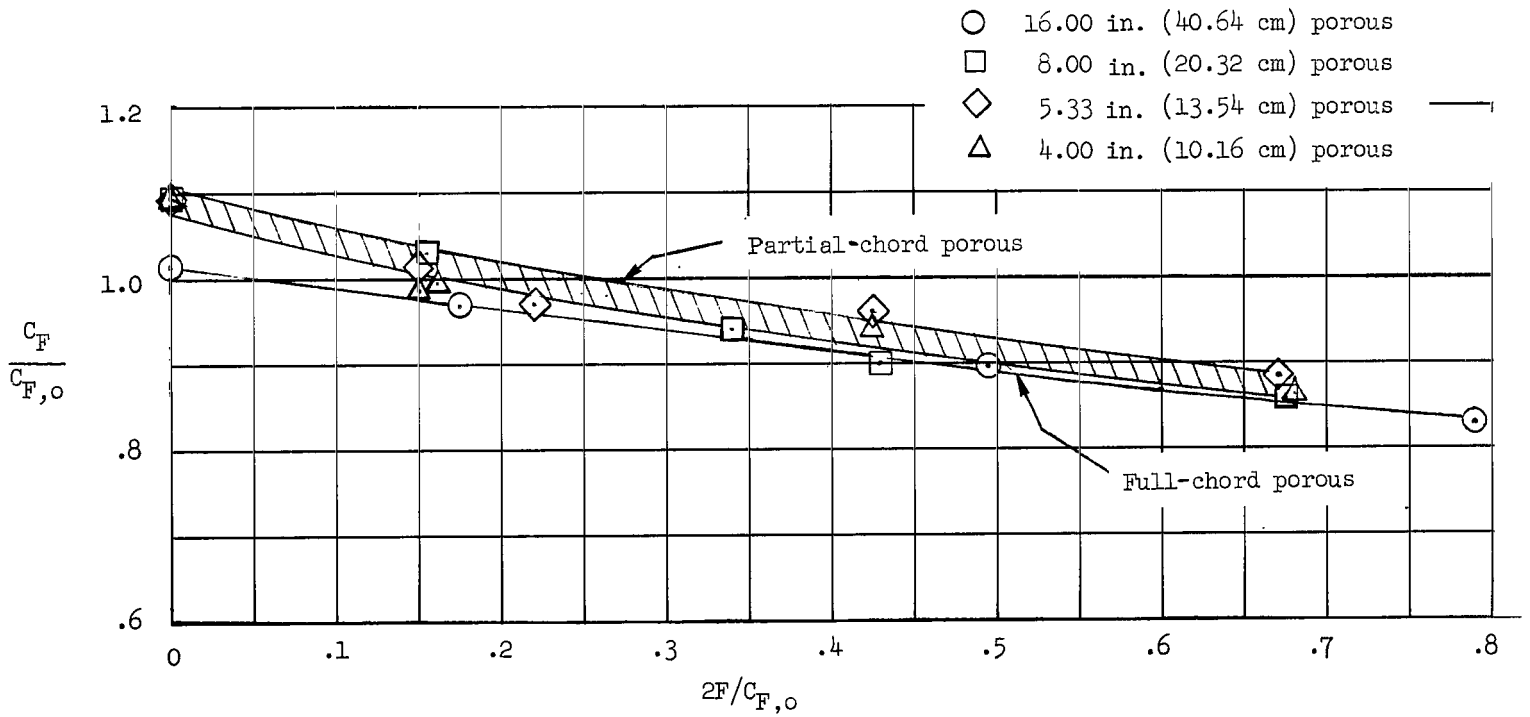


Figure 11.- Average skin-friction-coefficient ratios for porous configurations. x = 19.3 in. (49.02 cm).

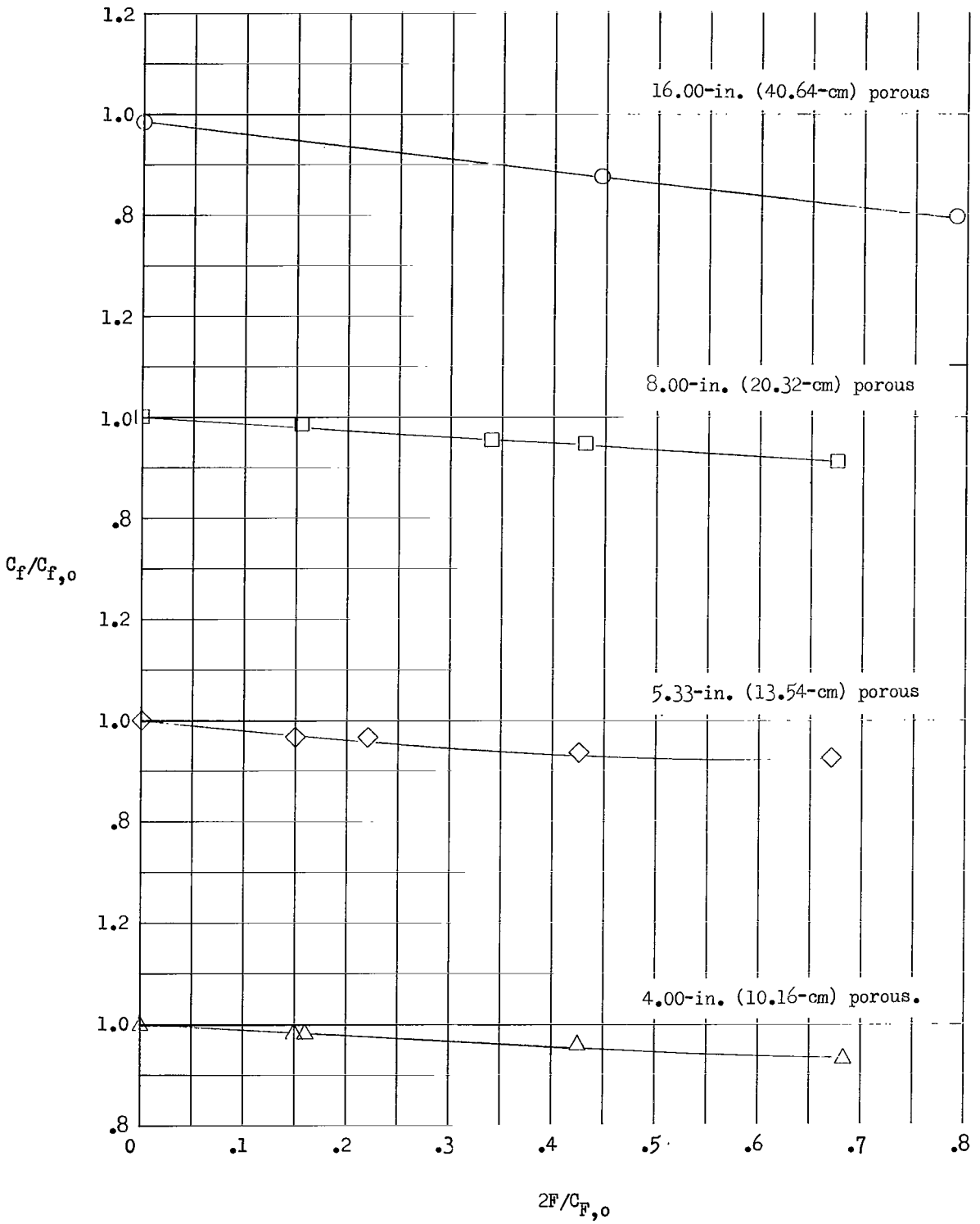


Figure 12.- Local skin-friction-coefficient ratios for porous configurations. x = 20.0 in. (50.8 cm).

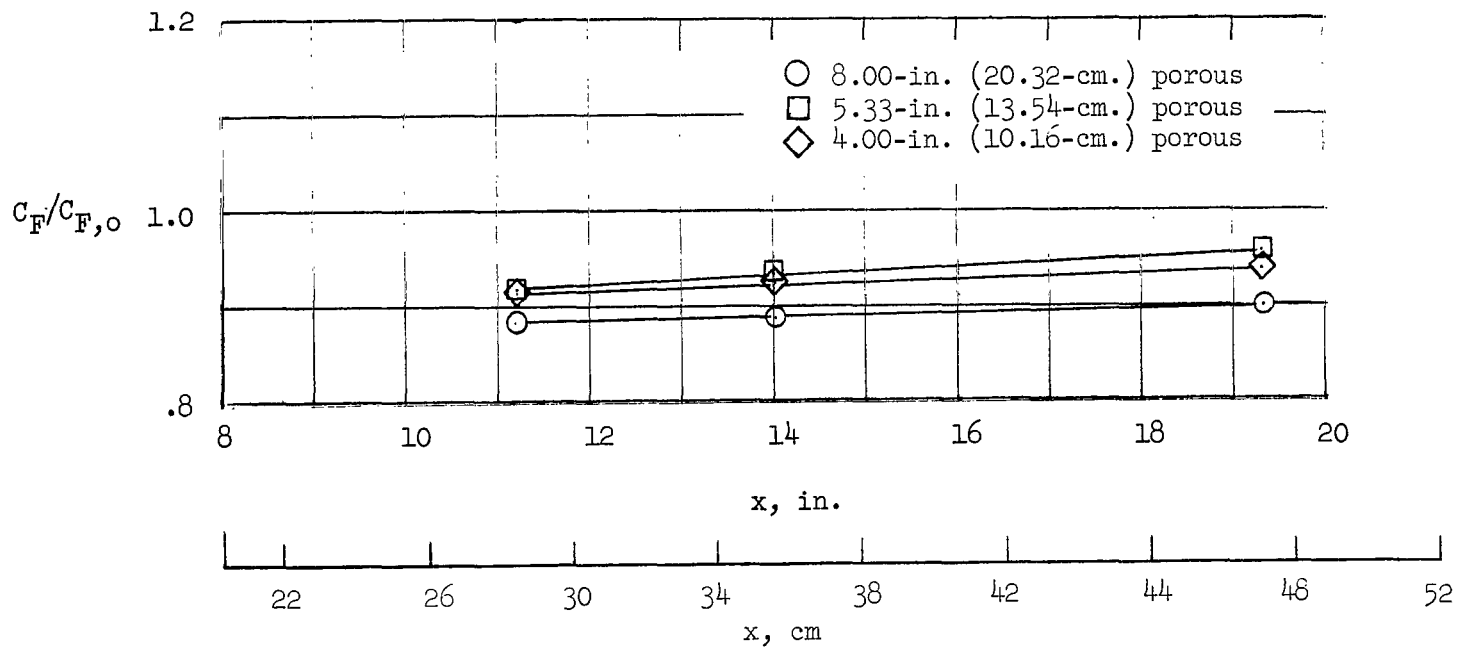


Figure 13.- Average skin-friction-coefficient ratios along the surfaces of the porous configurations for a mass-flow rate of 0.038 pound per second.

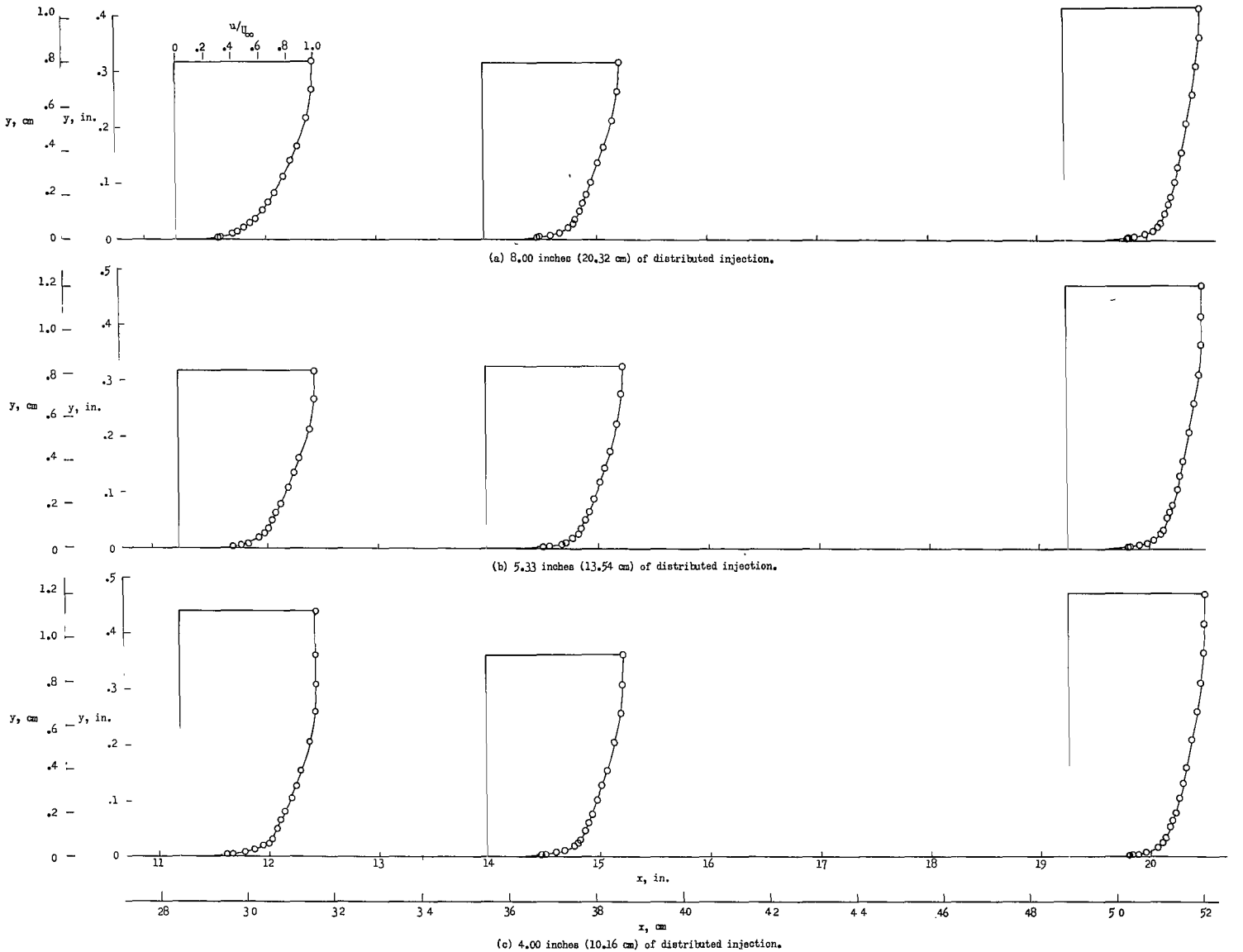


Figure 14.- Velocity profiles along surface of porous configurations. $2F/C_{F,0} = 0.43$.

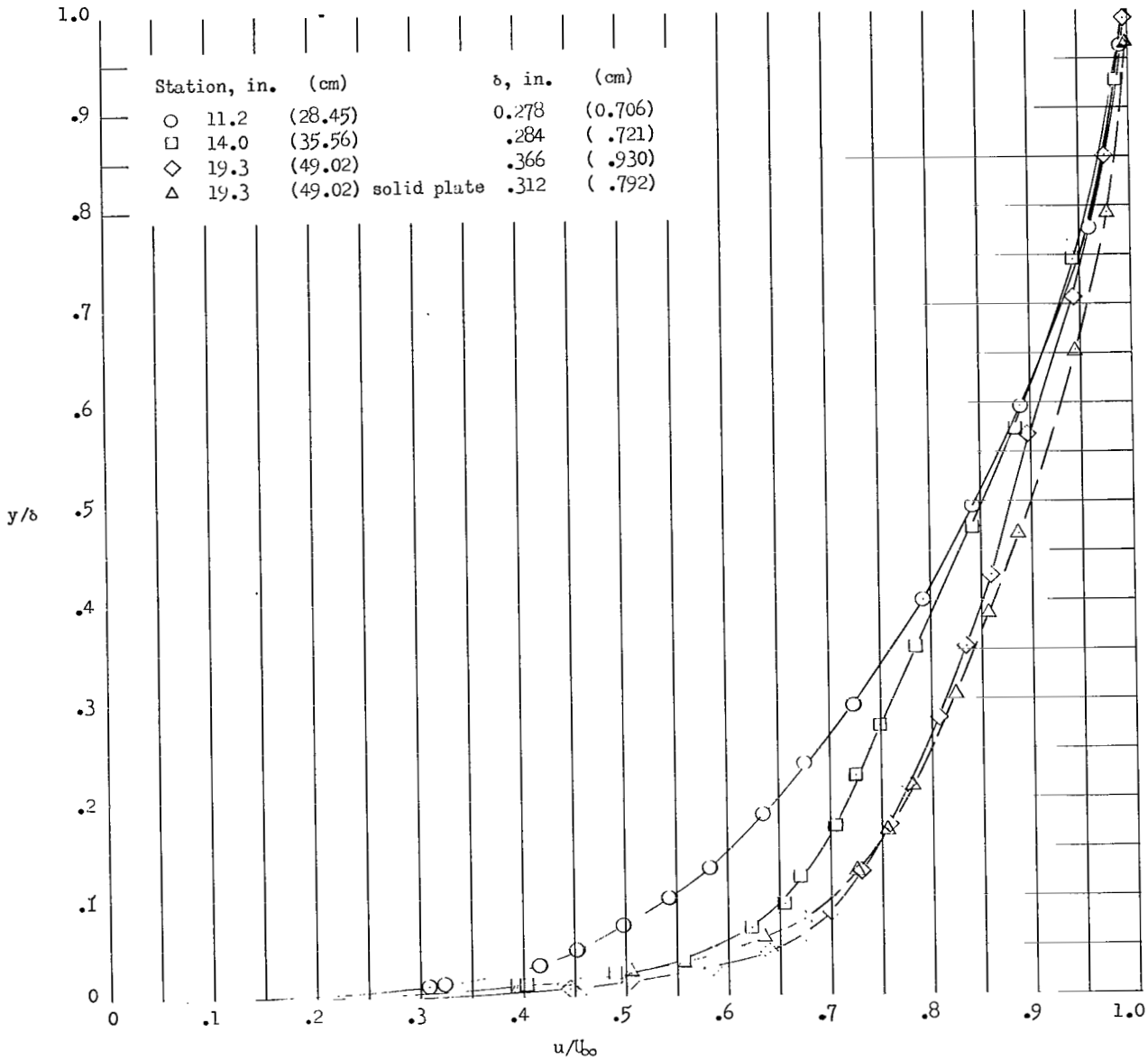


(a) 8.00-inch (20.32-cm) porous configuration.

Figure 15.- Nondimensional velocity profiles along surface of porous configuration for an injection mass flow of 0.038 pound (0.0172 kilogram) per second.

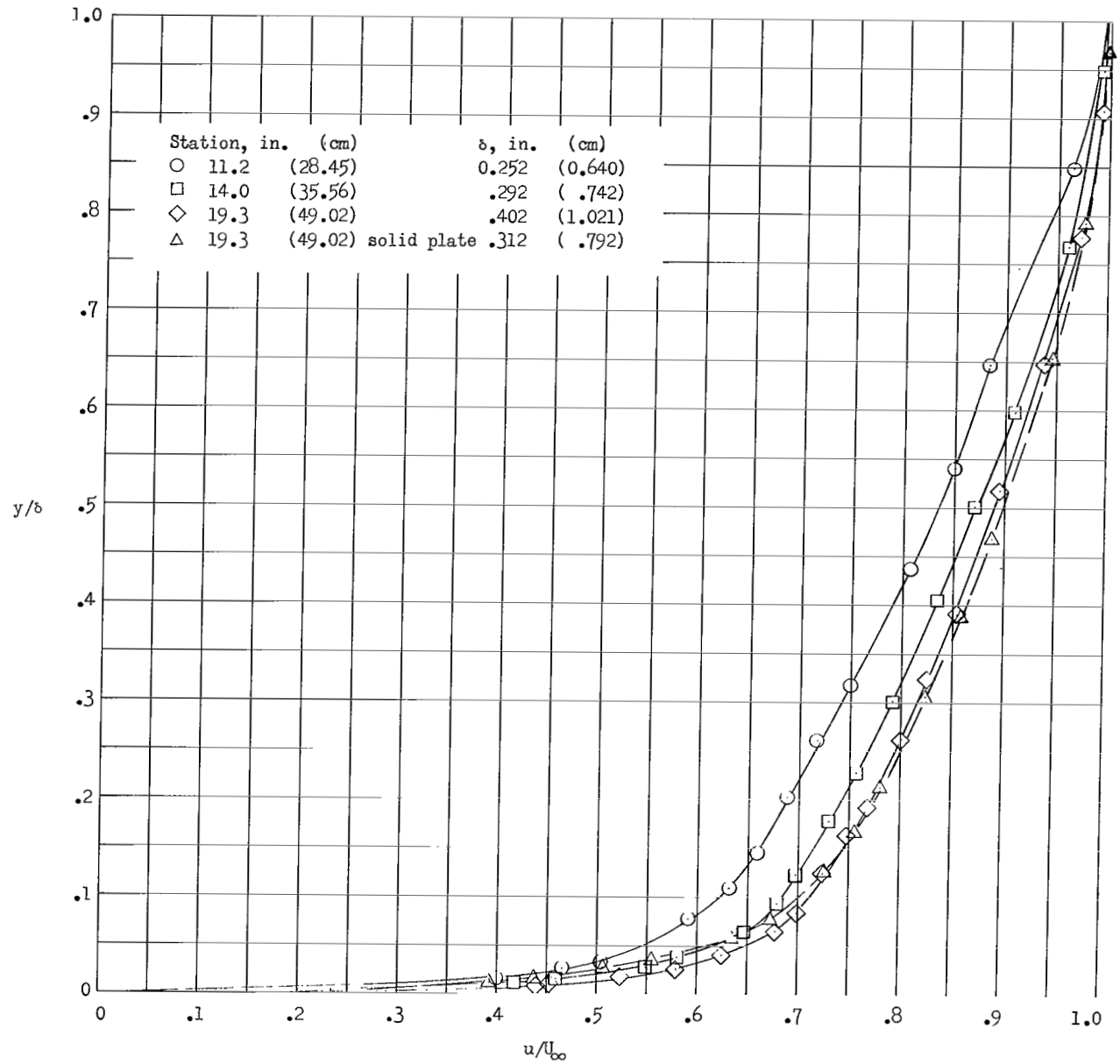


(b) 5.33-inch (13.54-cm) porous configuration.

Figure 15.- Continued.

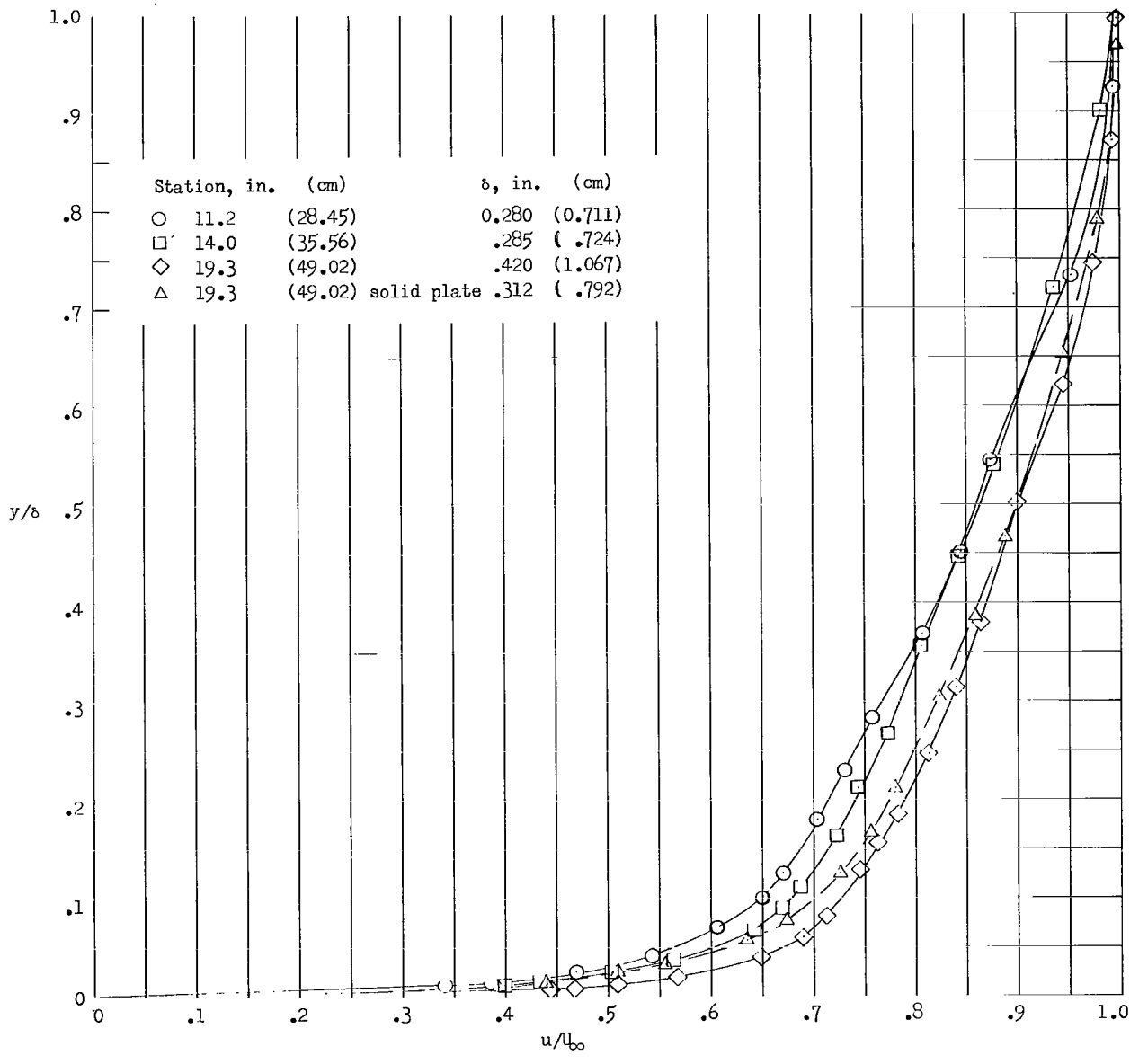


(c) 4.00-inch (10.16-cm) porous configuration.

Figure 15.- Concluded.

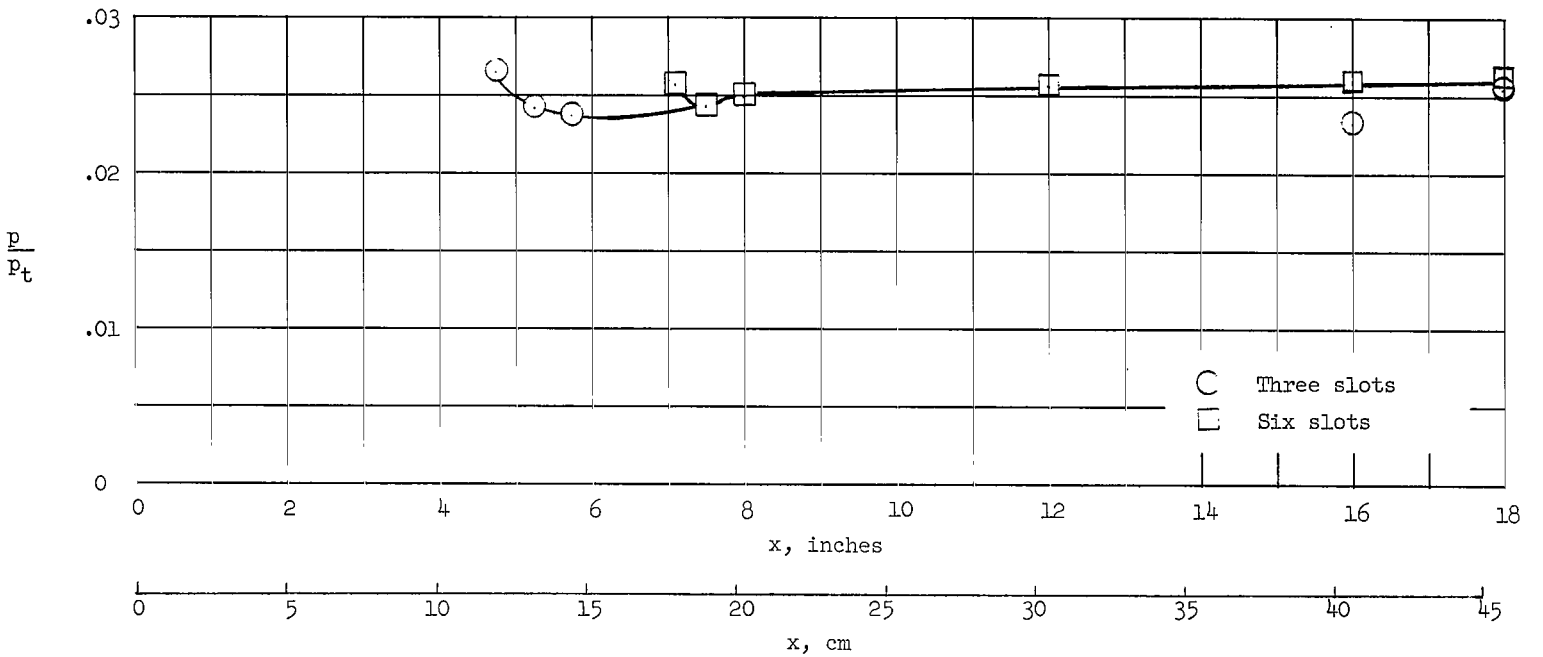


Figure 16.- Static-pressure distribution along surface of multiple-normal-flush-slot configurations with a mass-flow rate of 0.038 pound (0.0172 kilogram) per second.

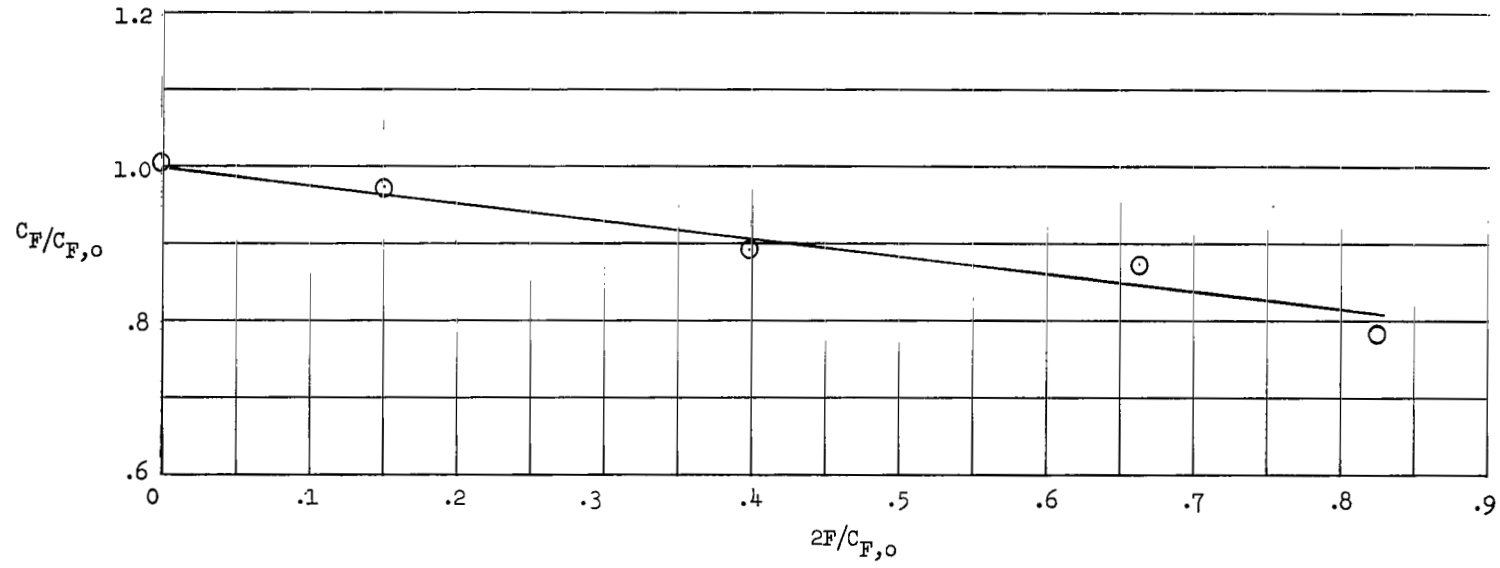


(a) Three-slot configuration.

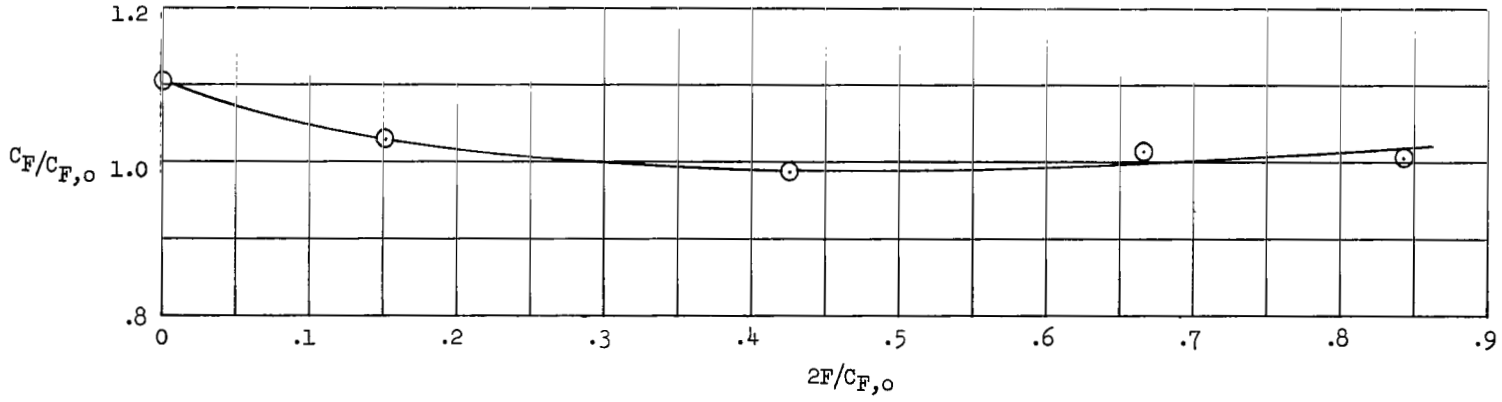


(b) Six-slot configuration.

Figure 17.- Average skin-friction-coefficient ratios for multiple-normal-slot configurations. x = 19.3 in. (49.02 cm).

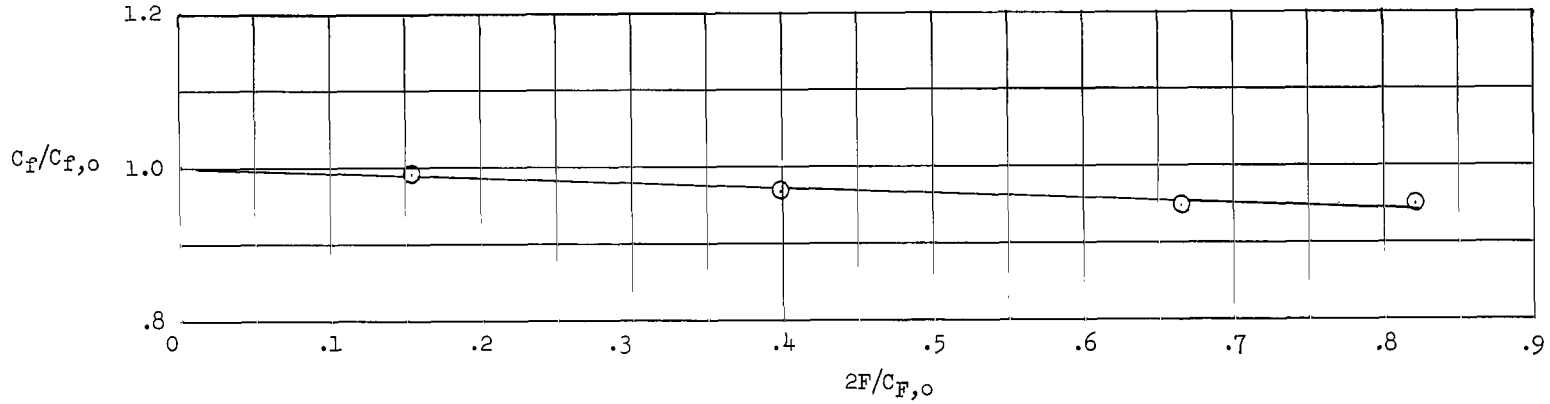


(a) Three-slot configuration.

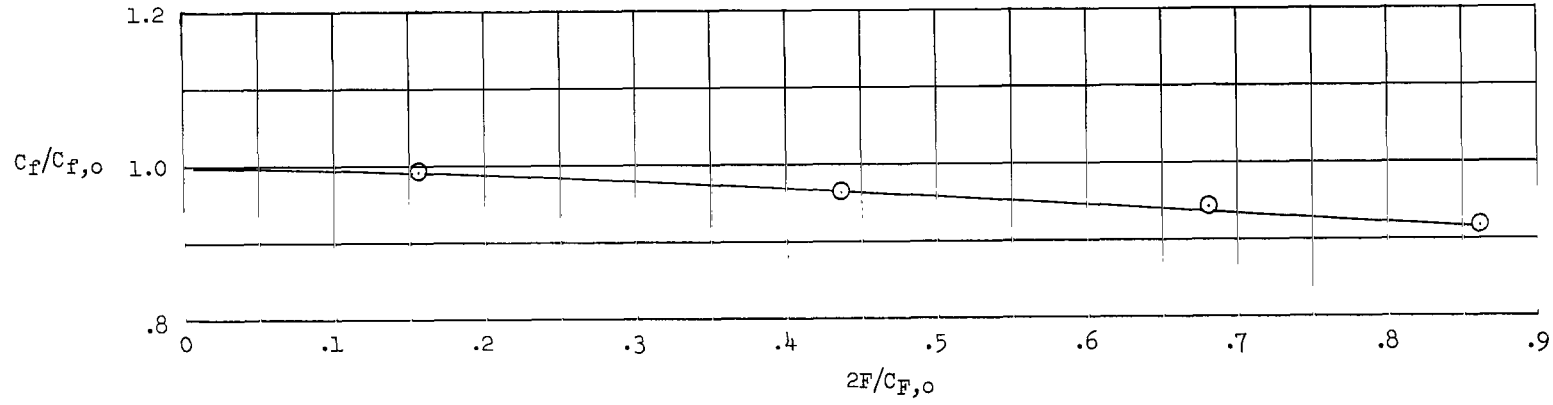


(b) Six-slot configuration.

Figure 18.- Local skin-friction-coefficient ratios for multiple-normal-slot configurations. x = 20.0 in. (50.80 cm).

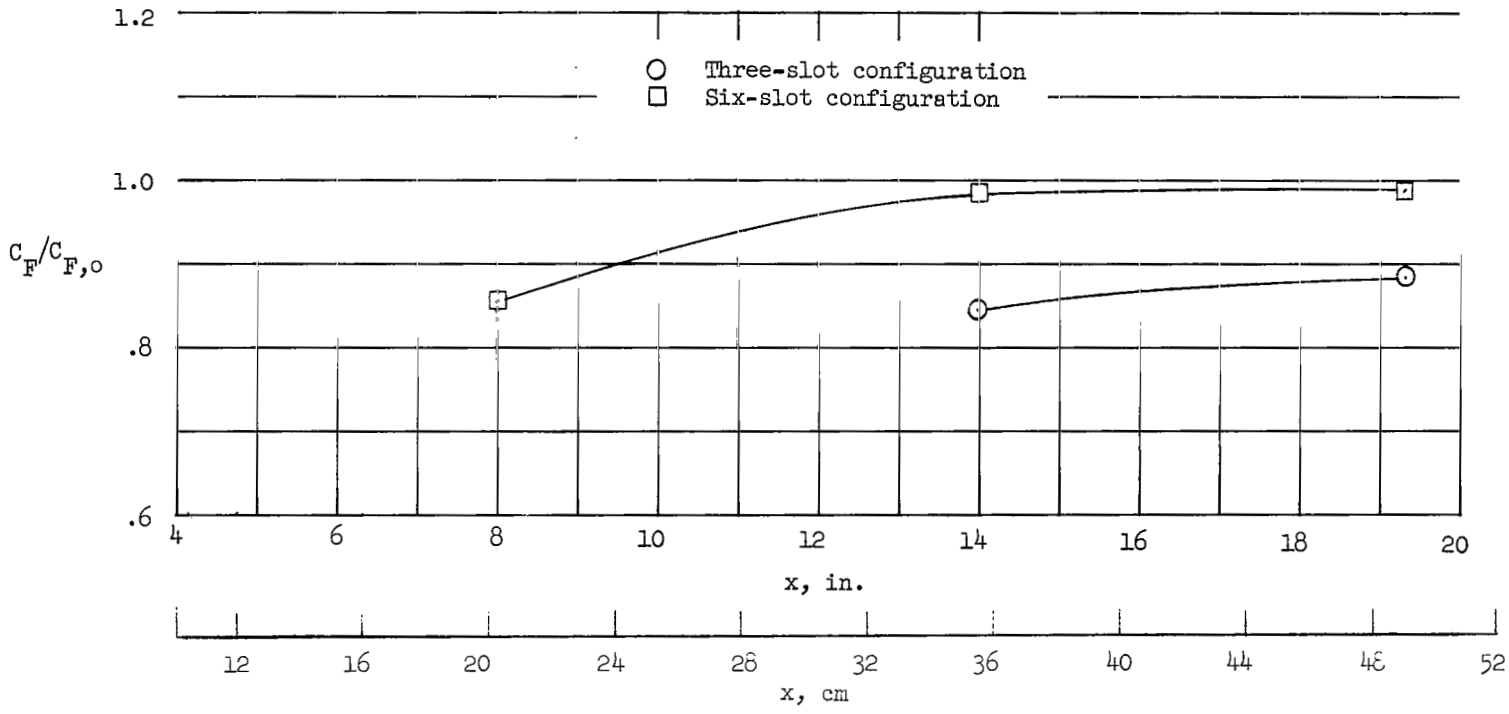


Figure 19.- Average skin-friction-coefficient ratios along surface of multiple-normal-slot configurations for a mass-flow rate of 0.038 pound (0.0172 kilogram) per second.

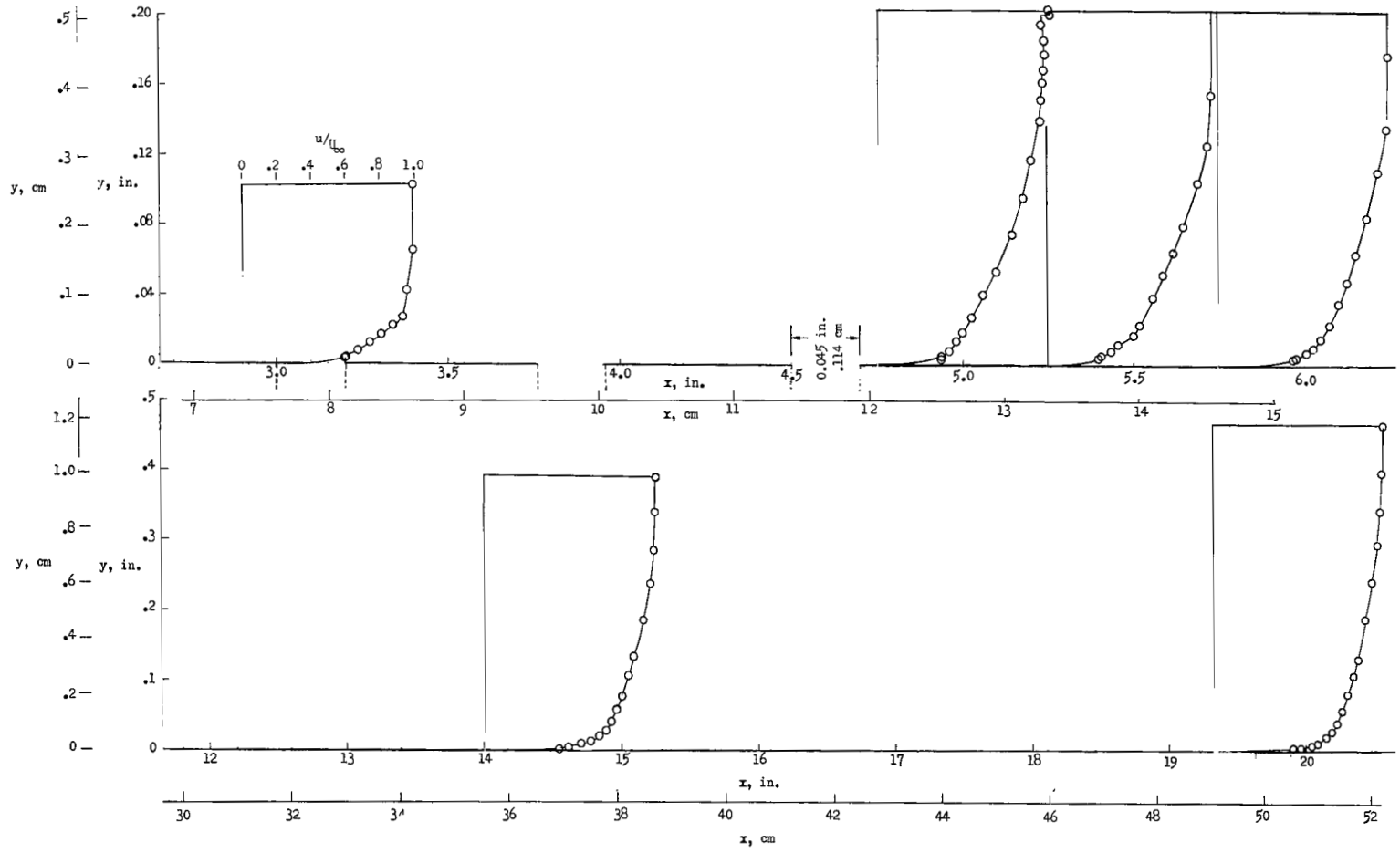


(a) Three-slot configuration.

Figure 20.- Velocity profiles along surface of multiple-normal-flush-slot configurations. $2F/C_{F,0} = 0.43$.

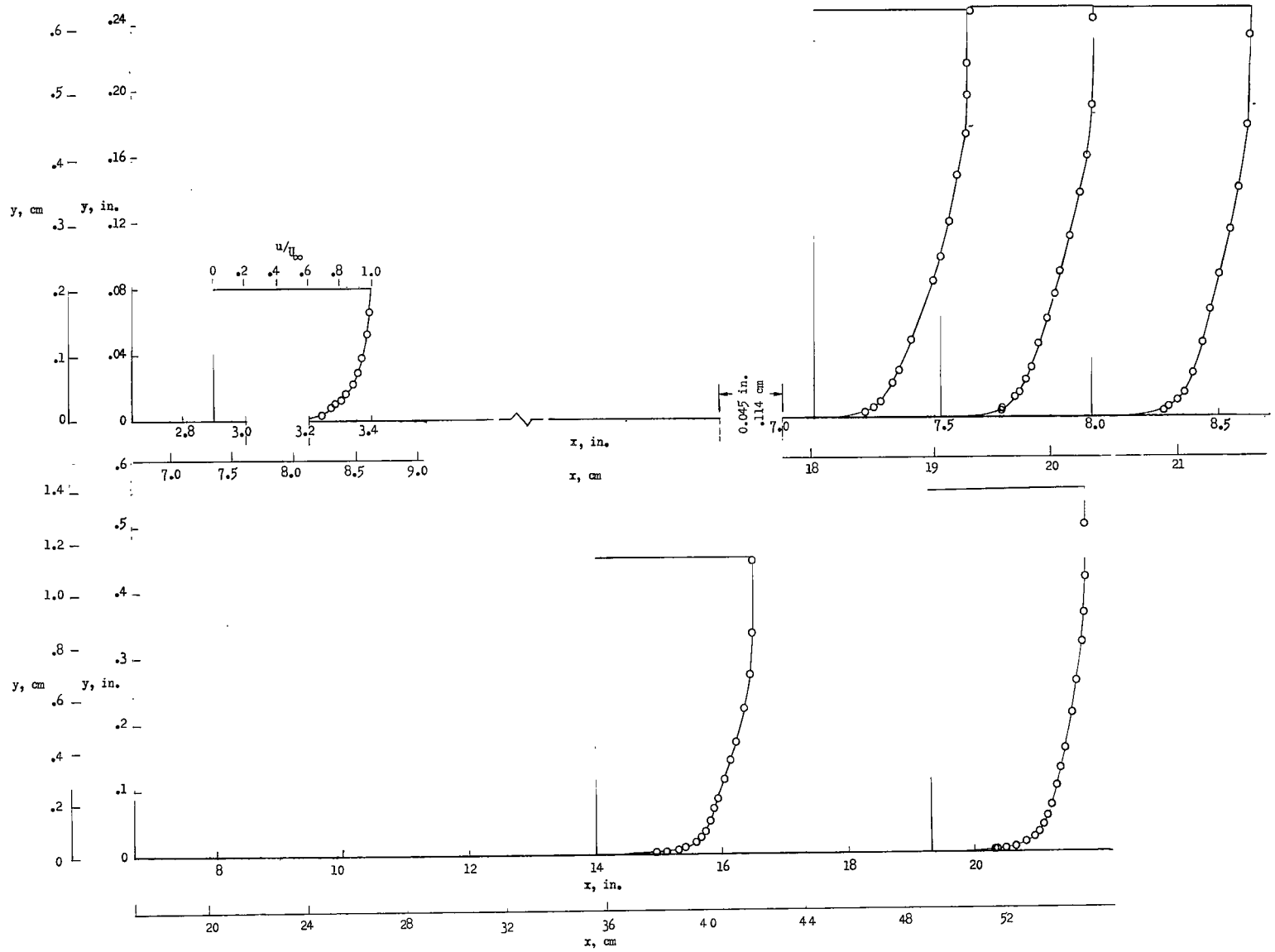


(b) Six-slot configuration.

Figure 20.- Concluded.

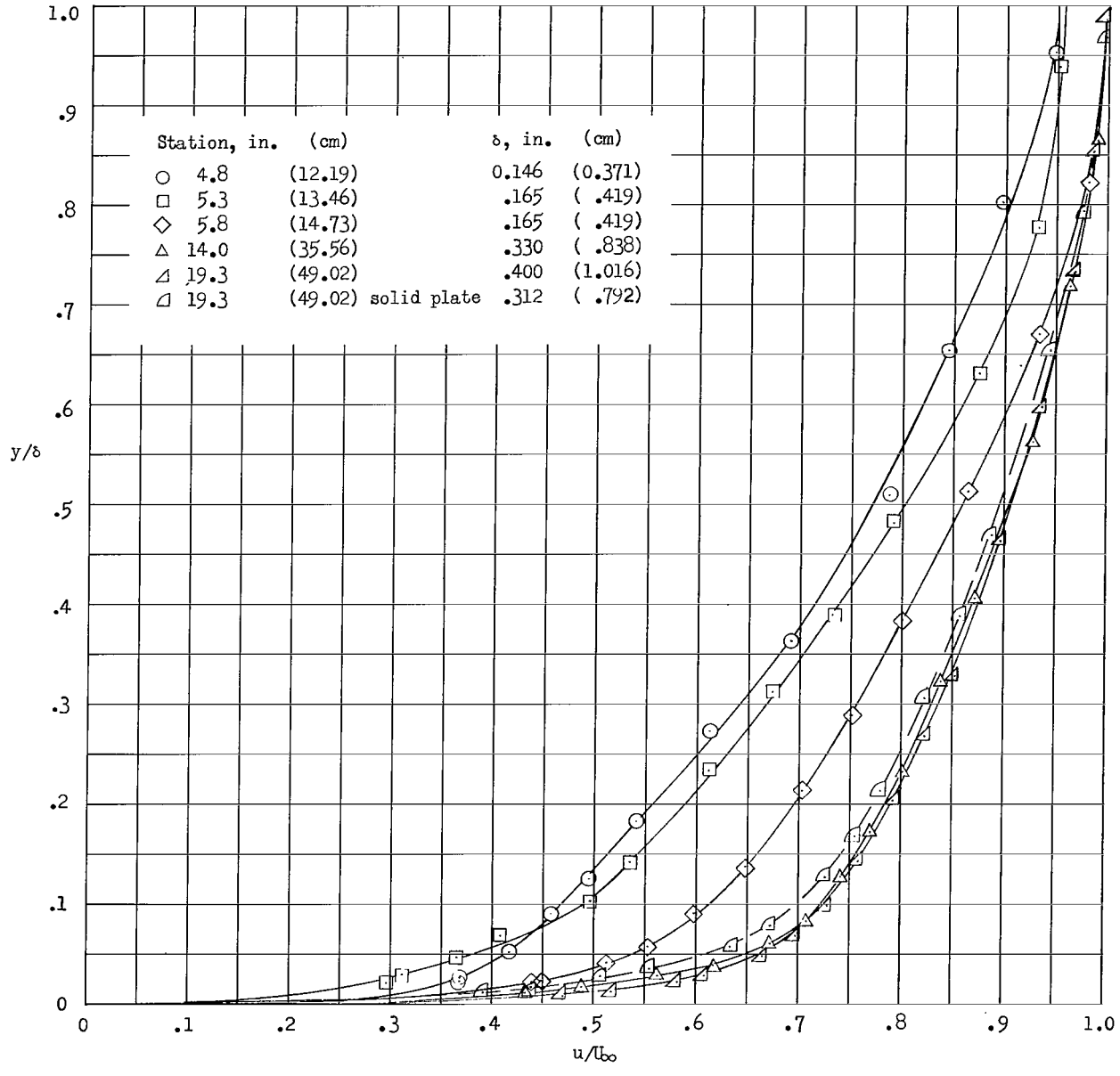


(a) Three-slot configuration.

Figure 21.- Nondimensional velocity profiles along surface of multiple-normal-flush-slot configurations for an injection mass flow of 0.038 pound (0.0172 kilogram) per second.

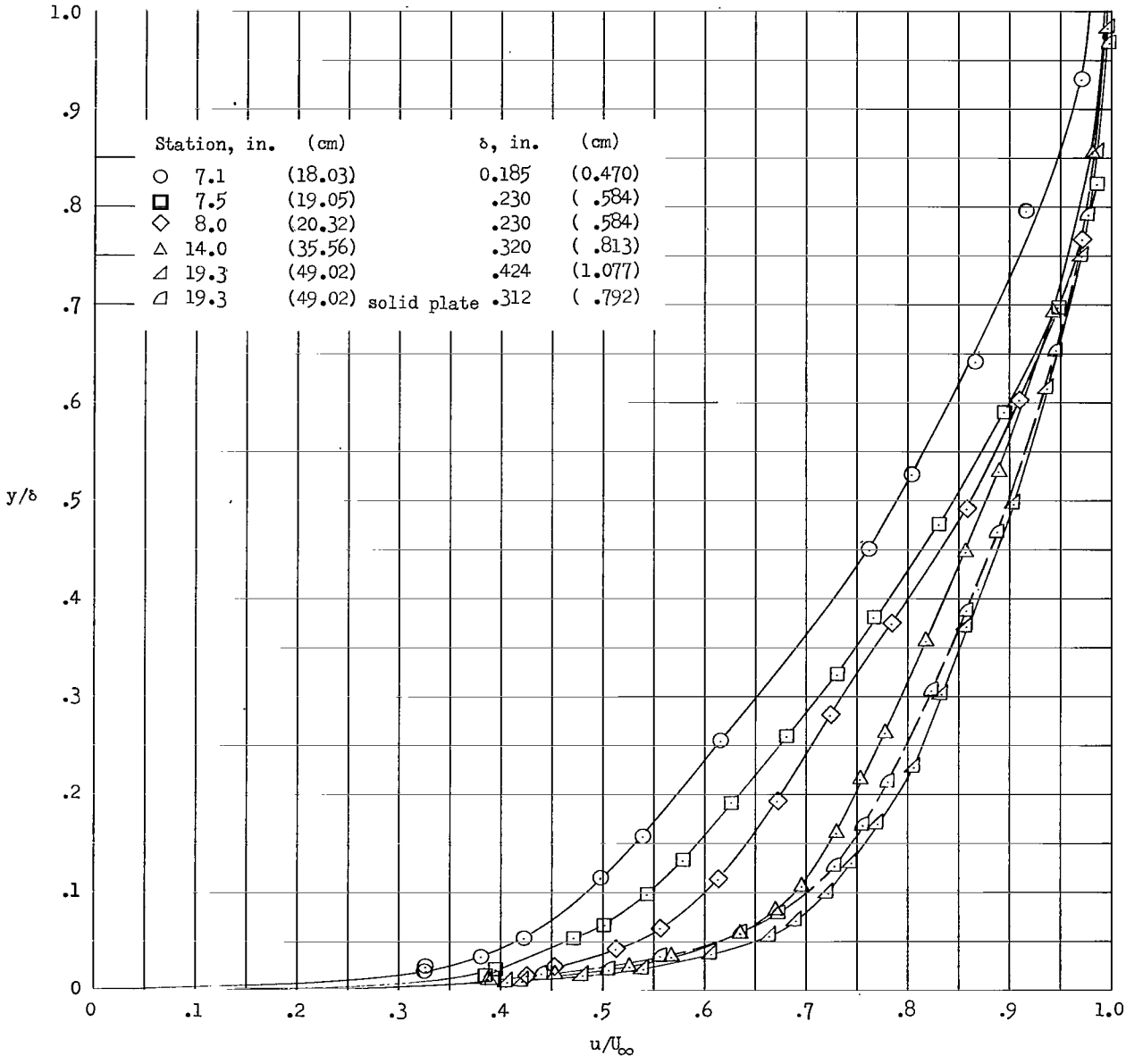


(b) Six-slot configuration.

Figure 21.- Concluded.

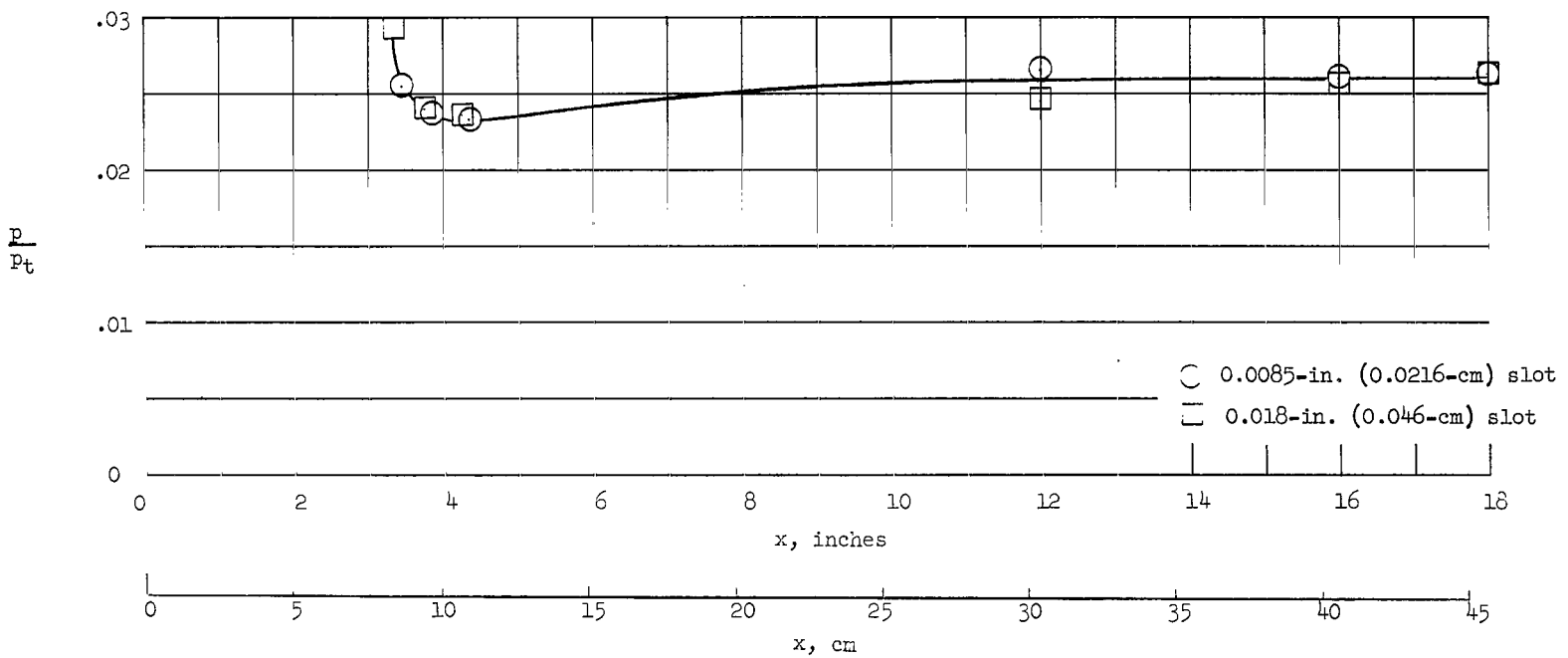


Figure 22.- Static-pressure distribution along surface of rearward-inclined flush-slot configurations with a mass-flow rate of 0.038 pound (0.0172 kilogram) per second.

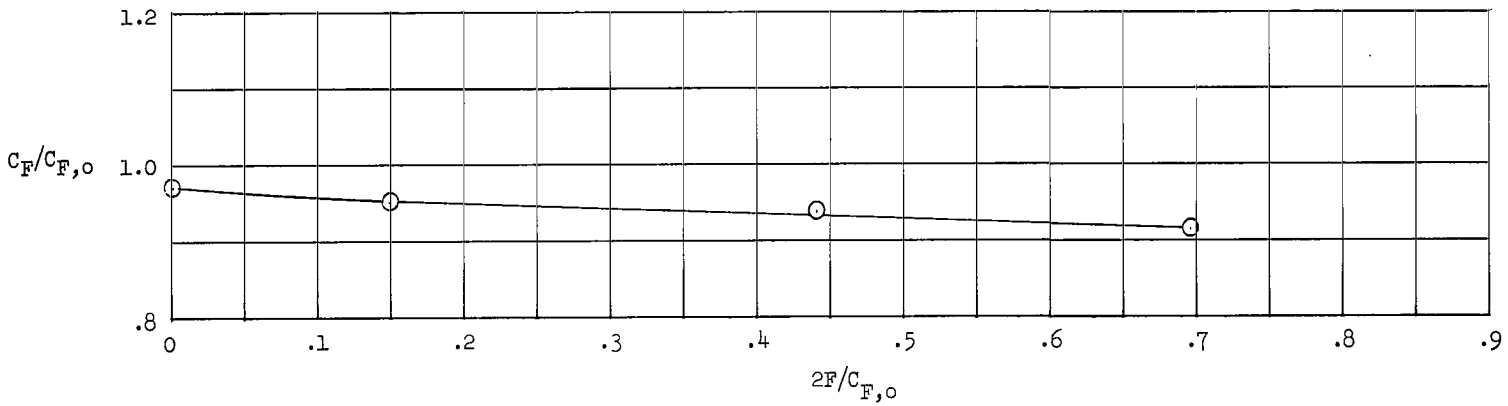


(a) 0.0085-inch (0.0216-cm) rearward-inclined flush slot.

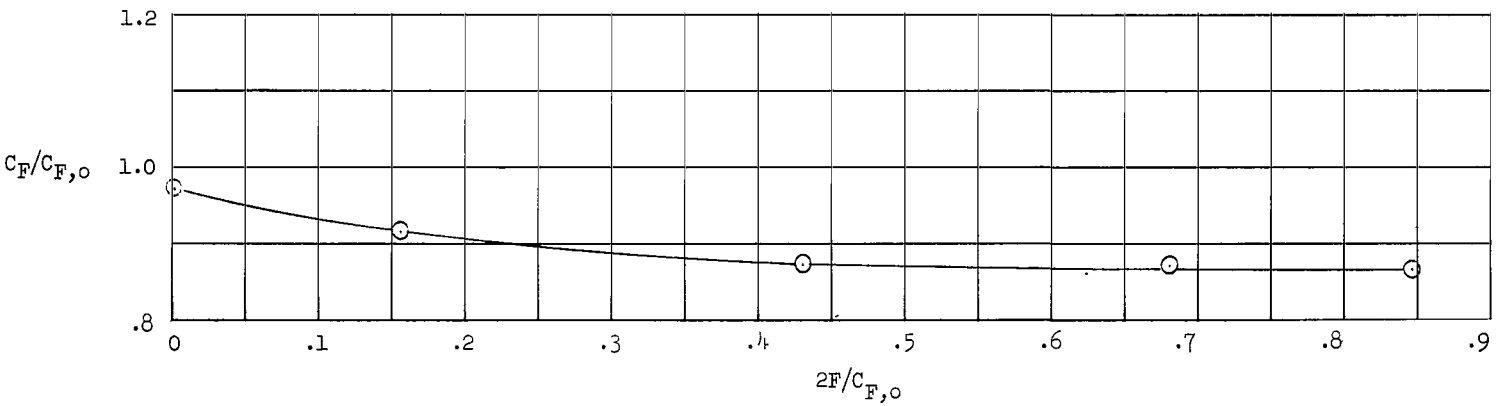


(b) 0.018-inch (0.046-cm) rearward-inclined flush slot.

Figure 23.- Average skin-friction-coefficient ratios for rearward-inclined flush-slot configurations. x = 19.3 in. (49.02 cm).

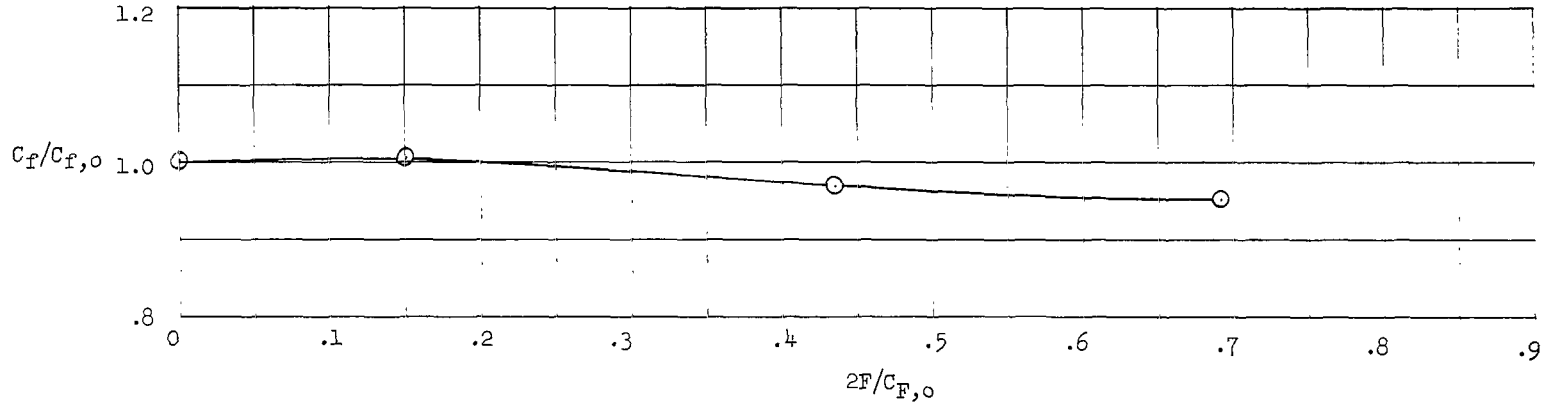


(a) 0.0085-inch (0.0216-cm) rearward-inclined flush slot.

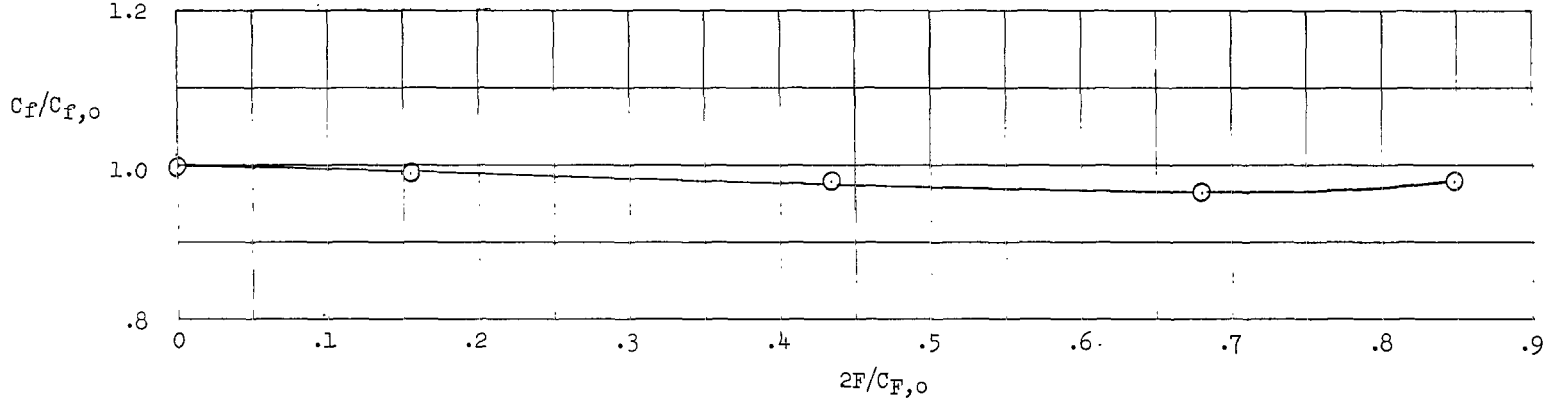


(b) 0.018-inch (0.046-cm) rearward-inclined flush slot.

Figure 24.- Local skin-friction-coefficient ratios for rearward-inclined flush-slot configurations. x = 20.0 in. (50.80 cm).

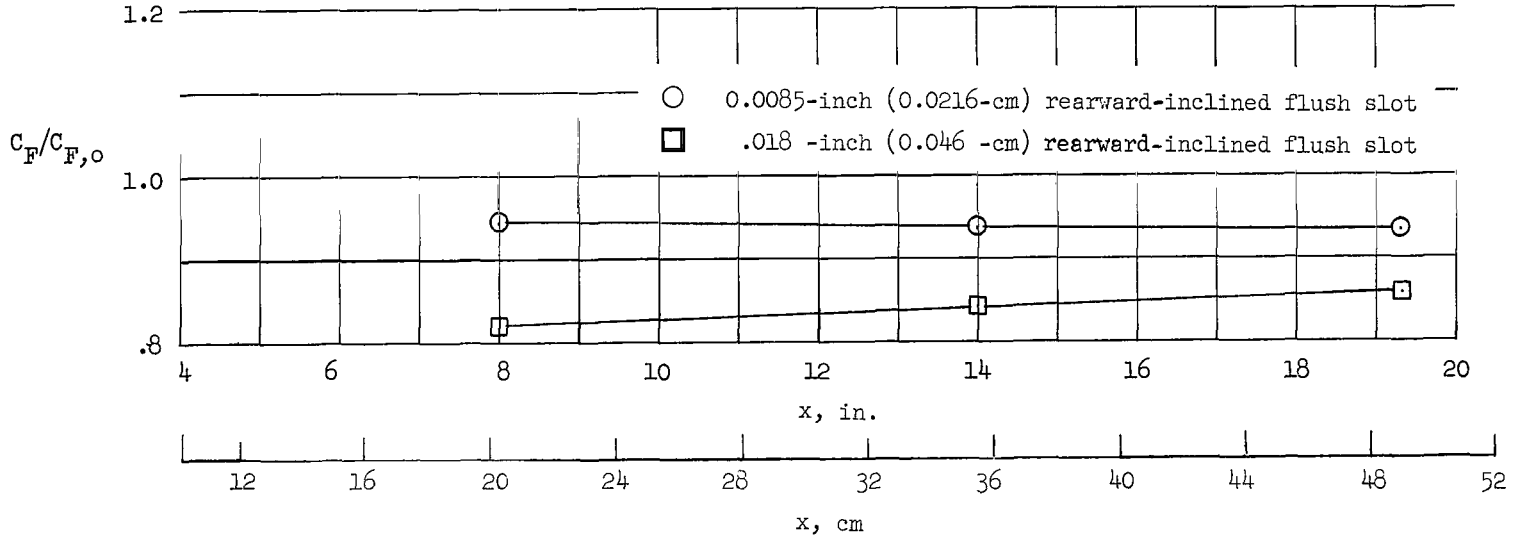


Figure 25.- Average skin-friction-coefficient ratios along surface of rearward-inclined flush-slot configurations with a mass-flow rate of 0.038 pound (0.0172 kilogram) per second.

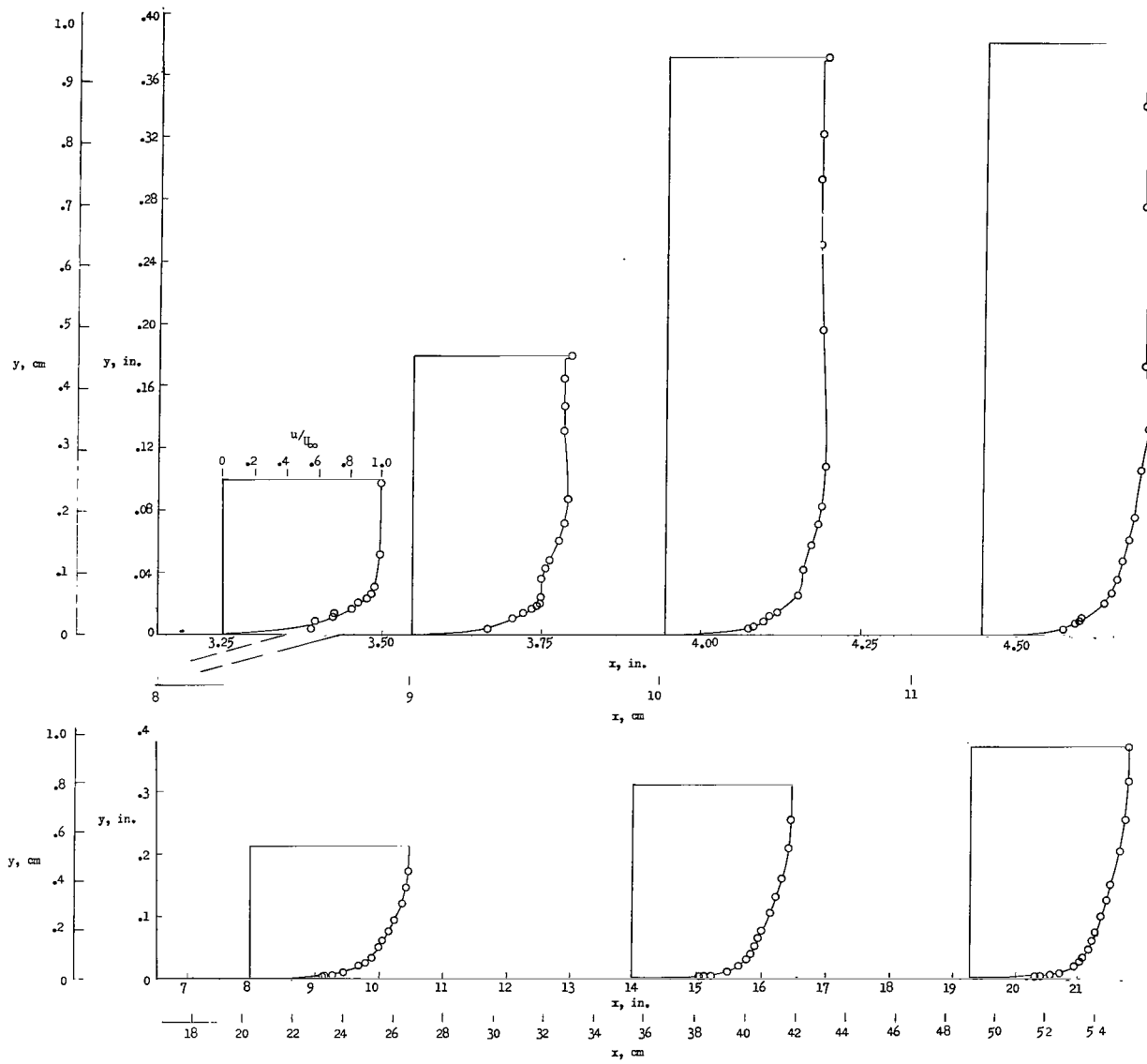


(a) 0.0085-inch (0.0216-cm) rearward-inclined flush slot.

Figure 26.- Velocity profiles along surface of rearward-inclined flush-slot configurations. $2F/C_{F,0} = 0.43$.

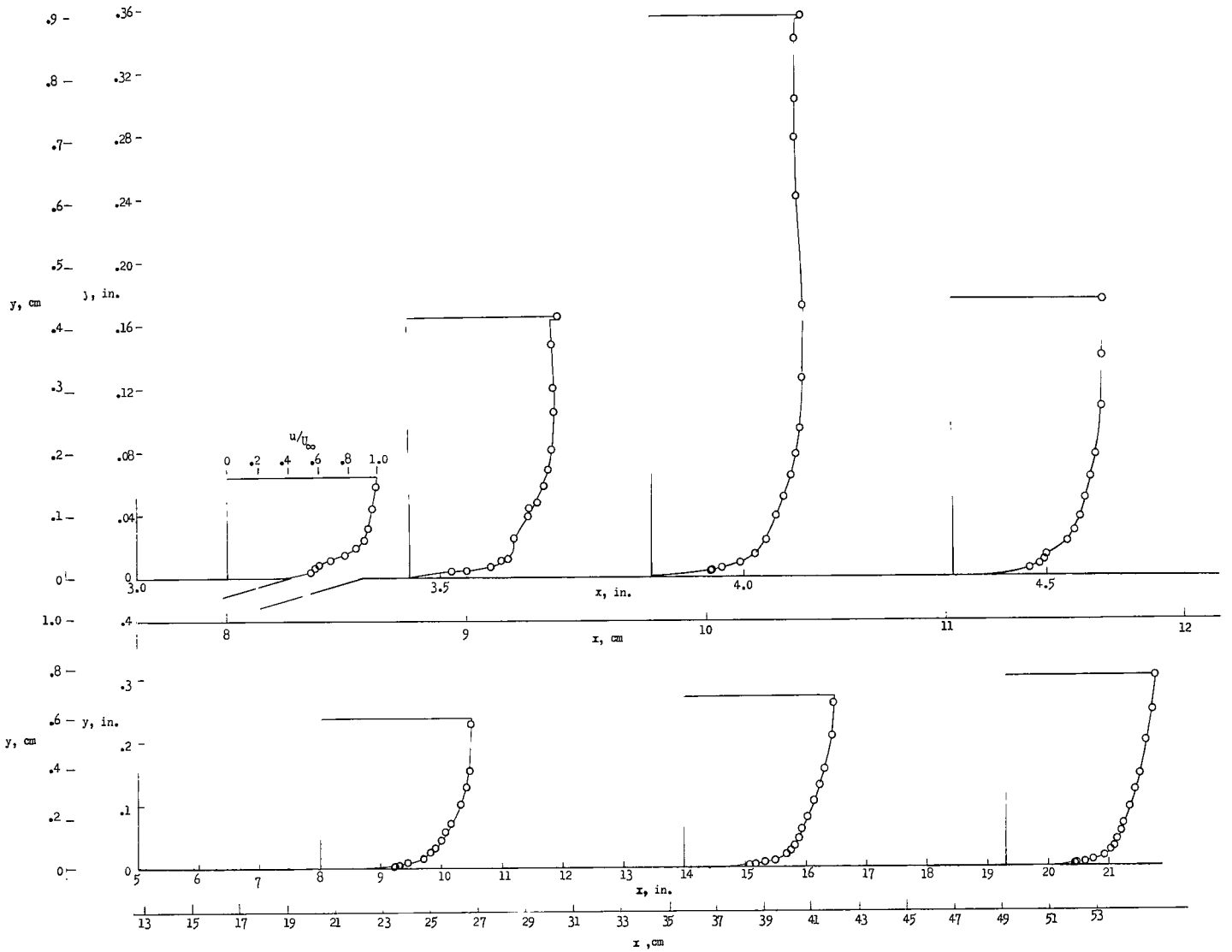


(b) 0.018-inch (0.046-cm) rearward-inclined flush slot.

Figure 26.- Concluded.

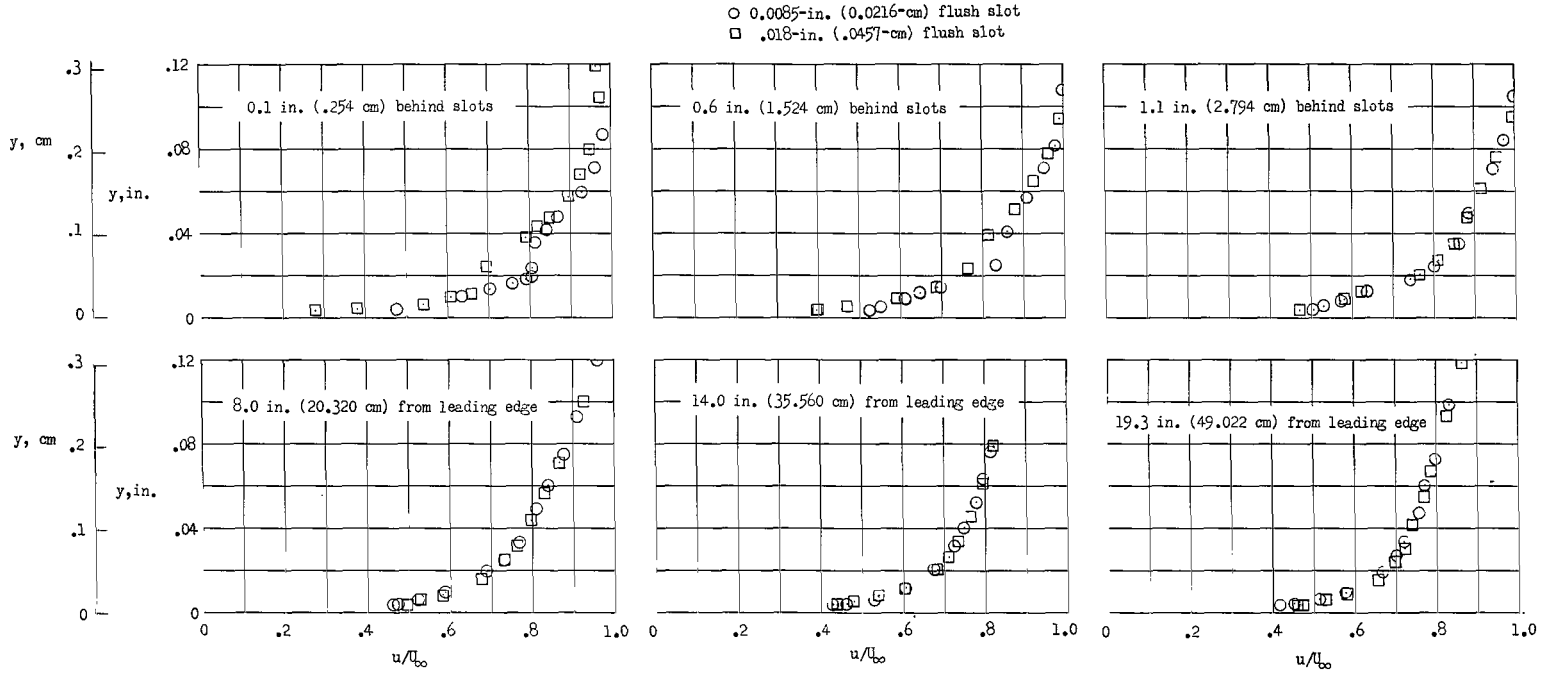


Figure 27.- Comparison of velocity profiles on surface of 0.0085-inch (0.0216-cm) rearward-inclined flush-slot and 0.018-inch (0.046-cm) rearward-inclined flush-slot configurations for an injection mass flow of 0.038 pound (0.0172 kilogram) per second.

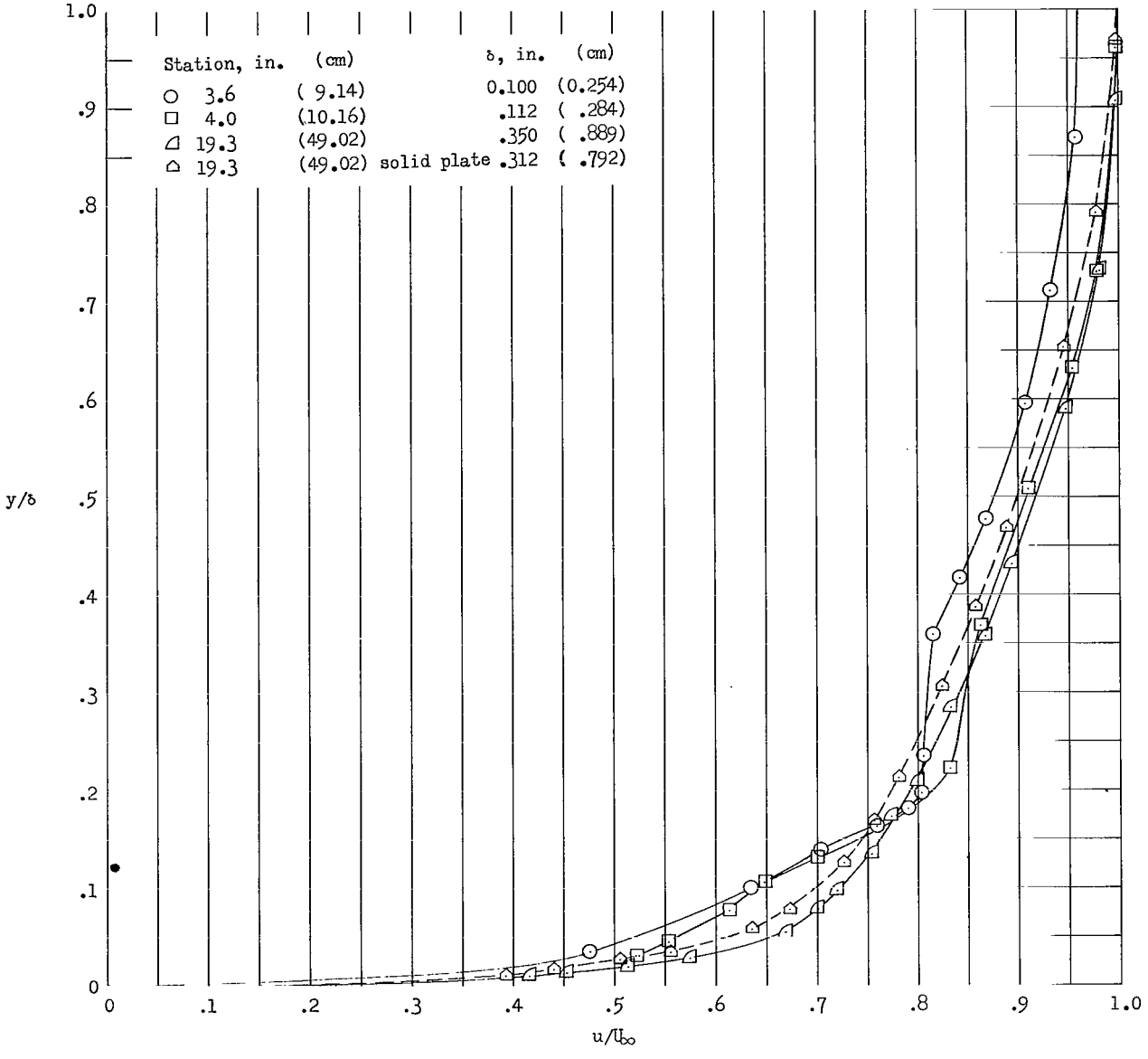


(a) 0.0085-inch (0.0216-cm) rearward-inclined flush slot.

Figure 28.- Nondimensional velocity profiles along surface of rearward-inclined flush-slot configurations for an injection mass flow of 0.038 pound (0.0172 kilogram) per second.

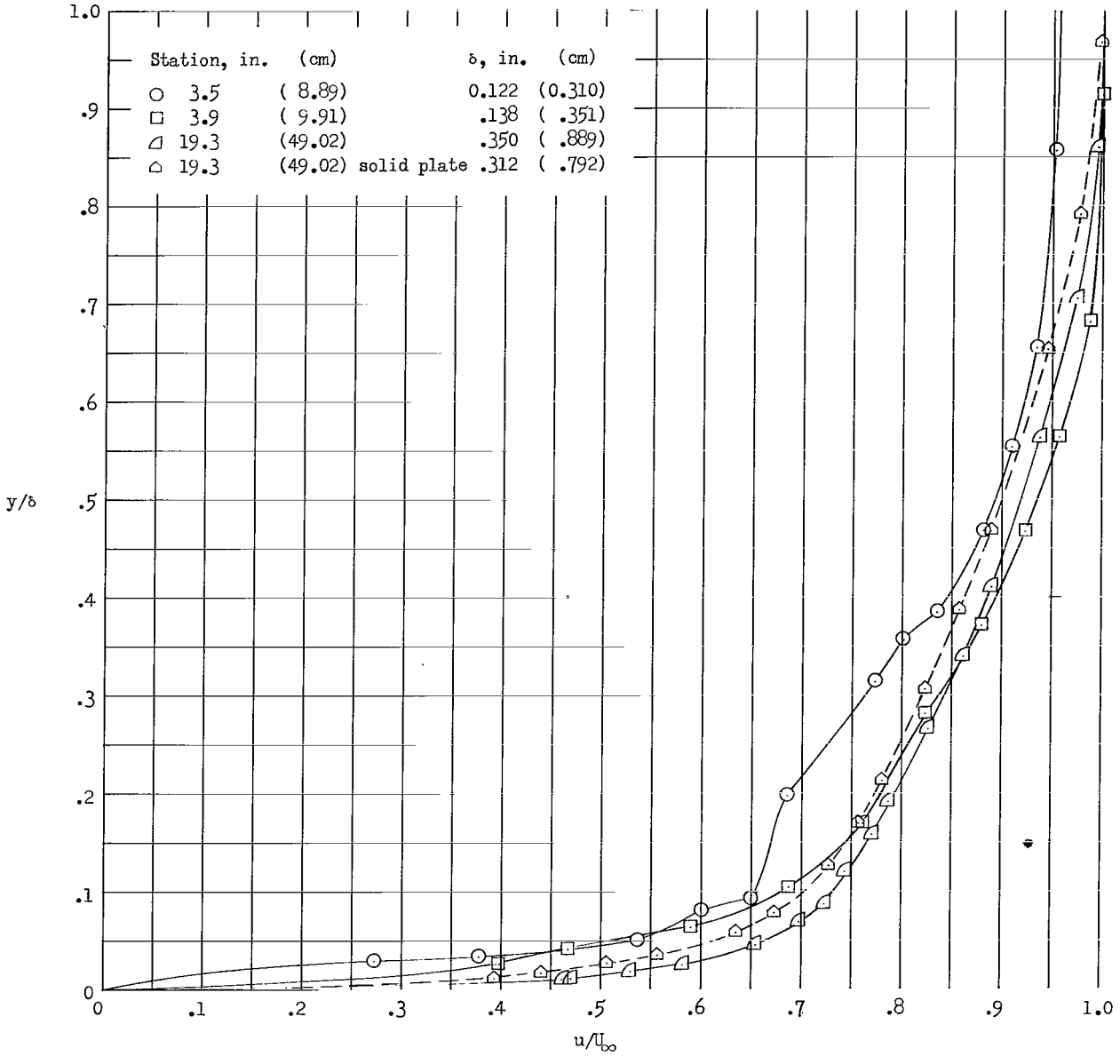


(b) 0.018-inch (0.046-cm) rearward-inclined flush slot.

Figure 28.- Concluded.

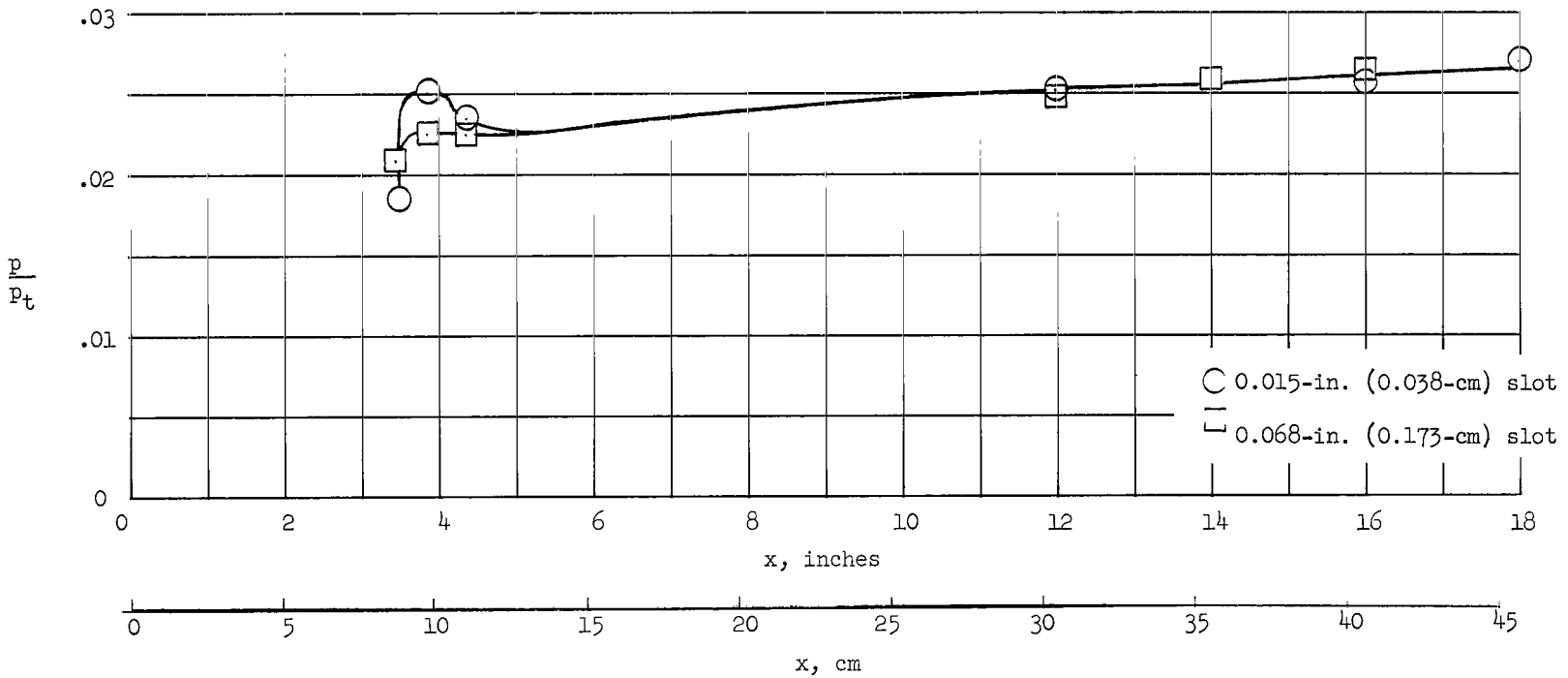


Figure 29.- Static-pressure distribution along surface of rearward-inclined step-slot configurations with a mass-flow rate of 0.038 pound (0.0172 kilogram) per second.

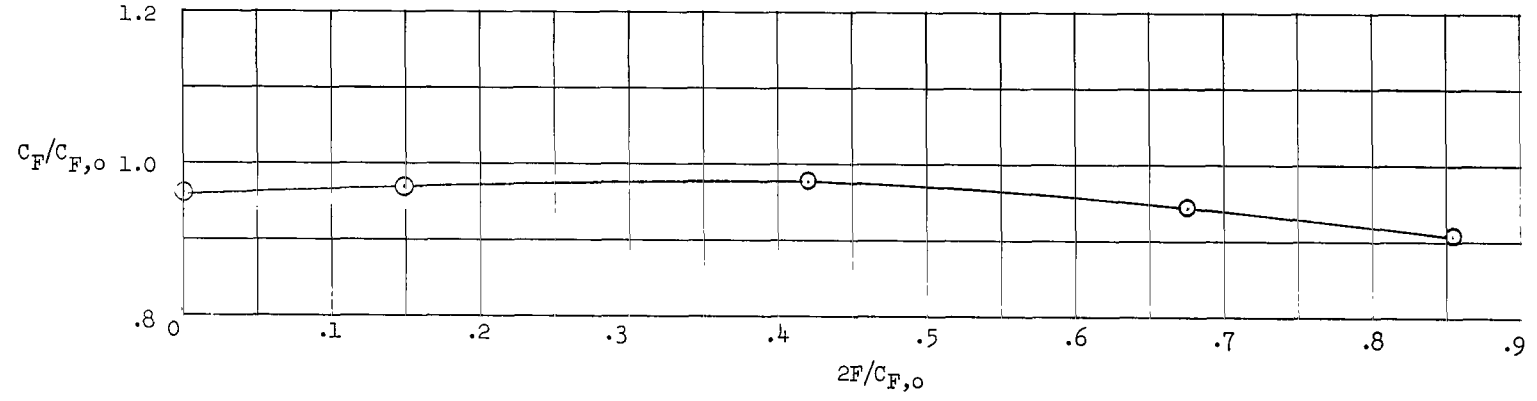


(a) 0.015-inch (0.038-cm) rearward-inclined step slot.

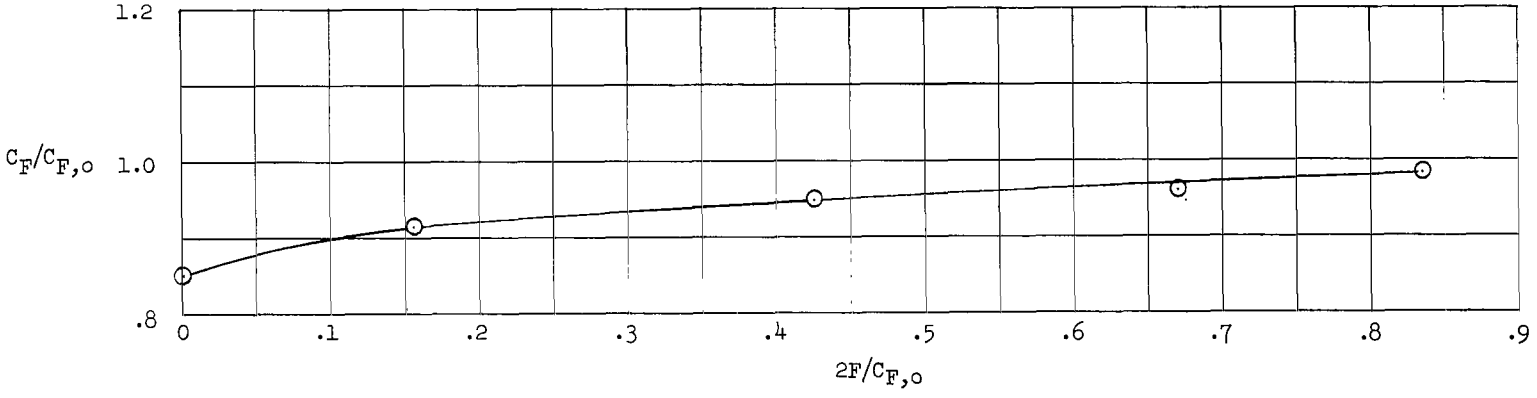


(b) 0.068-inch (0.173-cm) rearward-inclined step slot.

Figure 30.- Average skin-friction-coefficient ratios for rearward-inclined step-slot configurations. x = 19.3 in. (49.02 cm).

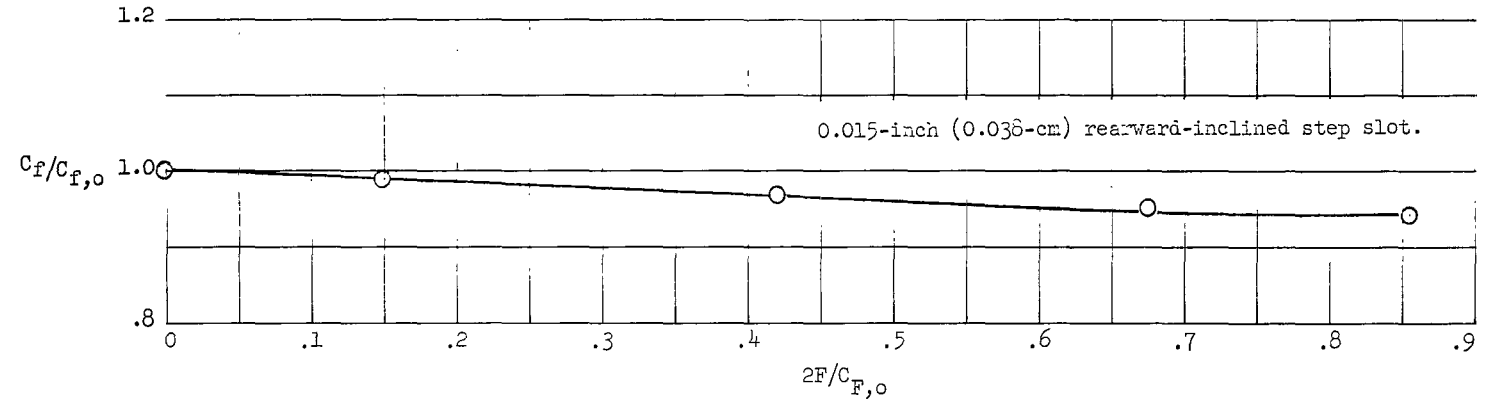


(a) 0.015-inch (0.038-cm) rearward-inclined step slot.

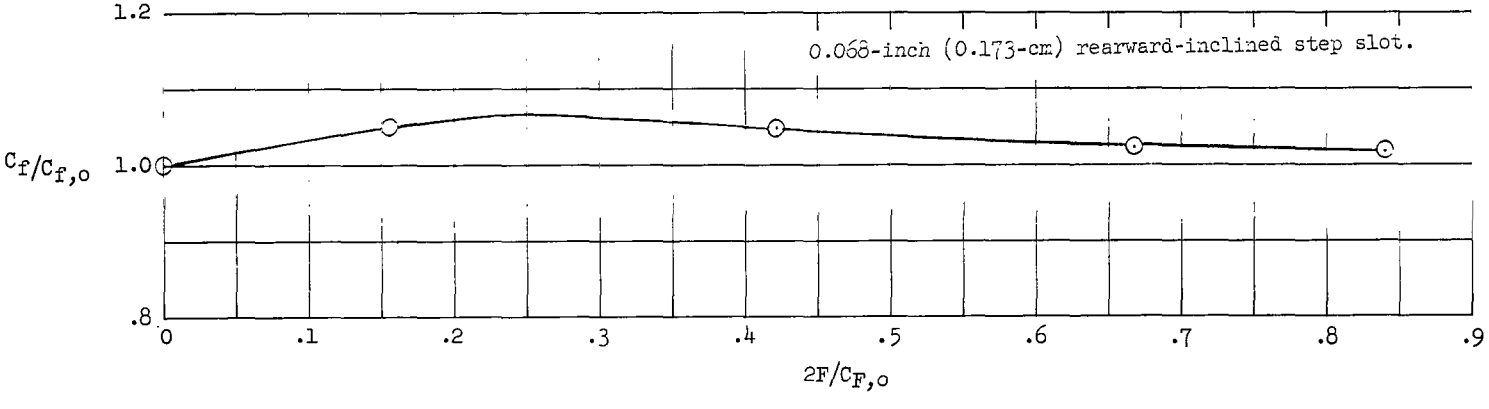


(b) 0.068-inch (0.173-cm) rearward-inclined step slot.

Figure 31.- Local skin-friction-coefficient ratios for rearward-inclined step-slot configurations. x = 20.0 in. (50.80 cm).

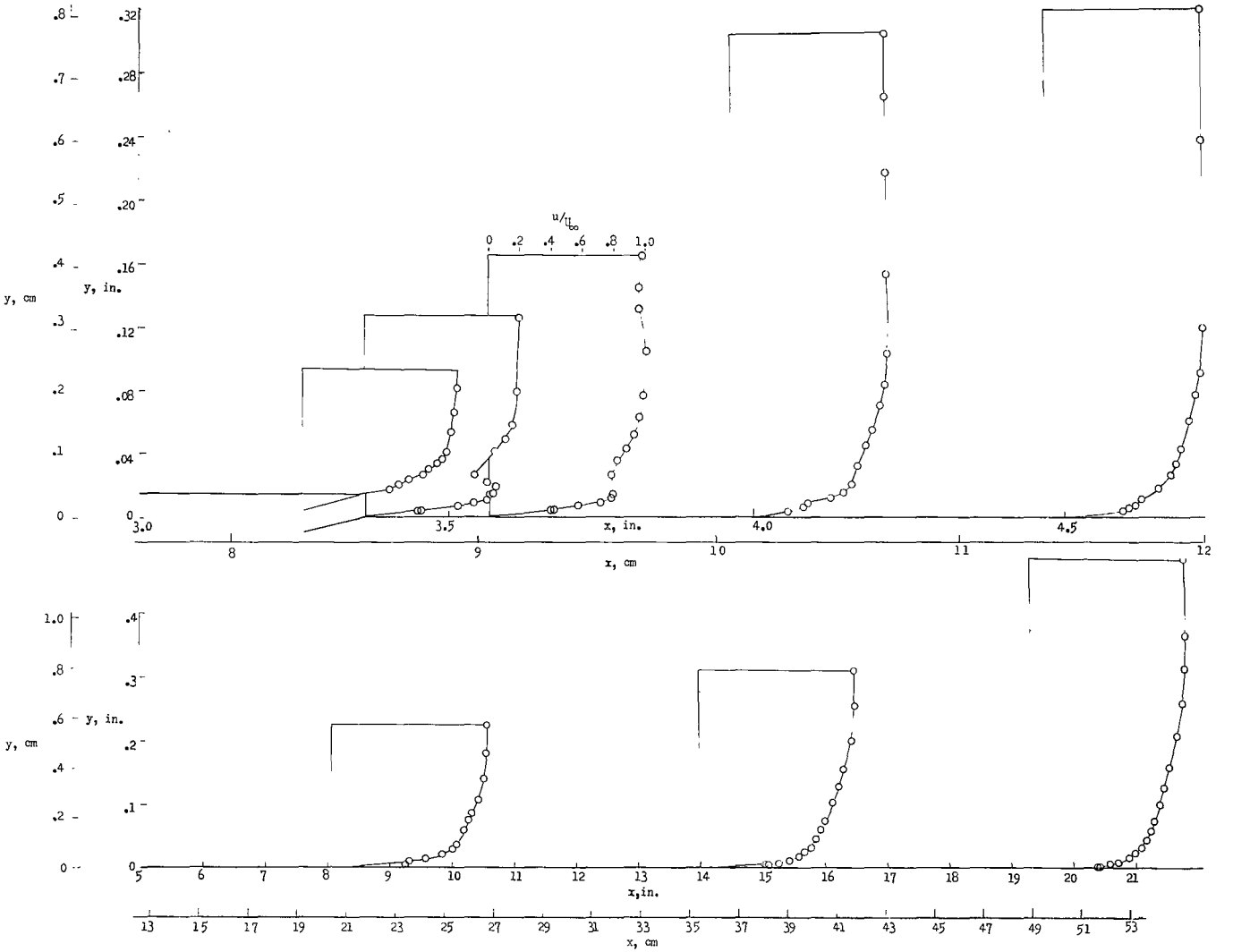


(a) 0.015-inch (0.038-cm) rearward-inclined step slot.

Figure 32.- Velocity profiles along surface of rearward-inclined step-slot configurations. $2F/C_{F,0} = 0.43$.

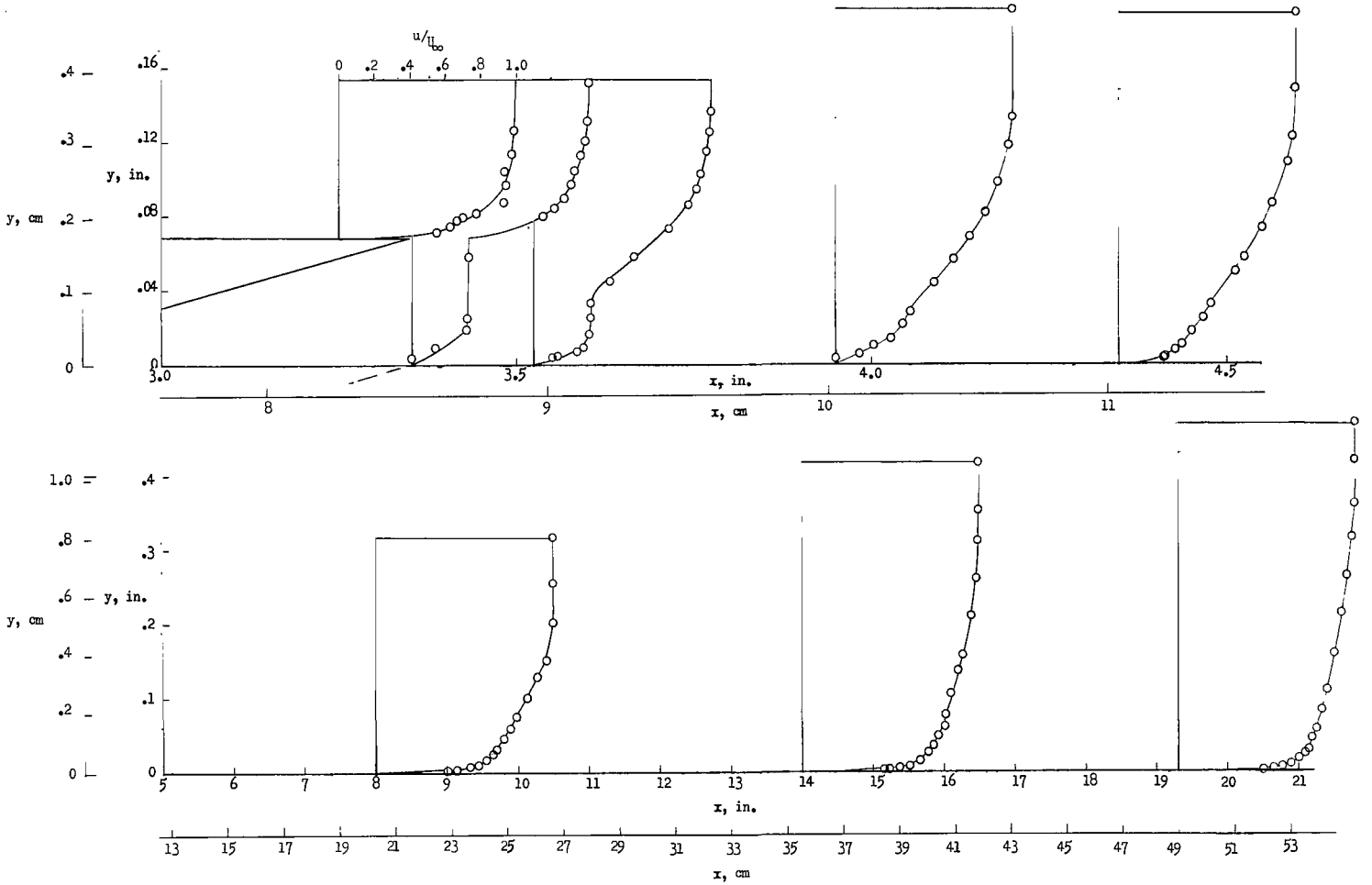


(b) 0.068-inch (0.173-cm) rearward-inclined step slot.

Figure 32.- Concluded.

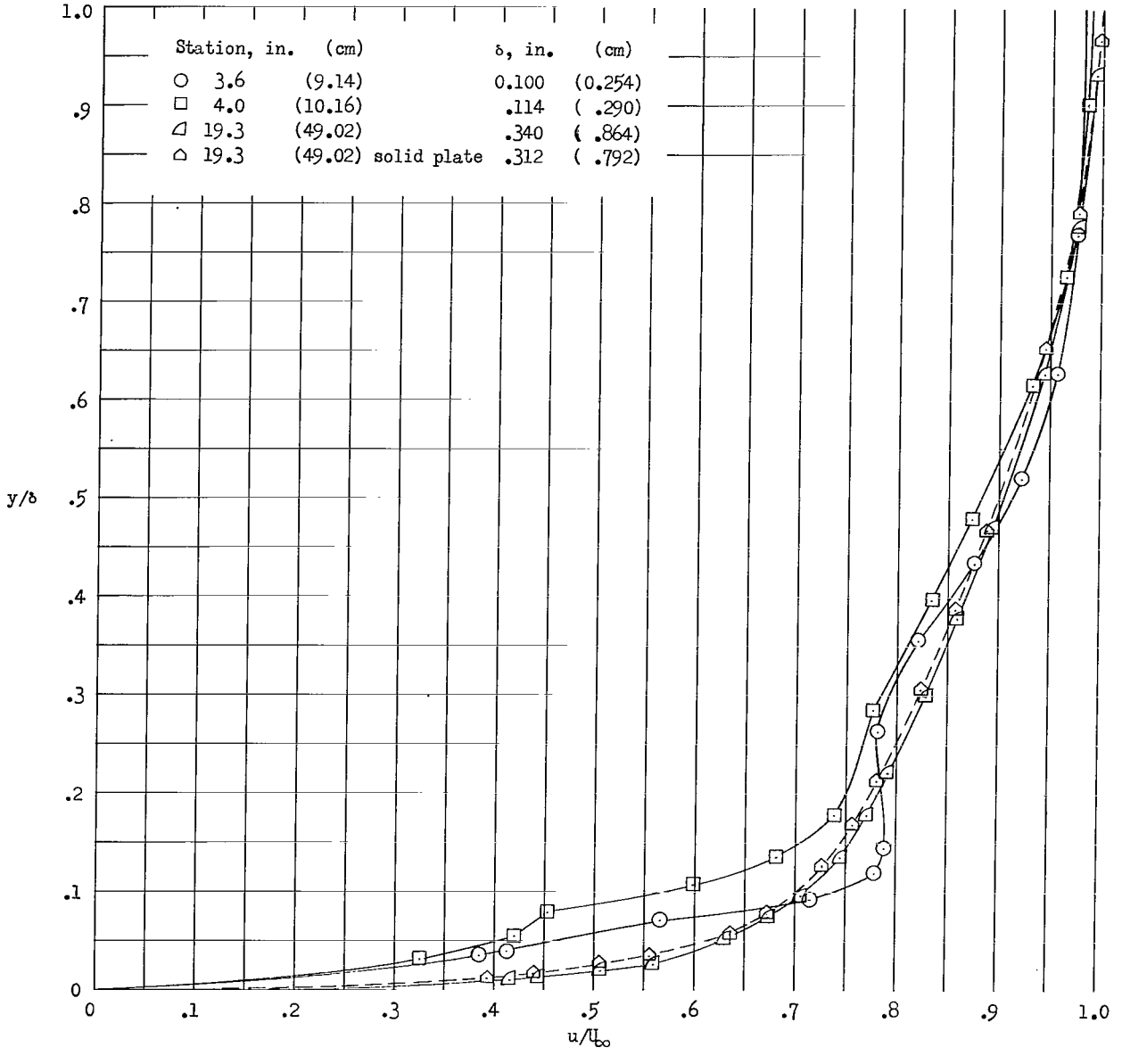


(a) 0.015-inch (0.038-cm) rearward-inclined step slot.

Figure 33.- Nondimensional velocity profiles along surface of rearward-inclined step-slot configurations for an injection mass flow of 0.038 pound (0.0172 kilogram) per second.

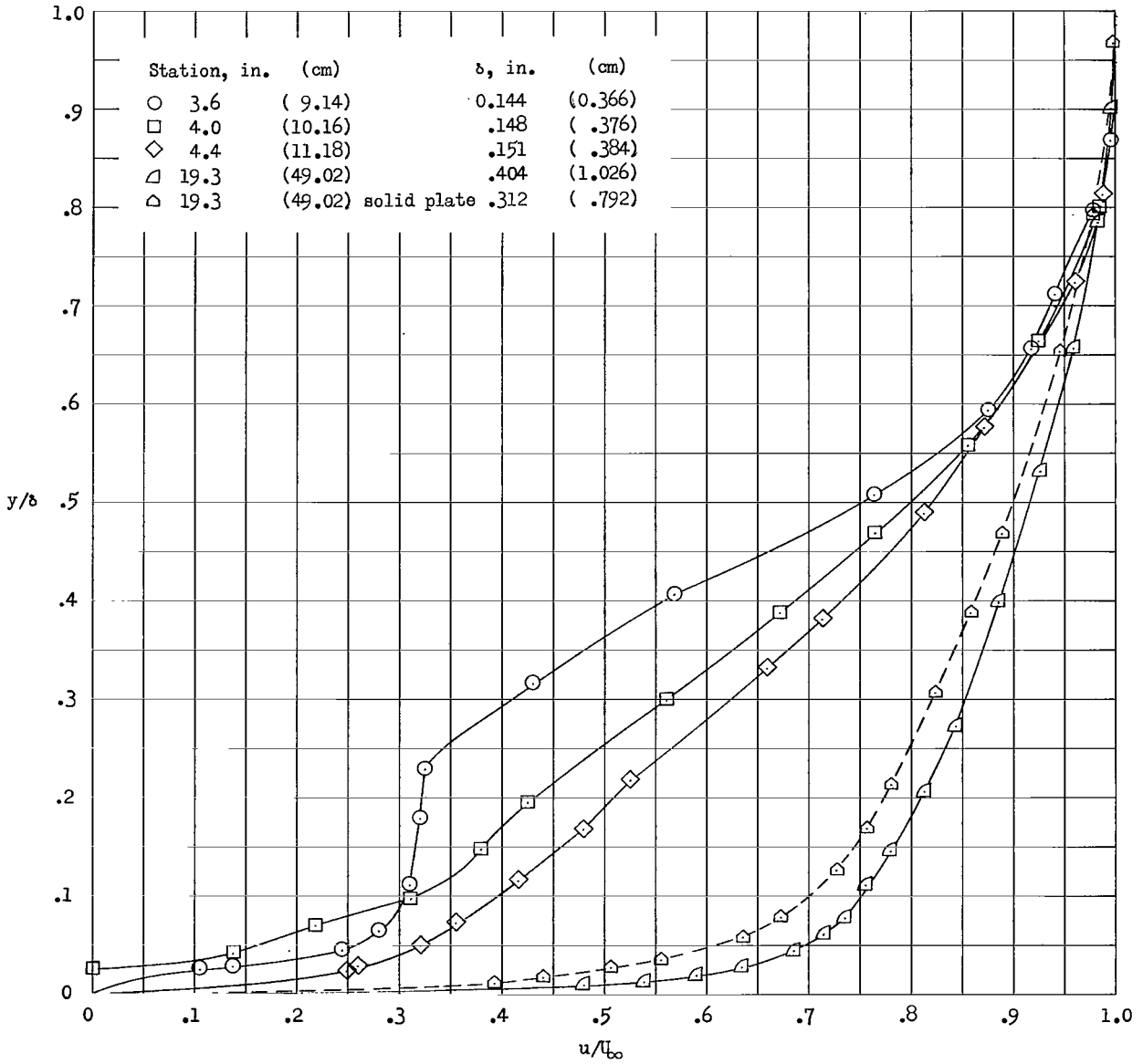


(b) 0.068-inch (0.173-cm) rearward-inclined step slot.

Figure 33.- Concluded.

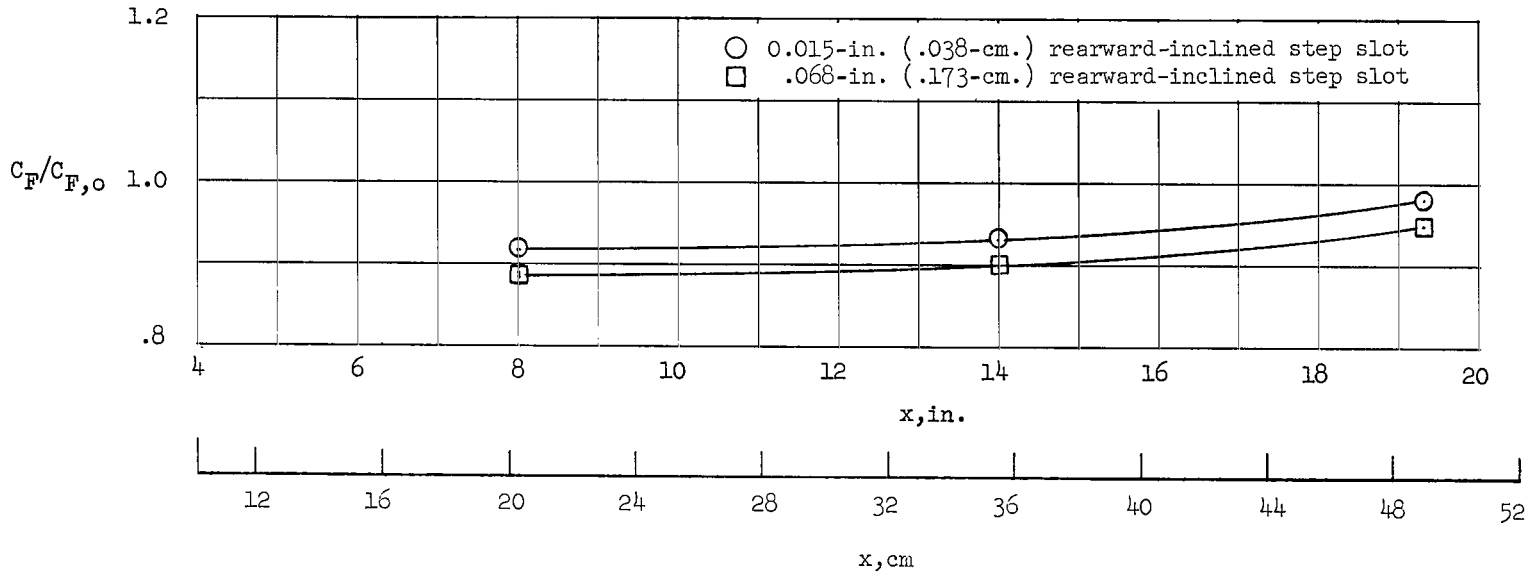


Figure 34.- Variation of average skin-friction-coefficient ratios along surface of rearward-inclined step-slot configurations with a mass-flow rate of 0.038 pound (0.0172 kilogram) per second.

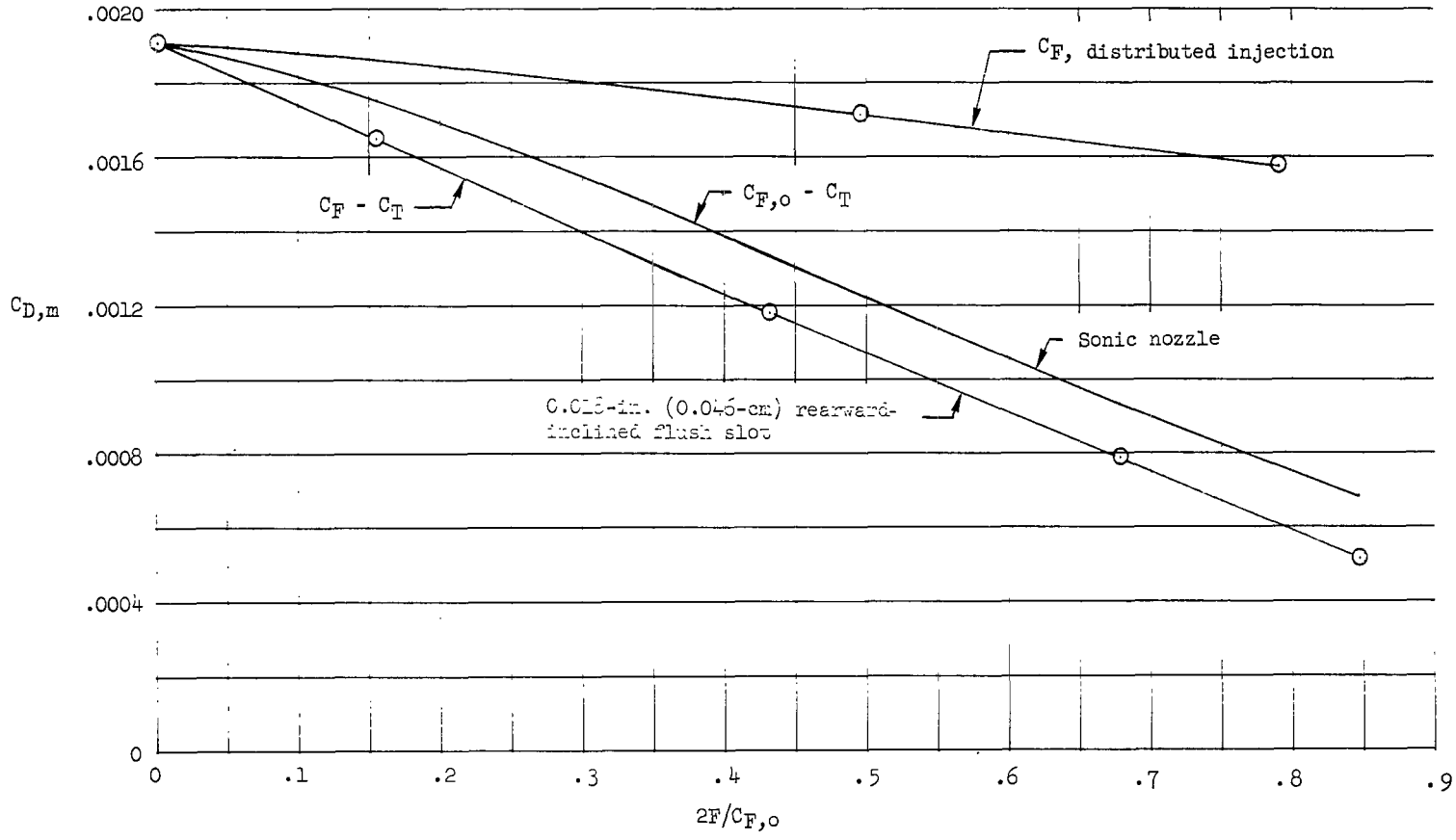


Figure 35.- Comparison of effectiveness of air for various applications.

*"The aeronautical and space activities of the United States shall be conducted so as to contribute . . . to the expansion of human knowledge of phenomena in the atmosphere and space. The Administration shall provide for the widest practicable and appropriate dissemination of information concerning its activities and the results thereof."*

—NATIONAL AERONAUTICS AND SPACE ACT OF 1958

# NASA SCIENTIFIC AND TECHNICAL PUBLICATIONS

TECHNICAL REPORTS: Scientific and technical information considered important, complete, and a lasting contribution to existing knowledge.

TECHNICAL NOTES: Information less broad in scope but nevertheless of importance as a contribution to existing knowledge.

TECHNICAL MEMORANDUMS: Information receiving limited distribution because of preliminary data, security classification, or other reasons.

CONTRACTOR REPORTS: Technical information generated in connection with a NASA contract or grant and released under NASA auspices.

TECHNICAL TRANSLATIONS: Information published in a foreign language considered to merit NASA distribution in English.

TECHNICAL REPRINTS: Information derived from NASA activities and initially published in the form of journal articles.

SPECIAL PUBLICATIONS: Information derived from or of value to NASA activities but not necessarily reporting the results of individual NASA-programmed scientific efforts. Publications include conference proceedings, monographs, data compilations, handbooks, sourcebooks, and special bibliographies.

***Details on the availability of these publications may be obtained from:***

SCIENTIFIC AND TECHNICAL INFORMATION DIVISION

NATIONAL AERONAUTICS AND SPACE ADMINISTRATION

**Washington, D.C. 20546**